PRECISION NEUTRON POLARIMETRY AND A MEASUREMENT OF PARITY VIOLATING ASYMMETRY IN N-P CAPTURE

by

Monisha Sharma

A dissertation submitted in partial fulfillment
of the requirements for the degree of
Doctor of Philosophy
(Physics)
in The University of Michigan
2008

Doctoral Committee:

Professor Timothy E. Chupp, Chair
Professor Ratindranath Akhoury
Professor Wolfgang B. Lorenzon
Professor Roseanne J. Sension
Associate Professor David A. Reis

Dedicated to my Maa & Papa

ACKNOWLEDGEMENTS

First of all I would like to thank my advisor Professor Timothy E. Chupp for his guidance and support during the last five years. I would also like to thank Professor W.B. Lorenzon for providing helpful suggestions. I also thank the members of my committee, Professor R. Akhoury, Professor R.J. Sension and Professor D.A. Reis.

I thank all the members of the NPDGamma collaboration. In particular, I would like to thank Dr. Seppo I. Penttila who helped me in all the experiments and Libertad Barrón-Palos for the technical and moral support she gave during all the ups and downs of my Ph.D. I also thank Dr. T.R. Gentile, Dr. Earl D. Babcock and the PF1B ^{3}He collaboration at ILL for taking the lead in investigating the ^{3}He polarization decay. I also thank Jason Medina for all the technical support he provided at LANSCE.

I would take the opportunity to thank my parents, Lakshmi Nath Sharma and Bhanu Sharma, for their faith, love and support. I owe loving thanks to my brothers, Amar Jeet and Bishwajit, for their love, support and encouragement. I also thank my sis-in-laws, Nandita and Namita, for their love and well wishes. My loving thanks to Dr. Sarin A. Deshpande for all his love, support and help. And lots of loving thanks to my cute, loving niece, Aashi, for making my days lovely.

I would also like to thank my labmates Behzad, Eric and Rob for their help during the last five years. Last but not the least, I thank Krithika and all my friends in Ann Arbor for making my stay here comfortable and memorable.

TABLE OF CONTENTS

LIST OF FIGURES

Figure

LIST OF TABLES

Table

LIST OF APPENDICES

Appendix

CHAPTER I

Introduction

This dissertation describes experimental studies with polarized neutrons. Polarized neutrons are sought for a variety of applications like electron scattering, hadronic parity violation and neutron β-decay experiments. In this dissertation the applications of polarized neutrons for hadronic parity violation and β-decay experiments, neutron polarization with ^{3}He spin filters and neutron beam polarization analysis are discussed.

Parity violation experiments aim to understand the weak interactions between nucleons. It is expected that weak interactions have the potential to provide new information on quark-quark correlations in the strong interactions limit of quantum chromodynamics (QCD). Weak interactions between nucleons are small as compared to the strong interactions, and since weak interaction violates parity, the only way to access weak interactions is by measuring the small parity-violating effects in experiments. Hadronic parity-violation experiments measure these small parity-odd interference effects amid the much larger effects of the strong interaction between the nucleons with high sensitivity and aim to provide a better insight on the hadronic weak interactions. On the other hand, the weak interactions in β-decay are well characterized but the goal of this field is the precision measurements of the correlation

coefficients between the neutron and the outgoing particles of the polarized neutron decay. It is believed that precision measurements of these correlation coefficients will lead to probe physics beyond the Standard Model [24]. Both hadronic parity violation and β-decay experiments employ polarized neutrons and both sensitive and precise measurements of observables need the knowledge of neutron polarization. This dissertation describes our efforts in polarizing neutrons using ^{3}He spin filter and the analysis for neutron beam polarization measurements.

Section 1.1 provides a brief history of weak interactions and parity violation. The section discusses the history of weak interactions and parity violation starting with the discovery of radioactivity to the demonstration of weak interactions in nucleon-nucleon interactions. Section 1.2 provides short discussions of the hadronic interactions, the meson-exchange model proposed to explain the weak interactions in nucleons and the NPDGamma experiment performed at Los Alamos Neutron Science Center (LANSCE). In the NPDGamma experiment, ^{3}He spin filters were used to polarize neutrons [26]. ^{3}He depolarization was observed in these spin filters when exposed to the neutron beam [67]. This depolarization effect is discussed in section 1.3. For precision measurements of the correlation coefficients in polarized neutron β-decay precise knowledge of the neutron polarization at 0.1% is essential to reduce the systematic effects. The experiment performed to reach this goal of 0.1% precision in neutron polarization is discussed in section 1.4.

1.1 History of Parity Violation and Weak Interaction

The story of weak interactions started in 1896 with the discovery of radioactivity by Becquerel. Chadwick in 1914 discovered that electrons in β-decay are emitted with a continuous spectrum of energies which appears to violate energy and momen-

tum conservation. To explain the apparent non-conservation of energy and linear momentum in the β-decay Pauli proposed the existence of the neutrino, a neutral particle with very small rest mass energy. Soon after this proposal E. Fermi came up with his theory of β-decay [33] based on the formulation created by Dirac and later developed by Heisenberg and Pauli.

The β-decay Lagrangian proposed by Fermi was

$$L_\beta = -\frac{G_F}{\sqrt{2}}\bar{\psi}_p\gamma_\mu\psi_n\bar{\psi}_e\gamma^\mu\psi_{\nu_e}. \tag{1.1}$$

This equation used the Dirac wavefunctions for the neutron, proton, electron and the neutrino. G_F is the Fermi coupling constant and experimentally determined to be $G_F = 1.03 \times 10^{-5} m_p^2$ in units of $\hbar = c = 1$. With the discovery of positron β-decays in 1934 the β-decay Lagrangian was modified to

$$L_\beta = -\frac{G_F}{\sqrt{2}}[\bar{\psi}_p\gamma_\alpha\psi_n\bar{\psi}_e\gamma^\alpha\psi_{\nu_e} + \psi_n\gamma_\alpha\psi_p\psi_{\nu_e}\gamma^\alpha\psi_e]. \tag{1.2}$$

With the discovery of muons in 1930's it was confirmed that there are other reactions in nature apart from β decay that have the same coupling strength and similar characteristics. The discovery of pions, hyperons and K-mesons led to the concept of a universal charged weak interaction governing the slow decays of unstable particles. Later, parity violation was discovered in these systems in which weak interaction occurs. In quantum mechanics P is a parity operator acting on a state $\psi(\vec{r})$ so that $P\psi(\vec{r}) = \psi(-\vec{r})$ [52].

Parity violation was discovered by T.D.Lee and C.N.Yang while solving the $\tau - \theta$ puzzle [49]. In their paper, they assumed that although θ^+ and τ^+ were closely identical in critical masses and lifetimes, the parities are different. They proposed that if parity is violated then τ and θ are the same particle with different parities, τ has odd parity and θ has even parity. They proposed an experiment to measure the

parity violation in β-decay and their thoughts were made practical by C.S.Wu *et. al.* in 1957 when they successfully measured parity violation in ^{60}Co by measuring a non-zero dot product between the beta particles momenta and the the spin of ^{60}Co [82]. Lee and Yang also suggested that parity violation is an intrinsic feature of weak interactions.

After admitting parity violation in weak decays the β-decay Lagrangian is no longer invariant under space inversion, therefore, corrections had to be made to it and a new form of the Lagrangian emerged which had both even and odd couplings. This new matrix element for allowed β decay is given by

$$M = \frac{g_F}{\sqrt{2}} \sum_{nucleons} \sum_j \int d^3x [\bar{\psi}_p O_j \psi_n][\bar{\psi}_e O_j (C_j - C'_j \gamma_5)\psi_{\bar{\nu}_e}]. \tag{1.3}$$

The coefficients C_j and C'_j had to be determined from the experiments and $C_j = C'_j$ for V-A couplings. Observation of the superallowed decays ($0^+ \rightarrow 0^+$) in (^{10}C+$\rightarrow$ ^{10}B) and (^{14}O+$\rightarrow$ ^{14}N) showed that $C_V = 1$. Measurement of the lifetime of free neutrons, where both axial and vector couplings enter, lead to

$$\lambda = C_A/C_V = 1.25. \tag{1.4}$$

This departure from unity showed the manifestation of strong interaction effects. Relative phases of C_A and C_V are determined by the observations of the β-decay and neutrino asymmetries of polarized neutrons. The final result for the matrix element of β decay is given by

$$M = \frac{g_F}{\sqrt{2}} \int d^3x \bar{\psi}_p \gamma_\mu (1 - \lambda\gamma_5)\psi_n \bar{\psi}_e \gamma^\mu (1 - \gamma_5))\psi_{\bar{\nu}_e}. \tag{1.5}$$

Immediately after the discovery of β-decay Tanner reported the first search of parity violation in the nucleon-nucleon interaction [71]. In 1958, Feynmann and Gell-Mann [36] and Sudarshan and Marshak [69] independently proposed a generalization

of Fermi's theory. According to this formulation, all charged weak processes: β-decay, muon decay etc. and the interaction between nucleons are described by an effective Lagrangian density in which a "universal" charged weak current $\mathcal{J}_\lambda$ is coupled to itself or to its Hermitian conjugate at a single space-time point,

$$L = -\frac{1}{2}\frac{G_F}{\sqrt{2}}(\mathcal{J}_\lambda \mathcal{J}^{\lambda\dagger} + \mathcal{J}^{\lambda\dagger}\mathcal{J}_\lambda), \tag{1.6}$$

where the weak current $\mathcal{J}_\lambda$ consists of leptonic and a hadronic portion given by

$$\mathcal{J}_\lambda = j_{l\lambda} + J_\lambda. \tag{1.7}$$

The leptonic part, $j_{l\lambda}$, is a generalization from β-decay. It describes the charged weak transformations like $\nu_l \rightarrow l^-$, $l^+ \rightarrow \bar{\nu}_l$ etc. The hadronic weak current term, J_λ, is expressed in terms of the quark model. For example, the valence quark compositions of neutron and protons are udd and uud, respectively. Neutron β decay therefore occurs due to the quark transformation $d \rightarrow u$ and the hadronic charged weak current contains a component proportional to $\bar{D}\gamma_\lambda(1-\gamma_5)U$ where U and D are the up and down-quark field operators, respectively. This theory thus predicted a parity violating weak contribution to the interaction between nucleons (p-p, n-p interactions etc.) and the verification of this theory proved to be an experimental challenge.

Many experiments have been designed to observe parity violation in nuclei e.g. measurement of circular polarization in ^{18}F [12, 6], proton-proton scattering [15], anapole moment measurements [81] etc. The NPDGamma experiment is one of the experiments designed to study the parity violation in the capture of neutrons by protons, $n + p \rightarrow d + \gamma$. The experiment measures parity-violating directional gamma-ray asymmetry in the n-p system by the use of polarized neutrons on a proton target. The observation of an asymmetry or absence, both have important implications on the correctness of the theories proposed for the NN interaction.

1.2 Weak Interactions, Parity Violation and the NPDGamma Experiment

When the parity-violating phenomenon was under investigation in nuclei, rapid progress was made in experiments and theory studying weak interactions and decays of particles. With the discovery of quarks, the electroweak theory was developed to explain the leptonic and semi-leptonic weak processes. Figure 1.1 shows the common classification of the weak interaction. The leptonic, semi-leptonic and $\Delta S = 1$ hadronic interactions are isolated as purely weak effects but nothing prevents the flavor-conserving hadronic interactions $\Delta S = 0$ such as $np \rightarrow np$ from passing through a strong channel. Flavor-conserving nucleon-nucleon interactions are modeled to have a strong Hamiltonian with a small perturbation from weak interaction. Experimental studies of the flavor-conserving hadronic interactions are therefore hindered by the smaller size of the weak couplings compared to the size of the strong couplings. The weak couplings are several magnitudes smaller than the strong couplings and therefore, the unique feature of the weak interactions: parity violation, is used to study the weak interactions in hadronic interactions.

Like pure leptonic and semi-leptonic weak interactions, pure hadronic weak interactions between nucleons can also be mediated by the exchange of $W^{\pm}$ and Z^0 bosons. The hard core repulsion between the nucleons keeps them farther apart from the range of weak gauge bosons, $\approx$0.02 fm. At momentum transfers typical of nuclear interactions $\approx$300 MeV, the appropriate degrees of freedom are mesons and nucleons. Therefore, the long range weak interaction is mediated by mesons ρ, ω or π as shown in figure 1.1(d) and the interaction is defined in terms of meson coupling constants. Several meson models have been proposed for weak interaction among hadrons. The most adopted model at present is the DDH model which is

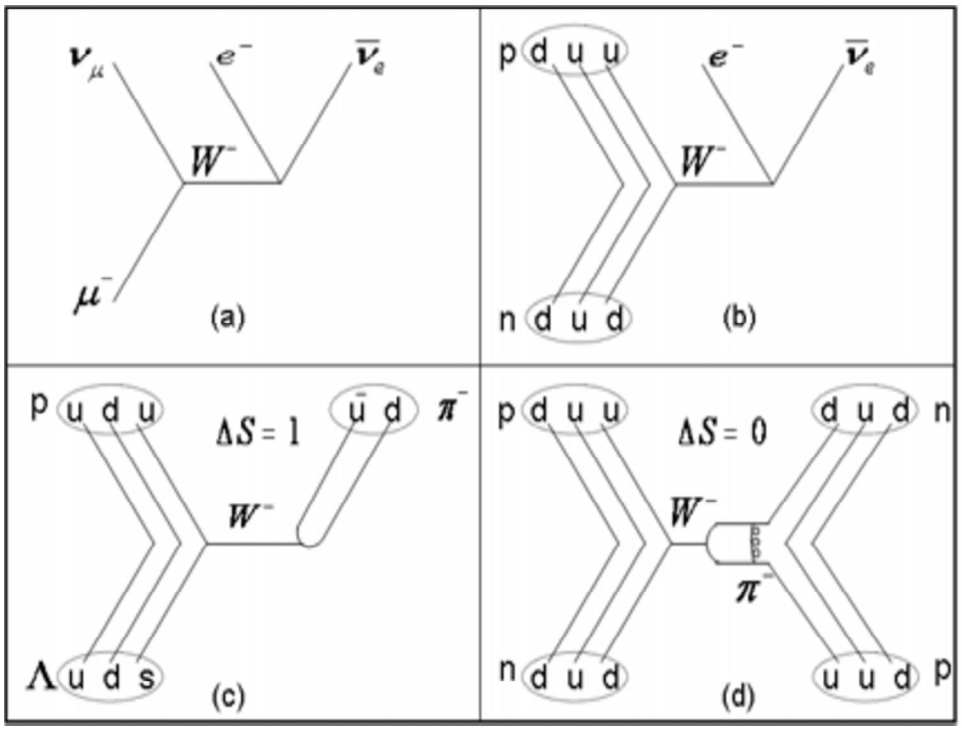

Figure 1.1: Illustration of various weak interactions: (a) Pure leptonic decay of muon (b) semileptonic β decay of a neutron (c) strangeness-non conserving pure hadronic decay of a Λ baryon (d) strangeness-conserving pure hadronic neutron-proton scattering

discussed in chapter II [30]. Many experiments have been performed and many more are being proposed for the measurement of these meson couplings. There are several parity-non-conserving observables for the NN system which are discussed in detail in chapter II. In heavy nuclei, the parity violating effects are generally much larger but difficult to interpret because of the structural uncertainties of the nuclei. The NPDGamma experiment proposes to measure the coupling constant for the pion exchange, f_π^1, in the nucleon-nucleon interaction of the DDH model. The NPDGamma experiment aims to measure the γ-ray directional asymmetry in the capture of neutrons by protons in $\vec{n}+p \rightarrow d+\gamma$. As the asymmetry will be measured in a two-body system, the results obtained will be free from the nuclear structure uncertainties and therefore will provide a clean result.

In terms of the meson coupling constants the γ-ray directional asymmetry in the

n-p capture is [37]

$$A_\gamma = -0.107 f_\pi^1 - 0.001 h_\rho^1 - 0.004 h_\omega^1. \tag{1.8}$$

The asymmetry is therefore to a very good approximation proportional to the pion-nucleon coupling constant as the other terms are small. The goal of the NPDGamma experiment is to measure the coupling constant f_π^1 to 10% of the predicted value from the DDH model. The DDH predicted value of this coupling is 4.56×10^{-7} and the given "reasonable range" is (0-11.4)$\times 10^{-7}$.

The NPDGamma experiment was performed at Flight Path 12 of Los Alamos Neutron Science Center (LANSCE). The experiment measured the γ-ray directional asymmetry, A_γ in the n-p capture. Chapter II gives the motivation behind the NPDGamma experiment. Experimental details and some of the results from the experiment are discussed in Chapter III. In the experiment, the γ-ray directional asymmetry was measured with respect to the neutron spin and therefore a polarized neutron beam was used. The neutrons were polarized using a ^{3}He neutron spin filter and both ^{3}He and neutron polarization were monitored continuously during the experiment. Details of the ^{3}He spin filter and the polarization analysis done for the NPDGamma experiment is presented in Chapter III. The NPDGamma experiment finished its first phase at Los Alamos Neutron Science Center and has been moved to Spallation Neutron Source (SNS) for the second run with higher neutron flux.

1.3 Depolarization in ^{3}He Polarizer Cells

During the NPDGamma experiment we monitored ^{3}He polarization continuously for a period of almost three months. The polarization measurements were performed by taking the ratio of the neutron transmission through a polarized ^{3}He cell to transmission through an unpolarized ^{3}He cell. ^{3}He polarization was also monitored over

time using Nuclear Magnetic Resonance (NMR). Both the methods showed us that ^{3}He polarization decreased over time when the ^{3}He polarizer cell was exposed to the neutron beam. Two types of relaxation were observed in the cell when polarization was monitored for a month in September 2006: (a) long term relaxation and (b) short term relaxation.

In long term relaxation, the polarization decreases continuously with time when the cell is exposed to the neutron beam and this decay is not reversible. Short term relaxation is an effect observed on shorter time scales, ^{3}He polarization decays when the cell is exposed to the neutron beam and with the beam off, polarization recovers, at least partially. This depolarization effect was observed in several different cells.

It is important to find the root cause of these decays and also to find out how the decay scales with the neutron flux. If the decay scales with the neutron flux then, it will not be possible to use the same kind of ^{3}He cells in a facility with higher neutron flux. In such a case an alternative to these cells will be required. To understand this relaxation an experiment was performed at LANSCE in Summer 2007 followed by another experiment at Institut Laue-Langevin (ILL) in Grenoble in France in November 2007. In the LANSCE experiment we measured the rubidium polarization by Electron Spin Resonance (ESR) technique in a cell with varying neutron flux. The ILL experiment measured the alkali metal polarization in Rb and Rb-K hybrid cells using ESR by measuring the Faraday rotation [9]. Spin destruction rate measurements, rate of electron spin-flips per alkali metal, were also performed on pure Rb and Rb-K hybrid cells by using relaxation in the dark technique [35]. These experiments confirmed the polarization decay in polarizer cells when exposed to neutron beam. Details of the experiment and results are presented in Chapter IV.

1.4 Importance of Polarized Neutrons and Precision Polarimetry Experiment

The discovery of β-decay led to the discovery of weak interactions and since then precision measurements in β-decay have played an important role in the development and understanding of the Standard Model and in probing new physics. There are three correlation coefficients in β-decay, A, B and C which measure asymmetries between the outgoing particle and the neutron spin. A measures the beta asymmetry, B measures the neutrino asymmetry and C measures the proton asymmetry.

The study of neutrons is important because the results can be related to the physics of fundamental fermion interaction with a small and reliable correction. Neutron decay is a four fermion interaction and can be used to understand fermion interactions better. In the Standard Model the ratio of the axial to vector coupling constants, $\lambda = g_A/g_V$, relates A, B and C. Thus the direct measurement of these parameters probes the Standard Model and the possibility of additional parameter which will lead to "new physics". Several experiments have measured A and B before but measuring the proton asymmetry C to probe the Standard Model is a new experiment. Precision measurement of C will provide new input into the analysis of β-decay. Combining the coupling constant λ calculated from a C measurement and V_{ud}, up and down quark mixing matrix element in the Cabibo-Kobayashi-Maskawa (CKM) matrix determined from super allowed neutron beta decays [63], will provide an indirect measurement of the neutron lifetime. Neutron lifetime is currently under extensive study due to the discrepancy of recent results [83, 66]. The only report of a measurement of C in the literature is by the PERKEO collaboration [63], where they reported a 1.5% measurement of kC, k is a kinematical factor which depends on the range of the proton energy spectrum that is measured.

PANDA (Proton Asymmetry in Neutron Decay) is a proposed experiment which aims to measure the proton asymmetry in β-decay, C, to 0.1%. In the V/A (Vector/Axial) theory a 0.1% measurement of the proton asymmetry can be interpreted as 0.15% measurement of λ [24]. A 0.1% measurement requires neutron polarimetry, background suppression and control of systematics effects at the 0.1% level. During the NPDGamma experiment we saw that it is possible to reach 0.1% polarization precision using polarized ^{3}He and time-of-flight discrimination of neutron velocity [26]. Precision polarimetry was therefore performed to understand the neutron polarization at 0.1% level using ^{3}He polarizers.

There are two main techniques for absolute neutron beam polarization measurement in the cold, thermal and epithermal neutron energy ranges [84],

- Relative intensity measurements of the spin components in a polarized beam after spatial separation using a magnetic field gradient (Stern-Gerlach effect).
- Transmission measurements using a second polarizing device, called the analyzer, along with a spin-flipper before the analyzer.

Both methods have their own limitations. For experiments in which neutrons need to travel in a uniform magnetic field, for a 0.1% measurement the first method cannot be used as an inhomogeneous magnetic field may cause field gradients in experimental set up and will lead to systematics in the experiment. Therefore, in our experiment neutron polarization measurements were performed using the second method by using a ^{3}He analyzer.

Polarization measurements in the NPDGamma experiment showed us that backgrounds play a major role in limiting the accuracy of the neutron polarization value. To understand the limitations caused by the backgrounds and other factors "Preci-

sion Polarimetry Experiment Using ^{3}He Spin Filters" was performed at LANSCE in Summer 2007. In this experiment the polarized neutron beam was analyzed using a ^{3}He analyzer. The polarized beam which comes out of the polarizer passes through an analyzer after passing through a spin flipper. We developed a method to measure the neutron polarization at two different positions in the experiment: after the polarizer and after the spin flipper. The details of the precision polarimetry experiment and the analysis developed are discussed in Chapter V.

CHAPTER II

Motivation for the NPDGamma Experiment

2.1 Introduction

The weak interaction between nucleons was first observed in 1964 by Abov [2]. The experiment used polarized neutrons on a Cd target. The gamma rays emitted due to neutron capture by Cd was analyzed for parity violation and a non-zero value was obtained for the asymmetry. Since then parity violating phenomena have been extensively studied experimentally. Circular γ-ray polarization [6], asymmetries from polarized nuclei [32] were studied and have been measured with good precision. Anapole moments of nuclear ground state measurements, another tool to probe the weak interactions, have been observed recently [81].

After decades of studies the weak interaction between the nucleon-nucleon interaction is yet not well established. In a nucleon-nucleon system it is difficult to access the weak interactions because of the much larger size of the strong interactions. Parity violation is an unique feature of weak interactions which is therefore used to probe the nucleonic system for weak interactions. Strong interactions do not violate parity, so any parity-odd effects must come from the weak interactions in the system. The study of nuclear parity have been, therefore, of interest for a long time in the hope it would provide information on weak interaction between nucleons.

It is important to understand the character of the weak interaction between nucleons for many reasons. Study of weak interactions between nucleons will improve the understanding of the strongly interacting limit of quantum chromodynamics (QCD). The weak interaction between leptons and quarks is well understood at the fundamental level. The range of weak interaction between the nucleons is much smaller than the size of the nucleon and also the strong repulsion of two nucleons does not allow the nucleons to come closer than a certain distance. Therefore it is proposed that the weak interaction between the nucleons must involve meson exchange. It is believed that weak interaction will provide new information on quark-quark correlations in QCD and will explain the meson exchange model of nucleon-nucleon (NN) interaction. Also, the NN interaction is the only way to study quark-quark neutral currents at low energy.

To understand the NN interaction, many models have been proposed in the last few decades [18, 30, 50]. The most popular model presently is the one in which the hadronic interaction is characterized by two vertices: a strong interaction vertex and a weak interaction vertex. The two vertices interact by the exchange of mesons. The hadronic interaction is dominated by the strong interaction with a small contribution from the weak interaction [30]. Many experiments have been proposed and are currently under development to validate the meson-exchange theory. The NPDGamma experiment is an experiment designed for achieving a better understanding of the weak interactions in nucleon-nucleon(NN) interaction. The experiment measures the asymmetry of the gamma-ray with respect to the neutron spin in the n-p capture, $n + p \rightarrow d + \gamma$.

2.2 Hadronic Interactions and DDH Model

Weak interactions are responsible for the decay of massive quarks and leptons into lighter quarks and leptons. The carrier particles of weak interaction are $W^{\pm}$ or Z bosons. The NN interaction has both a strong interaction and weak interaction vertex. A challenging problem of nuclear physics is to understand the weak interactions in the hadronic system because of the relatively small size of the weak interaction compared to the strong interactions. The Standard Model is successfully able to predict the weak interaction of the leptons and quarks, but is not fully successful in determining the weak interactions of composite hadrons.

After decades of study, knowledge of hadronic interactions is still limited because of the size of strong interactions in hadrons as compared to the size of weak interactions in them. Many theoretical frameworks for weak interactions using meson-exchange potential have been developed after the discovery of pion in 1947/48 [50]. In 1951 Taketani, Nakamura and Sasaki (TNS) proposed the pion exchange model for hadronic interactions for the first time [70]. Since then many meson-exchange models have been proposed but the validity of this meson-exchange description has not yet been established [50]. Experiments are in progress to establish the validity of the description.

The benchmark paper in the field of parity violation was published in 1980 by Desplanques, Donohogue and Holstein (DDH) [30]. They described the weak parity-violating nucleon-nucleon interaction using a meson-exchange potential involving seven weak meson-nucleon coupling constants. In this model, the parity non conserving NN interaction is written as a potential due to the meson(π, ρ, ω) exchange where one meson-nucleon vertex is governed by weak interaction and the other by

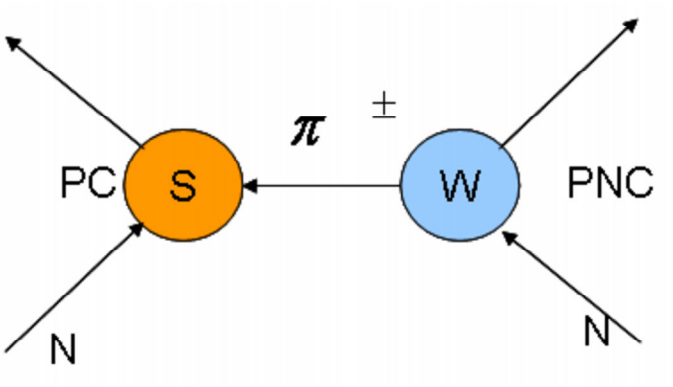

Figure 2.1: Diagram showing the weak and the strong vertex in the nucleon nucleon interaction in the DDH model.

Coefficient	*Equivalent*	*"Best Value"*($\times 10^{-6}$)	*"Reasonable Range"*($\times 10^{-6}$)
F_π	$g_{\pi NN} f_\pi / \sqrt{32}$	1.08	0:2.71
F_0	$-g_\rho h^0_\rho / 2$	1.59	-1.59:4.29
F_1	$-g_\rho h^1_\rho / 2$	0.027	0:0.053
F_2	$-g_\rho h^2_\rho / 2$	1.33	-1.06:1.54
G_0	$-g_\omega h^0_\omega / 2$	0.80	-2.39:4.29
G_1	$-g_\omega h^1_\omega / 2$	0.48	0.32:0.80
H_1	$-g_\rho h'^1_\rho / 4$	0.0	

Table 2.1: Weak coupling constants for the Weinberg-Salam model using the "best value" and "reasonable range" of results of DDH [4].

strong interaction. Figure 2.1 shows the diagram for the DDH model. In this figure, one of the vertices is weak (W), parity non-conserving (PNC), and the other vertex is strong (S), parity conserving (PC). The interaction between the two vertices is mediated by mesons. This meson exchange between nucleons is represented by nucleon nucleon meson exchange couplings in the DDH model.

DDH calculations of the Standard Model estimate of the parity non-conserving nucleon-nucleon meson couplings for this model were based on the Weinberg-Salam model, SU(6) symmetry and known hyperon decay amplitudes. The use of the quark model and the symmetry techniques did not require the precise knowledge of the nuclear wave functions and therefore, this technique overcame some of the challenges that affected some earlier calculations.

DDH provided "reasonable range" values of all the coupling constants in the exchange potential. The reasonable range was calculated taking into account the uncertainties so that any future correction in the model leads to a value within the range. They also provided an estimate of the most likely value from their model. These values are tabulated in table 2.1. The coupling constant h'^1_ρ was not evaluated by DDH and was later considered by Holstein and found to be small and therefore not considered in the DDH values [44].

2.3 Parity Non-Conserving NN Potential

The parity non-conserving nuclear effects take place at the level of nucleon-nucleon (NN) interaction. According to the DDH model as discussed before, there are two types of potentials in the NN interaction: parity conserving (PC) and parity non-conserving (PNC). The parity conserving part represents the strong interaction vertex and the parity non conserving vertex represents the weak interaction. The strong PC NN interaction has been successfully explained at low energies in terms of meson exchange potentials. This description is modified to include the PNC interaction by replacing one of the strong meson-nucleon couplings by a weak coupling. The range of $W^\pm$ and Z^0 is $\approx$0.02 fm [4], much shorter than the distance between nucleons. The hard core repulsion in the NN interaction keeps the nucleons farther apart from the range of weak gauge bosons. The long range weak force between the nucleons is therefore mediated by the exchange of light mesons. Figure 2.2 shows that a weak gauge boson is emitted by a quark from the weak vertex, it travels a short distance and changes to a π, ρ or ω which then couples strongly to another nucleon at the strong vertex. The coupling strengths of the meson exchanges between the vertices are modified by strong interactions of the bound quarks.

The relative strength of the PNC and PC NN interactions is roughly given by $4\pi G_F m_\pi^2/g_{\pi NN}^2 \approx 10^{-7}$ [4], indicating that the PNC effect is much smaller than the PC effect. Therefore, it is valid to introduce the weak interaction as a perturbation to the strong interaction and use the first order perturbation theory to the NN system. The Hamiltonian for the NN system can therefore be split into two terms: a parity conserving strong interaction term (H_S) and a weak parity non conserving potential (V_{PNC})

$$H = H_S + V_{PNC}. \tag{2.1}$$

Here V_{PNC} is the potential generated because of the π, ρ and ω mesons. V_{PNC} is a small perturbation to the system which mixes the parity conserving state ψ with the parity non conserving ϕ,

$$\psi' = \psi + \frac{<\phi|V_{PNC}|\psi>}{\Delta E}. \tag{2.2}$$

The NN potential (V_{PNC}) due to the exchange of π, ρ and ω mesons is given by

$$V_{PNC} = \sum_{\mu=\pi,\rho,\omega} \sum_{\Delta I=0,1,2} H_\mu^{\Delta I} V_\mu^{\Delta I}, \tag{2.3}$$

where V_{PNC} is a linear combination of terms each involving the exchange of a π, ρ or ω meson with a second index describing the isospin exchanged in the weak interaction. For example, $\Delta I = 1$ pion potential has the form

$$V_\pi^1 = \frac{i}{m}[\vec{\tau}_1 \times \vec{\tau}_2]_z(\vec{\sigma}_1 + \vec{\sigma}_2).\vec{u}_\pi(\vec{r}),$$

where m is the nucleon mass and

$$\vec{u}_\pi(\vec{r}) = \left[\vec{p}, \frac{e^{-m_\pi}}{4\pi r}\right],$$

where m_π is the pion mass, $\vec{r} = \vec{r}_1 - \vec{r}_2$ and $\vec{p} = \vec{p}_1 - \vec{p}_2$. The Yukawa function in the term $\vec{u}_\pi(\vec{r})$ gives the dependence of V_π^1 on the distance between the two interacting

nucleons. The exchange of light mesons, e.g. pion, determines the long-range part of the force and therefore, the range of V_π^1 is longer than that of the other weak meson potentials. The exchange of heavy mesons (ρ, ω) generates the short range part of the PNC NN force. The π exchange plays a dominant role in the $\Delta I = 1$ NN interaction. Both ρ and ω exchanges contribute to the $\Delta I = 0$ interaction and $\Delta I = 2$ interaction arises due to ρ exchange [4].

The parity violating asymmetry in a measurement in terms of coupling constant is given as

$$A = f_\pi^1 V_\pi^1 + h_\rho^0 V_\rho^0 + h_\rho^1 V_\rho^1 + h_\rho^2 V_\rho^2 + h_\omega^0 V_\omega^0 + h_\omega^1 V_\omega^1, \tag{2.4}$$

where the coefficients $(V_\mu^{\Delta I})$ are calculated from theory. In the last few decades a significant amount of experimental work has been done to get the values of these coupling constants. The following section discusses the experiments performed after 1980 (after the DDH model) to determine the coupling constants proposed in the DDH theory.

2.4 History and Motivation for the NPDGamma Experiment

The search for parity forbidden transitions has become very active in the last few decades after the benchmark paper of DDH. The weak interaction between nucleons in a nucleus was first observed in 1964 by Abov [2] when a parity violating signal was obtained due to γ-ray emission from a Cd target when it was hit by polarized neutrons. Since then parity violation in NN interaction has become an extensive field of research. Parity non conserving effects are usually studied by observing the transitions which are forbidden by parity conservation or by measuring the correlation between the spins and momenta. The relative strength of the PNC and PC NN interactions is $\approx 10^{-7}$, indicating that the PNC signal will be very small in the exper-

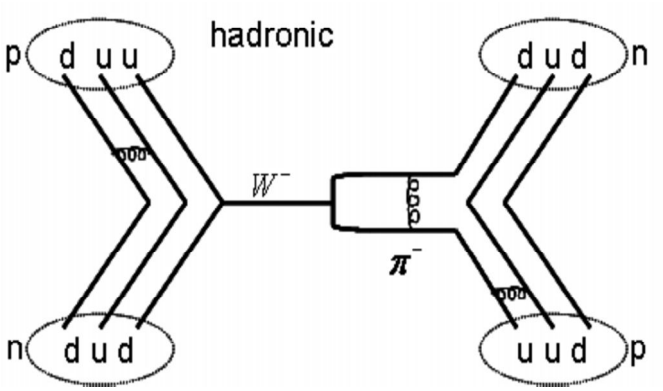

Figure 2.2: The figure shows the interaction between two hadrons and their quark composition. A weak boson is emitted from one nuclei which breaks up into quarks to produce a meson.

iments. Therefore, the important thing to consider in these experiments is to reduce the uncertainties due to the statistical and systematic errors. This section discusses some of the experiments performed in the past towards a better understanding of the weak interaction in the NN system.

2.4.1 History

There are several methods to detect the small signal in the NN interactions. Some of the experiments performed to understand the weak interactions in nucleonic systems and their results are discussed in this section

1. Longitudinal asymmetry measurements: These kind of experiments observe the scattering of a longitudinally polarized proton from an unpolarized target. If there is no parity violation, the scattering cross-section of spin up protons must be equal to the scattering cross sections of spin down protons. The asymmetry is defined as

$$A_L = \frac{\sigma_\uparrow - \sigma_\downarrow}{\sigma_\uparrow + \sigma_\downarrow}. \tag{2.5}$$

Here $\sigma_\uparrow$ is the cross section for scattering of spin up protons and $\sigma_\downarrow$ is the cross section for scattering of spin down protons. A number of experiments in this category, typically with polarized proton beam have been performed. This asymmetry

measures a linear combination of h_ρ^0, h_ρ^1 and h_ρ^2,

$$A_L = -0.028(h_\rho^0 + h_\rho^1 + h_\rho^2/\sqrt{6}). \tag{2.6}$$

For the E497 experiment at TRIUMF A_z was measured to be $(0.86 \pm 0.35) \times 10^{-7}$ [15, 72].

2. The second category of experiment involves a nucleus in an excited state decaying via photon emission to its ground state. Without parity violation in such a decay there will be equal number of right- and left-handed polarized photons. Therefore a non-zero polarization represents parity violation and can be used as a tool to understand hadronic interactions. In terms of coupling constants the circular polarization of photons emitted in the transitions of excited ^{18}F nuclei is,

$$P_\gamma = 4385 f_\pi^1 + 1.016 \times 10^{-4}. \tag{2.7}$$

The quantity has been measured in different experiments [6, 12] with consistent values of P_γ. From these experiments the value of P_γ is obtained to be $P_\gamma = (1.2 \pm 3.9) \times 10^{-4}$.

3. Another technique examines the decay of polarized nuclei's nuclear levels. Parity conservation requires that an equal number of decay products be emitted parallel and antiparallel to the direction of nuclear spin,

$$\text{Decay Prob}(\hat{k}_\gamma.\vec{J} > 0) = \text{Decay Prob}(\hat{k}_\gamma.\vec{J} < 0). \tag{2.8}$$

Such measurements were performed on ^{19}F, ^{180}Hf in the past [5, 47]. A similar experiment performed at Grenoble measured the asymmetry of the outgoing photon in the $n + p \rightarrow d + \gamma$ reaction. The γ-ray asymmetry value obtained from this experiment was [80]

$$A_\gamma = -(4.7 \pm 4.7) \times 10^{-8}. \tag{2.9}$$

4. Another experiment in the category of n-p experiment is the measurement of the spin rotation, ϕ_{PNC}, of polarized cold neutrons when transmitted through a medium. An experiment which will measure the spin rotation in ^{4}He is in progress at National Institute of Science and Technology (NIST) [14]. Polarized cold neutrons are used for this experiment. These polarized neutrons will experience a parity violating spin rotation when they travel through liquid helium due to the weak interactions with an angle proportional to a linear combination of the weak meson exchange amplitudes. In terms of the coupling constants the spin rotation is written as,

$$\phi_{PV}(n,\alpha) = -(0.97 f_\pi + 0.32 h_\rho^0 - 0.11 h_\rho^1 + 0.22 h_\omega^0 - 0.22 h_\omega^1) rad/m. \tag{2.10}$$

5. Anapole moment measurements: Anapole moments are produced due to the interaction of the nucleus with the electrons of the atom. Anapole moments of nuclear ground states are observed using laser spectroscopy on atomic beams. The anapole moment operator is a parity-odd rank one tensor given by

$$\vec{a} = -\pi \int r^2 \vec{J}(\vec{r}) d^3 r. \tag{2.11}$$

where $\vec{J}(\vec{r})$ is the electromagnetic current density operator. Nuclear anapole moments are parity-odd, time reversal-even E1 moments of the electromagnetic current operator. In addition to the exploration of physics of the Standard Model, high precision atomic PNC measurements also provide a different approach for the study of parity violation.

Existence of anapole moment was soon realized after the discovery of parity non conservation in 1958 [86].Recently in 1998 a new level of precision was reached in the atomic anapole by measuring the hyperfine dependence of atomic PNC in ^{133}Cs [81]. For ^{133}Cs, the anapole moment in terms of the coupling constants is written as [34]

$$\kappa_a = 2.0 \times 10^5 (28.2 f_\pi^1 - 7.8 h_\rho^0 - 1.9 h_\rho^1 + 0.5 h_\rho^2 - 4.5 (h_\omega^0 + h_\omega^1). \tag{2.12}$$

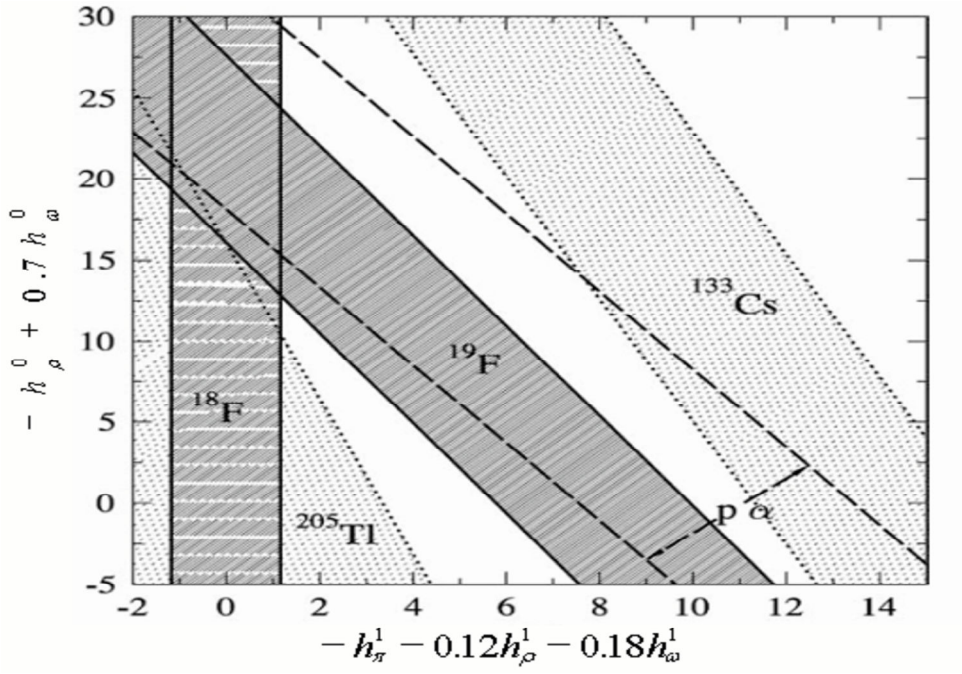

Figure 2.3: Plot showing the coupling constants determined from different experiments in the past [58].

Before the ^{133}Cs experiment anapole moment was performed on ^{205}Tl [74], the relation for ^{205}Tl anapole moment in terms of the coupling constants is [79]

$$\kappa_a = 1.12 \times 10^6 (f_\pi^1 - 3.23 h_\rho^0). \tag{2.13}$$

2.4.2 Motivation for the NPDGamma Experiment

The results obtained from the anapole moment of ^{133}Cs is controversial for two reasons. Firstly, the non-zero measurement of the ^{133}Cs was analyzed by Flambaum and Murray to extract a value of f_π^1 [34]. Their result is two times larger than the DDH value and a factor of seven larger than the limit set by ^{18}F experiments. Secondly, result from the ^{133}Cs are inconsistent with the anapole moment result obtained from an earlier experiment with ^{205}Tl where the anapole moment for the system was measured to be zero [74]. Assuming both the measurements are correct, the results suggest that the nuclear structure effects that were not included in the

analysis may play an important role in interpreting the measurements assuming the measurements are correct.

The nuclear structure affects make it difficult to measure the asymmetry in a large nuclei. Because of this smaller nuclei, few-nucleon systems whose interpretation is free from uncertainties in nuclear structure, are preferred and the coefficients can be calculated directly with small uncertainties.

The NPDGamma experiment was proposed with the idea to resolve the issue of the f_π^1 coupling constant [17]. The experiment uses neutron-proton capture ($n+p \rightarrow d+\gamma$) to measure an asymmetry with simple relation to the weak coupling constant and therefore a clear interpretation of the result. Due to the parity non-conserving part of nuclear forces in the system one expects a circular polarization and a forward-backward asymmetry of the emitted photon for unpolarized and polarized neutrons, respectively. In terms of the coupling constant the asymmetry is

$$A_\gamma = -0.107 f_\pi^1 - 0.001 h_\rho^1 - 0.004 h_\omega^1. \tag{2.14}$$

The asymmetry in the n-p capture will therefore measure f_π^1 as the contribution to asymmetry due to the two other terms is small. The n-p capture is discussed in detail in the next section. NPDGamma experiment finished its first phase at Los Alamos Neutron Science Center (LANSCE) in fall 2006 and has been approved for the (Spallation Neutron Source) SNS beamline.

2.5 The NPDGamma Reaction and Directional Gamma Asymmetry

The intrinsic interest in a clean measurement of f_π^1 in the NN system together with the considerations of experimental feasibility led to the development of the NPDGamma experiment at the LANSCE. The experiment aims to measure the value of A_γ with a goal of achieving $\pm 10\%$ of the DDH predicted value. The NPDGamma

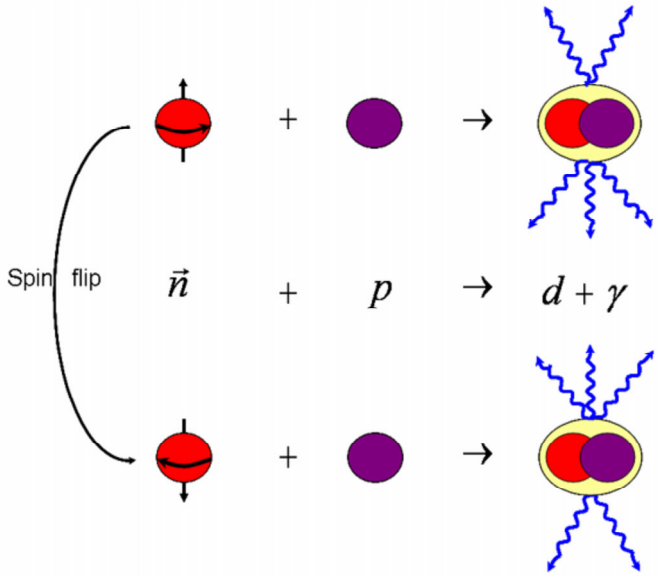

Figure 2.4: Figure showing the capture of a polarized neutron by a proton producing a deuteron and 2.2 MeV gamma-ray for both the spin states. The NPDGamma experiment plan to measure the parity-violating asymmetry in the gamma with respect to the neutron spin.

reaction is the thermal capture of spin polarized neutrons by the protons in a liquid para-hydrogen target. As a result of the capture a deuteron is formed and a 2.2 MeV photon is emitted,

$$\vec{n} + p \rightarrow d + \gamma(2.2MeV). \tag{2.15}$$

The $n + p \rightarrow d + \gamma$ experiment was first performed at ILL in 1977 [20]. This is the simplest internucleon system possible for the study of NN interactions. The study becomes easier because of the absence of the nuclear structure complexities. The goal of the NPDGamma experiment is to measure the parity-violating directional gamma-ray asymmetry in this clean system. This asymmetry is measured in the angular distribution of the 2.2 MeV γ-rays relative to the direction of the neutron spin. Parity is violated if the cross section for photon emission for neutron spin up is different than the emission for neutron spin down. This leads to an asymmetry in the experiment, if any.

Let $d\sigma/d\Omega$ is the probability per unit solid angle Ω for emission of a γ and $\theta_{\vec{s}_n,\vec{k}_\gamma}$ is the angle between the direction of the neutron spin and the emitted photon. The parity non-conserving asymmetry, A_γ, is the coefficient that determines the cosine dependence of $d\sigma/d\Omega$ on $\theta_{\vec{s}_n,\vec{k}_\gamma}$. The cross section for photon emission is given by

$$\frac{d\sigma}{d\Omega} = \frac{1}{4\pi}(1 + A_\gamma \cos\theta_{\vec{s}_n,\vec{k}_\gamma}) \tag{2.16}$$

and

$$\cos\theta_{\vec{s}_n,\vec{k}_\gamma} = \frac{\vec{s}_n.\vec{k}_\gamma}{|\vec{s}_n|.|\vec{k}_\gamma|}. \tag{2.17}$$

As $d\sigma/d\Omega$ is an observable scalar quantity and since $\cos\theta_{\vec{s}_n,\vec{k}_\gamma}$ is reversed by parity transformation, a non-zero A_γ implies the violation of parity. It is impractical to produce a parity transformation of an entire experimental set up. Therefore to perform the parity violating measurement in the NPDGamma experiment direction of the neutron polarization was flipped using a spin flipper. As the proton target is left-right symmetric the neutron spin reversal is equivalent to the interchange of left and right of the incident beam and the target and is therefore equivalent to parity transformation. Under parity transformation the correlation between the neutron spin and the photon momentum is odd as $\vec{s}_n$ does not change sign but $\vec{k}_\gamma$ does (figure 2.5). Therefore, non-zero A_γ will indicate the violation of parity in the reaction. Figure 2.4 shows that the resulting gamma cross-section carries the signature of parity violation if the gamma emission in the angular directions are different for spin up and spin down. The difference in cross section or the measured asymmetry is

$$A_\gamma = \frac{\frac{d\sigma}{d\Omega}(\vec{s_n}.\vec{k_\gamma} > 0) - \frac{d\sigma}{d\Omega}(\vec{s_n}.\vec{k_\gamma} < 0)}{\frac{d\sigma}{d\Omega}(\vec{s_n}.\vec{k_\gamma} > 0) + \frac{d\sigma}{d\Omega}(\vec{s_n}.\vec{k_\gamma} < 0)}. \tag{2.18}$$

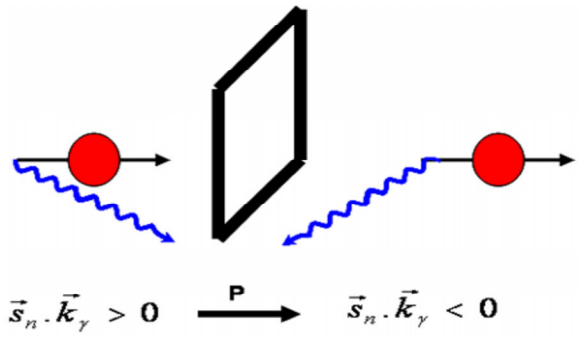

Figure 2.5: Parity violation between the neutron spin and gamma momentum is shown in this figure. Looking at the mirror reflection, the neutron spin remains unchanged but the direction of momentum changes, therefore parity is violated.

2.6 Origin of the Asymmetry in n-p Capture

The cross-section $d\sigma/d\Omega$ is obtained from the transition amplitude of the electromagnetic part of the Hamiltonian between initial and two nucleon states. In the n-p system the unbound system can be expanded in terms of spherical harmonics and is represented by an S wave. Figure 2.6 shows the level diagram for the n-p system. Parity violation arises when the P states mix with the S states. P states that conserve J mix with the S states of the unbound system. The isospin of each state is determined by the rule that wavefunction of two-fermion system is antisymmetric with respect to the particle exchange. For states of two-nucleon system, the sum of the quantum numbers $l + S + I$ must be an odd integer. Therefore, for the $^3S_1$ state of the deuteron $I = 0$ whereas for the $^3S_0$ state $I = 1$ [19]. The transitions from an unbound n-p system to a bound deuteron occurs due to the electromagnetic transitions between the energy levels. The allowed transitions for this system are labeled in figure 2.6. These transitions obey the angular momentum and parity selection rules. E1 transitions are between the states of opposite parity and the M1 transitions are between the states of same parity. All E1 and M1 transitions are labeled in the figure. Also, $\Delta I = 0$ transitions are not allowed for a self conjugate

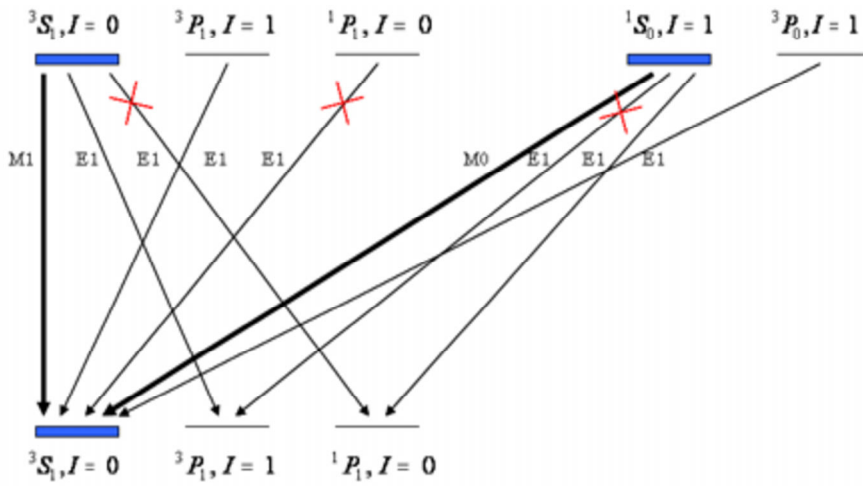

Figure 2.6: Spin and isospin assignments for the bound and low energy continuum levels of the n-p system and the electromagnetic transitions linking the levels. Parity violation in this system is caused by the interference of the E1 and M1 transitions shown. A_γ is caused by the E(1)M(0) interference.

nucleus and therefore those transitions are not taken into consideration. As M1 transitions are between the states of same parity, it is considered to be of positive parity and E1 transitions are considered to be of negative parity as they are between the states of opposite parity. The interference of these two opposite parity transitions or M1-E1 interference leads to the parity violating asymmetry in the n-p system.

The parity violating parameters for this system can be obtained by using these transitions. For a neutron beam polarized along the z-axis the differential cross section in terms of $E1$ and $M1$ is given by

$$\frac{d\sigma}{d\Omega} \propto \frac{1}{4\pi}\left(1 - 2\sqrt{2}\frac{< E1 >}{< M1 >}\cos\theta_{\vec{s}_n,\vec{k}_\gamma}\right), \tag{2.19}$$

where $\theta_{\vec{s}_n,\vec{k}_\gamma}$ is the angle between the neutron polarization and momentum of the outgoing photon and

$$A_\gamma = -2\sqrt{2}\frac{< E1 >}{< M1 >}. \tag{2.20}$$

The relation between A_γ and the coupling constant $f_\pi^{\Delta I=1}$ was calculated by several

groups and is given to be [37, 62],

$$A_\gamma \approx -0.107 f_\pi^{\Delta I=1}. \tag{2.21}$$

In the NPDGamma experiment A_γ was measured by measuring the cross section for each spin direction of the neutrons (equation 2.18). This measured value is used to calculate the value of the coupling constant $f_\pi^{\Delta I=1}$ using equation 2.21.

As mentioned before, only one experiment was performed before the NPDGamma experiment to measure $f_\pi^{\Delta I=1}$ using the n-p system where the gamma asymmetry was obtained to be $A_\gamma = (6 \pm 21) \times 10^{-8}$. NPDGamma experiment is the second experiment which aims to measure $f_\pi^{\Delta I=1}$ using the n-p system. As the signal obtained is very small because of the dominant strong interaction the experiment needs a very high statistics and also the systematics have to be reduced. The NPDGamma experiment finished its first run at Los Alamos National Laboratory in Fall 2006 and the analysis is in progress. The experiment has been moved to Spallation Neutron Source at Oak Ridge National Laboratory where it plans to take advantage of the higher neutron flux.

CHAPTER III

The NPDGamma Experiment

The NPDGamma, $\vec{n} + p \rightarrow d + \gamma$, experiment at the LANSCE aimed to measure the parity-violating directional asymmetry in the $\vec{n} + p \rightarrow d + \gamma$ reaction to 0.1 level of A_γ. It was performed on Flight Path 12 (FP12) at the Manuel Lujan Jr. Neutron Scattering Center (Lujan center) of the Los Alamos Neutron Science Center (LANSCE). FP12 at Lujan center is the only currently operating neutron beamline in the US dedicated to fundamental neutron physics where neutrons are produced from a 20 Hz pulsed neutron source. To reach the proposed sensitivity it is important to have the high counting rate provided by the high flux neutron beam.

Figure 3.1 shows a schematic of the experimental set up of the NPDGamma experiment. The experiment was enclosed in a 10 Gauss magnetic field. Magnetic field was required for the polarization and transportation of the neutrons downstream of the polarizer. The unpolarized neutrons from the source pass through the ^{3}He polarizer and become transversely polarized. A radio frequency spin flipper (RFSF) which can flip the neutron spin on a pulse to pulse basis was also installed in the neutron beam path . After the spin flipper, the neutrons enter a 16 L liquid H_2 target where neutrons were captured by the H_2 target due to the n-p capture, $\vec{n}+d \rightarrow d+\gamma$. The 2.2 MeV γ-rays from this capture reaction were detected by an array of 48

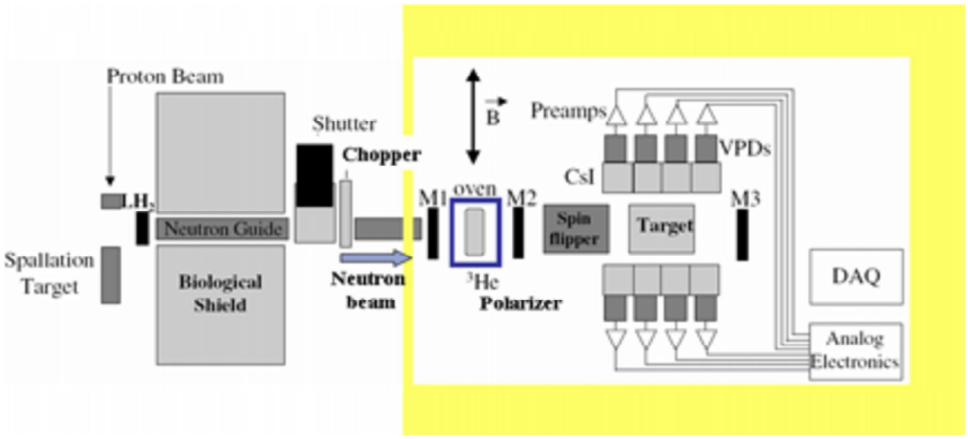

Figure 3.1: Experimental set up for the NPDGamma experiment. Proton beam hit the spallation target producing neutrons. Neutrons were transported to the experiment using a supermirror neutron guide. A chopper was installed in the flight path to select the correct wavelength neutrons. Outer box in the figure is the experimental cave. The experiment was enclosed in a magnetic field of 10 Gauss. The position of the monitors, polarizer, spin flipper, LH_2 target and the detectors are shown in the figure.

CsI detectors. There were three neutron detectors (also called monitors) placed at different positions along the beamline as shown in figure 3.1. These monitors were used to monitor the incident neutron beam intensity, neutron polarization, the spin flipper efficiency and the ortho-para ratio of the liquid hydrogen target.

This chapter gives a description of the components of the NPDGamma experiment. As the dissertation is more focused on neutron polarization, the chapter will have a detailed discussion of ^{3}He polarizers and the polarization analysis for the NPDGamma experiment.

The NPDGamma experiment took its final set of data with LH_2 at LANSCE in the Fall of 2006 and has been moved to Spallation Neutron Source (SNS) at Oak Ridge National Laboratory (ORNL) for another set of runs with higher sensitivity at the higher neutron flux at SNS.

3.1 The Flight Path and the Frame Overlap Chopper

The pulsed neutron beam at FP12 is produced by spallation when 800 MeV protons from a proton storage ring are incident on a Tungsten target at 20 Hz. The protons are first accelerated using the linear accelerator and then they enter the storage ring to be compressed in time to hit the tungsten target. The neutron flux incident on the experiment depends on the proton current and the energy delivered to the target. The neutrons are then thermalized in a 12 x 12 cm^2 hydrogen moderator kept at a temperature of 20 K. The neutrons are transported to the experiment using a supermirror neutron guide [64].

A neutron guide uses the concept of total internal reflection for a range of angles up to the critical angle. In a neutron guide the neutrons are reflected about twice or thrice until they reach the experiment. The maximum glancing angle, or the critical angle, at which total internal reflection occurs is

$$\theta_c = m\theta_c(^{58}Ni), \tag{3.1}$$

where $\theta_c(^{58}Ni)$ is the critical angle of the natural nickel and m is the ratio of the effective critical angle of the supermirror to that of natural nickel [31]. The FP12 neutron guide is made of several layers of ^{58}Ni and ^{47}Ti with m=3 and 9.5×9.5 cm^2 in cross section.

A picture of the flight path is shown in figure 3.2. The length of the flight path was calculated to be 21.123 $\pm$ 0.032 m using the Bragg edge technique [29]. The pulsed neutron beam was transmitted through a beryllium block and the time of flight spectrum was recorded. For Be the Bragg edges are at 3.483 $\mathring{A}$, 3.957 $\mathring{A}$ and 3.98 $\mathring{A}$. The length of the flight path was calculated by comparing the known Be Bragg edges with the time of flight spectrum. As the neutron beam was pulsed, we

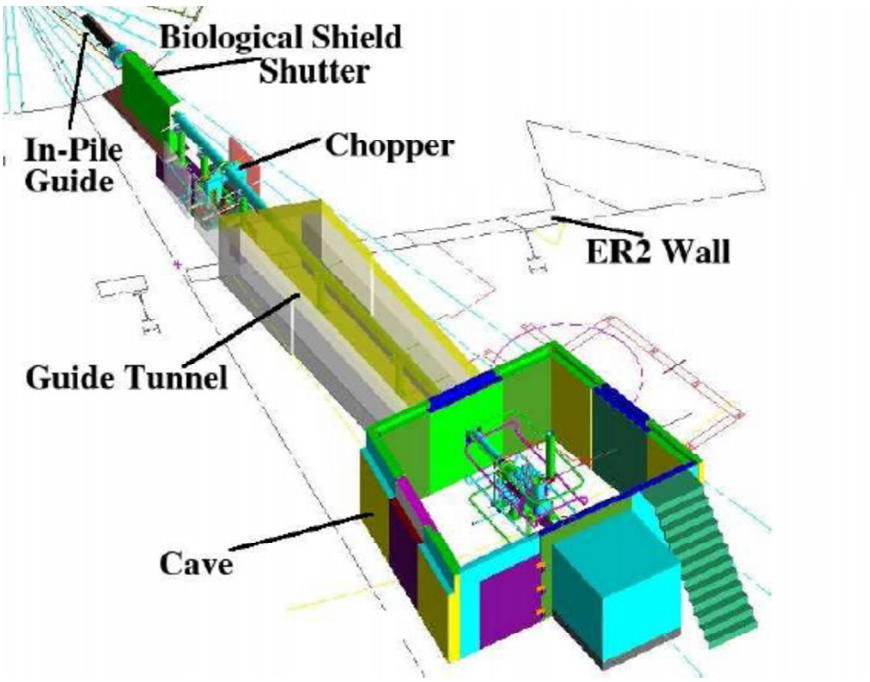

Figure 3.2: An overview of the flight path 12. The figure shows the location of the chopper in the flight path. The area indicated as "Cave" is the area where the experiment was carried out [37].

were able to measure the time of flight of the neutrons accurately and thus we knew the velocity of the neutrons we were working with. Velocity range for the neutrons was selected using a chopper installed in the flight path before the neutrons enter the experimental area (seen in figure 3.2).

Frame overlap chopper is a device which selects a desired wavelength or the velocity range in the neutron time of flight (tof) spectrum for an experiment. It prevents the overlap of slow neutrons of a previous pulse with fast neutrons of the next pulse. Neutrons with energy less than 1 meV are stopped by the chopper located between the moderator and the experiment.

The chopper had two blades which were able to rotate independently up to 1200 rpm and was located at a distance of 9.38m from the surface of the H_2 moderator[37]. When either one or both blades covered the neutron beam opening, the slow neutrons at the tail end of the neutron spectrum were blocked, thus stopping the overlap of

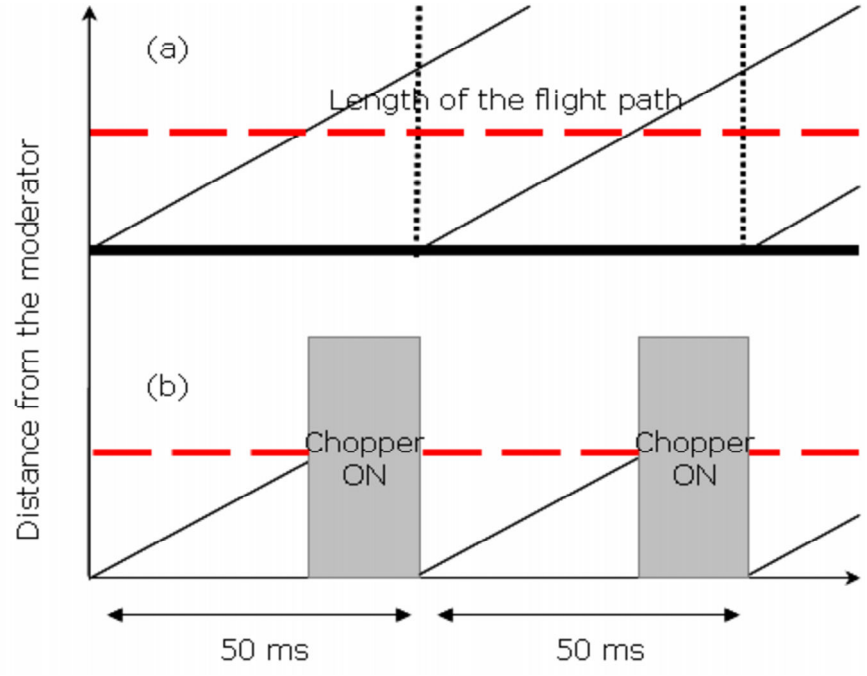

Figure 3.3: Diagram explaining the functioning of a chopper. The dashed lines indicate the point where the neutrons are needed. Y axis is the length of the flight path and X axis is time of flight. When there is no chopper, neutrons from two different pulses can interfere (a) but when the chopper is on it cuts off the slow neutrons from the pulse and prevent them from reaching the next pulse (b).

fast neutrons from the penultimate pulse with the slow neutrons in the previous pulse. The functioning of a chopper is shown in figure 3.3. When the chopper is not present, neutrons with all wavelengths pass through and thus are confused with the neutrons from the previous pulse (figure 3.3(a)). But when the chopper is on, these undesired neutrons from each pulse are blocked (figure 3.3(b)). Difference between the neutron time of flight spectrum when the chopper is working and when it is not is shown in figure 3.4. As can be seen from the figure, the tail of neutrons is removed by the use of chopper which otherwise interfere with the next pulse.

3.2 Monitors

The experiment used three neutron detectors (also called monitors) at different positions in the beamline for monitoring the neutron transmission through various

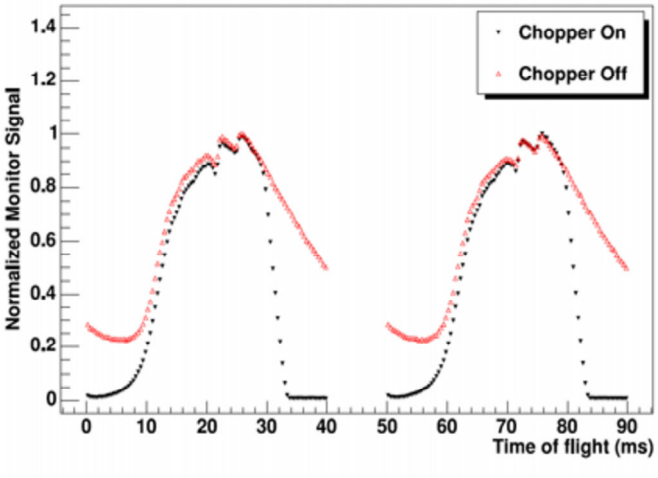

Figure 3.4: M1 spectrum of two pulses for chopper on and chopper off state. The red curve is for chopper off and black curve is for chopper on. When the chopper is functioning it chops off the tail neutrons and prevent them from interfering with the next pulse.

components of the experiment. The position of the three monitors can be seen in figure 3.1. Monitors used in the NPDGamma experiment were parallel plate ion chamber with an active area of 12 x 12 cm^2. Each monitor had three 0.5 mm thick Aluminium electrodes. The two outer electrodes were provided with -5 kV and the neutron current signal was obtained from the central electrode. The schematic of the monitor is shown in figure 3.5.

The monitors were held at a pressure of 1 atm and are filled with 50% He, both ^{3}He and ^{4}He, and 50% N_2. The thickness of a monitor depends on the ratio of ^{3}He to ^{4}He. The first two monitors, which were thin, contained mostly ^{4}He with a very small fraction of ^{3}He, less than 3% and therefore absorbing about 3% of the neutron beam at 10 meV The ^{3}He thickness was measured to be $(1.01\pm0.07)\times10^{18}$ cm^{-2} for M1 and $(0.99\pm0.07)\times10^{18}$ cm^{-2} for M2 [39]. The thick monitor, the third monitor, contained 50% of ^{3}He and absorbed almost 40% of the neutron beam at 10 meV. When neutrons are captured by ^{3}He in the monitors due to the capture reaction n+^{3}He$\rightarrow$^{1}H+^{3}H+764 keV, 764 keV energy is also released. This energy causes ionization of N_2 inside the

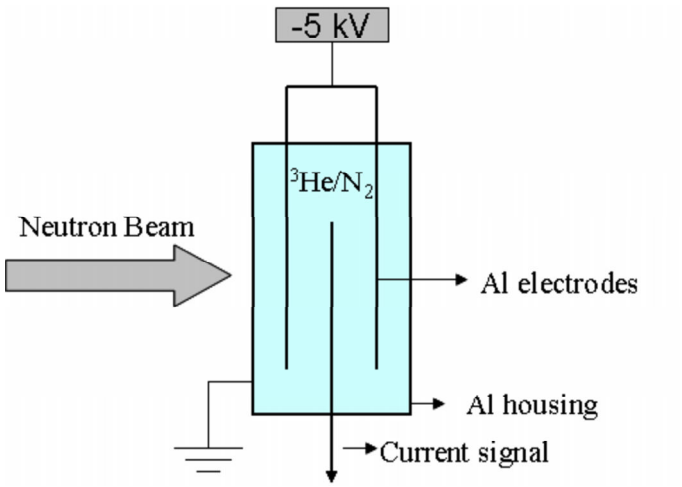

Figure 3.5: Schematics of a monitor is shown in the figure. ^{3}He, ^{4}He and N_2 gases are enclosed in a Al housing. The neutron causes ionization of N_2 inside the monitor due to the energy emitted in the capture reaction n+^{3}He$\rightarrow^1$H+^{3}H+764 keV and these ions are collected by the central electrode which is converted to voltage.

monitor. These ions are collected by the central electrode and the current signal is obtained. Therefore, the current signal is proportional to the incident neutron flux and hence also an indirect measurement of the varying neutron flux. A photograph of the monitor used in the experiment is shown in figure 3.6.

3.3 The Polarizer

There are two types of neutron polarizers: supermirror polarizers and ^{3}He polarizers. Both the types are discussed in this section. For the NPDGamma experiment, we used the ^{3}He polarizers, therefore they will be discussed in more detail.

3.3.1 Supermirrors

A supermirror polarizer is made of ferromagnetic material and is based on the reflection of neutrons from a ferromagnetic surface. For a ferromagnetic material the refractive index is

$$n_{\pm} = 1 - \frac{\lambda^2 N(b_{coh} \pm p)}{2\pi}, \tag{3.2}$$

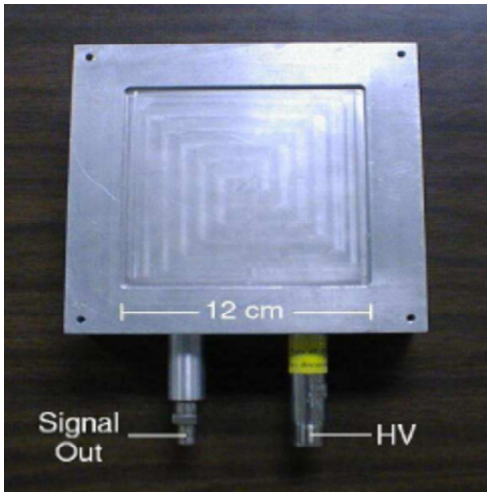

Figure 3.6: A photograph of one of the monitors used for the experiment.

where n_+ and n_- is the refractive index for neutrons whose moments are aligned parallel and antiparallel to the magnetic field, respectively, b_{coh} is the mean coherent scattering length, and p is the magnetic scattering length

$$p = \frac{2\mu(B - H)m\pi}{h^2 N}, \tag{3.3}$$

where m is the neutron mass, μ is the magnetic moment and B is the magnetic induction in an applied field H. Thus, the refractive index of the material is different for spin up neutrons and spin down neutrons giving rise to two critical angles of total reflection γ_+ and γ_-. Reflections at an angle between these two critical angles will produce a polarized beam [31].

A new technique in using the supermirrors for neutron polarization is the crossed supermirror polarizer. The crossed supermirror polarizer was recently developed in ILL to overcome the limitations of single supermirror polarizer[48]. Neutron polarization obtained by the use of single polarizer is limited by angular and wavelength dependence of polarization across the beam phase space. With a set of crossed supermirrors, polarization was measured up to 99.7% over the range of 3-7 $\AA$ using ^{3}He spin filter as analyzer.

3.3.2 ^{3}He Polarizer

The use of polarized ^{3}He gas targets as neutron polarizers provide a promising technique for absolute neutron beam polarization measurement first demonstrated by Coulter et al.[28]. Polarized ^{3}He can be used as a nearly perfect neutron spin filter as it has a very large spin dependent cross section for neutron capture. There are both elastic and inelastic scattering channels available for the neutrons on ^{3}He. The two available inelastic channels where neutrons interact with ^{3}He are:

$$n +^3 He \rightarrow^3 H + p \tag{3.4}$$

$$n +^3 He \rightarrow^4 He + \gamma. \tag{3.5}$$

The absorption cross sections for both the reactions obey the $1/v$ law which means:

$$\sigma = \sigma_0 \frac{v_0}{v} = \sigma_0 \frac{\lambda}{\lambda_0}, \tag{3.6}$$

where σ_0 is the absorbtion cross section for neutrons at wavelength λ_0. For equation 3.5, the reaction cross section is 54 barns at 1.8 $\mathring{A}$. But, equation 3.4 has a high cross section of 5333 ± 7 barns at 1.8 $\mathring{A}$ [7], due to the presence of a broad $J^\pi = 0^+$ excited state of the ^{4}He compound nucleus and as this resonance is open only in the 0^+ channel, the cross section is very spin dependent and is dominated by the absorption of neutrons with spin anti-parallel to the ^{3}He polarization. Therefore, an unpolarized beam of neutrons incident on a target of polarized ^{3}He emerges parallel to the target polarization.

To understand the spin dependence of equation 3.4, lets consider the low energy regime where only $l = 0$ partial waves contribute . For a spin $\frac{1}{2}$ target we have singlet and triplet states. Let σ_s and σ_t be the cross section for these two states. If I is the

spin of the target, the spin independent cross section, σ_{Re}, for the target is [60]

$$\sigma_{Re} = \frac{I+1}{2I+1}\sigma_t + \frac{I}{2I+1}\sigma_s. \tag{3.7}$$

For a particular spin state the cross section, σ_P, is given by,

$$\sigma_P = \frac{I}{2I+1}(\sigma_s - \sigma_t) \tag{3.8}$$

and if P_T is the target polarization the experimental cross sections for neutrons and target spins parallel(+) or antiparallel(-) is,

$$\sigma_+ = \sigma_{Re} \mp P_T\sigma_P. \tag{3.9}$$

If the target polarization is 100%, for I=1/2,

$$\begin{aligned} \sigma_{Re} &= \frac{3}{4}\sigma_t + \frac{1}{4}\sigma_s \\ \sigma_P &= \frac{1}{4}(\sigma_s - \sigma_t). \end{aligned} \tag{3.10}$$

For the case of ^{3}He, $\frac{\sigma_P}{\sigma_{Re}} = 1.010 \pm 0.032$ [55], and therefore

$$\sigma_+ = 0, \sigma_- = 2\sigma_{Re}. \tag{3.11}$$

Thus, if the ^{3}He target is 100% polarized, all the neutrons which have the same spin as the target will pass through and the neutrons with spin antiparallel to the target will get absorbed with an absorption cross section of σ_-. Thus, ^{3}He targets with 100% polarization are ideal neutron polarizers, but 100% is practically not achievable because of experimental limitations.

The transmission of unpolarized neutrons through a ^{3}He spin filter cell with neutron spins parallel and anti-parallel to the ^{3}He spins is

$$t_+ = \exp(-nl\sigma_a(1 \mp P_{He})), \tag{3.12}$$

where t_+ is the transmission of neutron spins aligned parallel to the ^{3}He spins and t_- is the transmission of neutron spins aligned anti-parallel to the ^{3}He spins, P_{He} is the ^{3}He polarization, l is the target length, n is the number density of ^{3}He, and $\sigma_a = \frac{\sigma_0 \lambda}{\lambda_0}$ is the wavelength dependent absorption cross section. Therefore, the neutron transmission through an unpolarized cell (P_{He}=0)is

$$T_0 = \exp(-nl\sigma_a). \tag{3.13}$$

The neutron transmission through a polarized ^{3}He spin filter ($P_{He} \neq 0$) is

$$T_P = \frac{t_+ + t_-}{2} = \exp(-nl\sigma_a)\cosh(nl\sigma_a P_{He}) = T_0 \cosh(nl\sigma_a P_{He}) \tag{3.14}$$

and neutron polarization of the transmitted beam, P_n, is

$$P_n = \frac{t_+ - t_-}{t_+ + t_-} = \tanh(nl\sigma_a P_{He}) = \sqrt{1 - \frac{T_0^2}{T_P^2}}. \tag{3.15}$$

For the NPDGamma experiment ^{3}He spin filter was chosen over supermirror neutron polarizers because of the following reasons:

- Spin of ^{3}He can be quickly reversed with respect to the static magnetic field which is of great value in reducing the systematic errors associated with the experiment. But, in supermirrors as it is a magnetic device the static magnetic field has to be reversed to reverse the neutron polarization.
- A supermirror requires an analyzer to measure the polarization but for ^{3}He polarizers polarization can be measured using the transmission ratio method described above.

3.4 Optical pumping and ^{3}He Polarization

There are two techniques to produce polarized ^{3}He: spin exchange optical pumping (SEOP) and metastablity-exchange optical pumping (MEOP). MEOP was first

observed in 1962 when Colgrove *et al.* demonstrated optical pumping of metastable $^1S_0$ helium in a discharge and thus the possibility of polarizing ^{3}He gas via metastablity exchange between a polarized metastable ^{3}He and a ground state ^{3}He [78]. MEOP polarizes pure ^{3}He at low pressure typically 1 mbar, at rates of about 1 std-liter/hour with ^{3}He polarizations of 70% or more [56]. MEOP polarizer stations compress the ^{3}He into cells and are transported to the point of use where the ^{3}He polarization decays very slowly, with a time constant that can be a week or longer. In SEOP, the ^{3}He cell is polarized by the hyperfine interaction during collisions of the ^{3}He nuclei with polarized valence electrons of optically pumped alkali-metals. For applications that require several days or weeks of stable polarization operation, such as targets for electron scattering, neutron scattering experiments and long running fundamental neutron physics experiment (e.g. NPDGamma Experiment), it is practical to have a SEOP system pumping continuously with stable polarization for weeks or months.

For the NPDGamma experiment ^{3}He was polarized by spin exchange with laser polarized rubidium. Spin-exchange from optically pumped Rb vapor was discovered by Bouchiat *et al.* in 1960 [16]. The spin exchange is mediated by the hyperfine interaction of the Rb outer shell electron with the ^{3}He nucleus during the binary collisions time, order of 10^{-12} seconds [25]. The rate equation which governs the evolution of ^{3}He polarization is

$$\left[\frac{\Gamma}{2}+\gamma_{SE}\rho_A\left(+\frac{1}{2}\right)\right]\rho\left(-\frac{1}{2}\right)-\left[\frac{\Gamma}{2}+\gamma_{SE}\rho_A\left(-\frac{1}{2}\right)\right]\rho\left(+\frac{1}{2}\right)=\frac{d}{dt}\rho\left(+\frac{1}{2}\right), \tag{3.16}$$

where $\rho\left(\pm\frac{1}{2}\right)$ are the occupation probabilities for $m_S=\pm\frac{1}{2}$ states in ^{3}He and Γ is the relaxation rate for ^{3}He in the absence of Rb due to the dipole-dipole relaxation, wall relaxation, relaxation from diffusion through magnetic field gradients and other mechanisms. For the ^{3}He polarization rate to be much higher than the wall relaxation

rates target-cell wall material has to be chosen carefully, and high density of Rb is needed. A small amount of nitrogen buffer gas is added to the cells to suppress radiation trapping [22] The time evolution of ^{3}He polarization is

$$\begin{aligned} P_{He}(t) &= \rho\left(+\frac{1}{2}\right) - \rho\left(-\frac{1}{2}\right) \\ &= \frac{\gamma_{SE} P_{Rb}}{\gamma_{SE}+\Gamma}(1 - e^{-(\gamma_{SE}+\Gamma)t}). \end{aligned} \tag{3.17}$$

Here P_{Rb} is the Rubidium polarization and $\gamma_{SE} = k_{SE} n_{Rb}$ is the spin exchange rate per atom of ^{3}He, $k_{SE} =< \sigma_{SE} v >$ is the velocity averaged rate constant and n_{Rb} is the Rubidium number density. Γ is the intrinsic cell relaxation rate due to the combined contributions of dipole-dipole relaxation [54], wall relaxation [61] and other mechanisms [11]. Cell temperature is a complicated variable which affects wall relaxation, diffusion, Rb-Rb collisions [77] and absorption of laser light [87]. And, Rb polarization P_{Rb} is

$$P_{Rb}(\vec{r}) = \int_{cell} \frac{\gamma(\vec{r})}{\gamma_{opt}(\vec{r}) + \Gamma_{SD}(\vec{r})} d^3 r, \tag{3.18}$$

$\gamma_{opt}(\vec{r})$is the position dependent convolution of the laser intensity and photon absorption cross section and Γ_{SD} is the spin-destruction rate per rubidium atom, it is dominated by the Rb-Rb collisions with contributions from Rb-^{3}He and Rb-N_2 collisions. The spin destruction is stronger near the walls of the cell due to diffusion [76].

The principal of optical pumping for Rb is illustrated in figure 3.7. For Rb in ground state $j = \frac{1}{2}$, the two states are $S_{1/2}$ and $P_{1/2}$ each with two magnetic substates $m_S = \pm\frac{1}{2}$. Circularly polarized light with magnetic projection $+1(\sigma_+)$ is incident on the system and is only absorbed by $S_{1/2}$ with $m_S = -\frac{1}{2}$ state and it populates $P_{1/2}$ state with $m_S = +\frac{1}{2}$ which can decay to either sublevel of the ground state. The Clebsch Gordon coefficient for the two transitions $P_{1/2}, m_S = 1/2 \rightarrow S_{1/2}, m_S = -1/2$

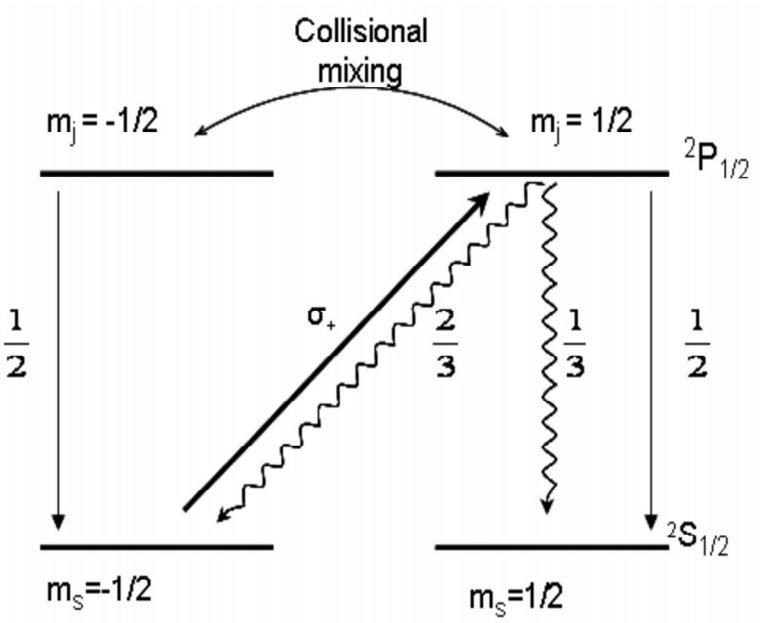

Figure 3.7: Illustration of optical pumping in Rb levels with the nuclear spin neglected. The wavy lines are the radiative decay without the buffer gas and the lines correspond to the presence of buffer gas.

and $P_{1/2}, m_S = 1/2 \rightarrow S_{1/2}, m_S = 1/2$ are 2/3 and 1/3, respectively. The buffer gas, (N_2) collisions randomize the P states changing the relative decay rates to each sublevel of the ground state to 1/2. Thus all the electrons move to one state and Rb gets polarized. The polarized Rb interacts with ^{3}He nucleus via hyperfine interaction and transfers its spin to ^{3}He making ^{3}He polarized.

3.5 Experimental Set Up for the Polarizer

3.5.1 ^{3}He Polarizer Cells

The cells used in the NPDGamma experiment were made at National Institute of Standards and Technology (NIST), Maryland. These cells had an inside diameter of about 10 cm or greater and length of about 5 cm. Boron free alumino-silicate GE180 was used to make these cells as ^{10}B has a very high absorption cross section for neutrons, $\sigma = 38376$ barns at 1.8 $\AA$ [53] and natural boron has 19.9% of ^{10}B. GE180 was used to make these cells because of its high neutron transmission. The neutron

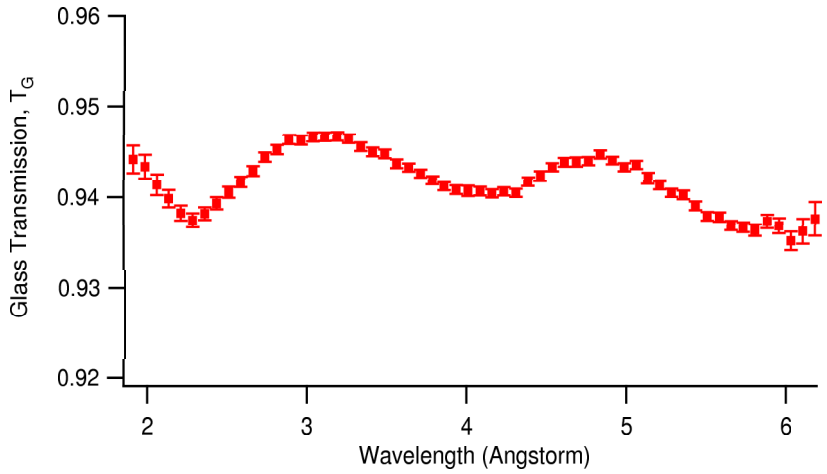

Figure 3.8: Transmission of neutrons through a 3.5 mm thick piece of GE180 glass.

transmission through a 3.5 mm thick piece of GE180 glass over the wavelength range important for the NPDGamma experiment is shown in figure 3.8. The wavelength dependence of the neutron transmission through GE180 is relatively flat. The average transmission through the cell is ≈94%. These cells were blown from glass melted from 15 mm stock tubing [59]. A cell is attached to the glass manifold and a Rb ampoule is placed in the side arm. The cell was baked for at least 48 hours at 400 ^{0}C to a base vacuum below 10^{-7} mbar. Then it was filled with 67 mbar of N_2 followed by about 800 mbar of ^{3}He and then sealed at a pull off with a torch. Table 3.1 shows a list of cells made for the NPDGamma experiment. The table also indicates the diameter, volume, thickness, lifetime and maximum polarization attained for the respective cells. A broadband laser system was used to produce the polarization values shown in the table and were measured by transmission measurements on the NG6M monochromatic beam line at the NIST.

3.5.2 Cell Heating and Temperature Control

The ^{3}He cell used in the NPDGamma experiment was mounted in a box made of heat stabilized nylon (MC901 from GE Polymer Shapes) which acted as the oven for

cell name	diameter (cm)	volume (cm^3)	thickness ($10^{20} cm^{-2}$)	lifetime (hours)	$Maximum P_3$ ($\pm 5\%$) (%)
Astro	11.3	640	1.4	730	58
Pebbles	11.1	508	1.1	350	61
Dino	10.6	452	1.2	700	61
BooBoo	12.6	587	1.4	520	55
Kirk	10.5	624	1.5	600	
Rocky	13.4	773	1.2	100	
Elroy	11.0	430	1.0	100	

Table 3.1: Cells made at NIST for the $n + p \rightarrow d + \gamma$ experiment. Maximum ^{3}He polarization improves with longer lifetimes. The ^{3}He polarization values were measured using a monochromatic neutron beam at NIST [26].

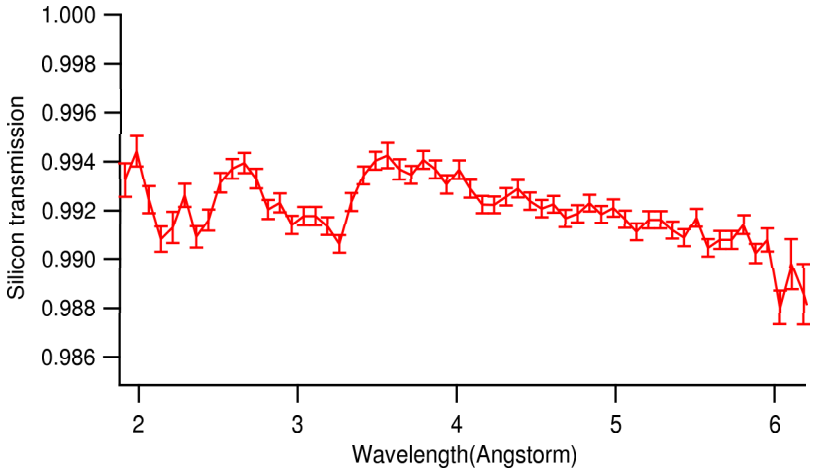

Figure 3.9: Neutron transmission through four silicon wafers. Silicon wafers were used upstream and downstream of the polarizer because of its high neutron transmission.

the system. The box was 33 cm wide × 30 cm deep × 26 cm high and had the ability to maintain the cell at 140-165 ^{0}C . For maximum neutron transmission through the oven, silicon wafers were used upstream and downstream of the oven. The neutron beam passes through pairs of 0.2 mm thick and 15 cm in diameter single crystal silicon wafers both upstream and downstream of the polarizer cell. Si wafers have a good transmission for neutrons, shown in figure 3.9. The average transmission through four pieces of silicon wafers in our wavelength range is ≈0.99%.

To heat the oven to the desired temperature hot air hoses were provided. This air used to flow through two 750 W in-line air heater in series. One of the air heaters

was located inside the shielded cave and it used to provide a constant power. The second heater was located outside the cave, controlled with a proportional-integral-derivative controller (PID controller). The temperature required for the cell was selected in this PID controller and was modulated here to maintain the selected process temperature within a few degrees, ± 5 ^{0}C. This controlled air heater was placed outside the cave, the experimental area, to minimize any noise or pick-up of control signals by the detector or the data acquisition system. The temperature in the cells was monitored using a thermocouple temperature sensor. The sensor was mounted on the cell to get the actual temperature on the cell surface.

The initial design of the oven is shown in figure 3.10, where the cell was held from the sides with teflon screws, and the cell center was aligned with the neutron beam center. During the commissioning period of the NPDGamma experiment it was observed that the cell was drooping down with time and therefore leading to the misalignment of the cell with respect to rest of the experiment. To overcome this problem a new oven was designed. A picture of the new oven is shown in figure 3.11. In this new design, the polarizer cell was held from both top and bottom inside a 0.7 mm thick glass cylinder, making the position of the cell very rigid. This design proved helpful in solving the problem of cell misalignment.

3.5.3 Lasers and Optics

Coherent FAP (Fiber Array Package) systems were used to provide the laser light to the neutron spin-filter system. FAP systems were selected because they are considered to be stable robust light sources that could run for months without major adjustments. The FAP systems provide light from a fiber-optic bundle coupled to a system of lenses to provide a roughly rectangular "spot" on the cell. The unpolarized light from the fiber passes through a polarizing beam splitter producing two linearly

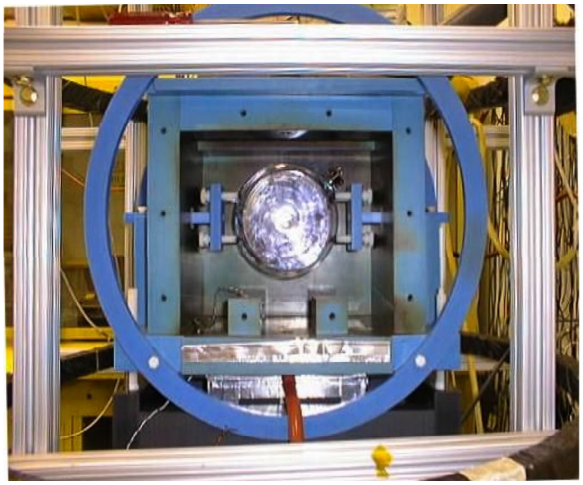

Figure 3.10: Old oven which was used during the commissioning period of the experiment. As there was no support from the bottom, the cell was drooping down with time.

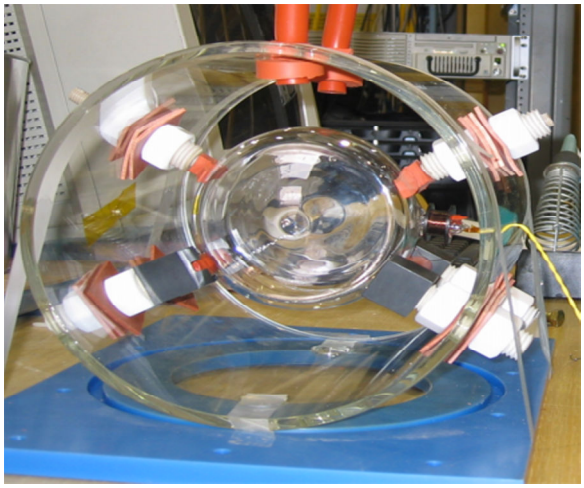

Figure 3.11: The new oven which was built to solve the drooping problem in the oven in figure 3.10. This oven holds the cell rigidly from top and bottom preventing the cell from moving.

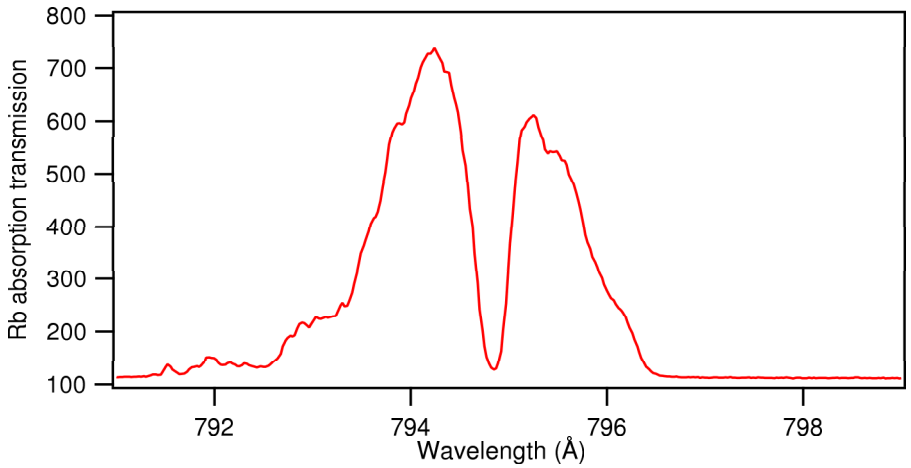

Figure 3.12: Transmission spectrum of 795 nm laser light passing through polarizer cell. The dip at 795 nm is due to Rb absorption.

polarized beams. Each of these two beams then passes through a $\lambda/4$ plate producing two circularly polarized beams polarized in the same direction. They then overlap at the cell, about 1 m away from the cell. The direction of the ^{3}He polarization, either in the direction of the magnetic field or opposite, depends on the orientation of the $\lambda/4$ plates. To change the direction of ^{3}He polarization in the experiment the orientation of these $\lambda/4$ plates were changed.

Laser light needed to polarize Rb and therefore to polarize ^{3}He was initially provided by two fiber coupled 30 W Coherent FAP systems tuned at 795 nm (D1 wavelength of Rb), when the experiment was run with the test targets. The laser light used to pass through the cell from the top and bottom of the cell. One laser beam pair was incident from above and one was incident from below the cell. Before starting the experiment with the LH_2 target, one more laser was added to the experiment to reach higher polarization. The laser light from the first two lasers were coupled and they used to be incident on the cell from above and the light from the third laser used to be incident on the cell from the bottom. The laser power and wavelength for these lasers were monitored using a power meter and a spectrometer respectively.

Figure 3.12 shows the laser light transmission through an optically pumped ^{3}He cell. The plot shows the dip at 795 nm confirming Rb was absorbing the light at the right wavelength.

3.6 Polarization monitoring

3.6.1 Using Monitors

Monitors were placed at different positions in the experiment to monitor the neutron flux, neutron transmission through the various components of the experiment, neutron polarization etc. with time. Signals obtained from the first two monitors in the experiment, one upstream (M1) and one downstream (M2) of the polarizer were used for the polarization analysis. M1 sees the neutron beam directly coming from the neutron source and is a good measure of the incident neutron flux. The data from M1 is therefore used to normalize the data recorded at M2 (after the polarizer) for every run. From equation 3.15, the neutron polarization determination depends on the transmission through the spin filter when it is polarized and when it is unpolarized. Thus, with these two measurements neutron polarization in the experiment can be monitored with time. Details of the analysis are presented in section 3.9. In the NPDGamma experiment we were taking data from these monitors in real time and therefore, were able to monitor the neutron polarization in the experiment continuously.

3.6.2 NMR Monitoring

The polarizer was instrumented with pulsed and adiabatic fast passage (AFP) NMR for diagnostics, monitoring of ^{3}He polarization with time and to reverse the ^{3}He spin. For pulsed NMR, a small 2.5 cm diameter pick-up coil was used which probed only a small fraction of the cell volume. This coil was mounted on the small

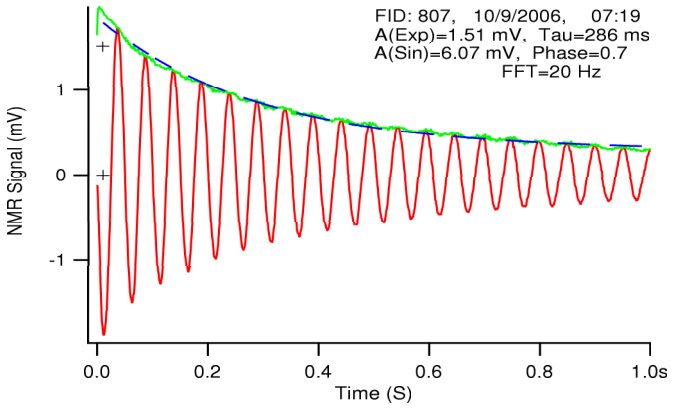

Figure 3.13: NMR signal is picked up by the pick up coil placed on the cell. The amplitude of the signal is an indirect measure of ^{3}He polarization in the cells.

protrusion coming out of the side of the cell. The pulsed NMR circuitry switched the coil from the excitation pulse to the read out electronics. Pulse angles of a few degrees were sufficient to monitor the polarization. This technique was used to check whether we had the polarization in the cells without the use of neutrons. Figure 3.13 shows a typical signal from the pulsed NMR. The amplitude of the signal is proportional to the ^{3}He polarization in the cell and if calibrated with neutron polarization is an indirect method to determine the value of ^{3}He polarization. Details of the pulsed NMR systems are discussed in appendix A.

The advantage of using ^{3}He spin filter cells for the polarization of the neutrons is that the direction of neutron polarization can be reversed very easily without flipping the direction of magnetic field. This is done by flipping the direction of ^{3}He polarization in the spin-filter using AFP with respect to the vertical magnetic field. A set of 30 cm diameter Helmholtz coil provided the oscillating field in the direction of the neutron beam propagation. The oscillation frequency was ramped from far below to far above resonance and thus flipping the direction of the ^{3}He polarization. The losses in AFP reversal depend on many factors like uniformity of the static and

oscillating field, sweep rate and the strength of the oscillating field. If the sweep rate and the strength of the field is tuned properly so as to satisfy the conditions of AFP, losses of much less than 1% can be achieved.

3.7 The Neutron Spin Flipper

In an asymmetry measurement experiment, false asymmetries should be taken care of if one wants to measure the asymmetry to the desired level of accuracy. If the asymmetry measurement is done by simply measuring the signal in one detector with a certain neutron spin direction at one time and then measuring the signal in the same detector after flipping the neutron spin in the opposite direction at a later time, the accuracy cannot be achieved because of the pulse to pulse variations due to the fluctuations in the beam current, drift in the detector efficiency, gain non-uniformities with time etc. and will lead to false asymmetries affecting the final result. We therefore need to minimize these falsely generated asymmetries. This is achieved by fast reversal of neutron spin. Using this method, the asymmetries in the detectors can be measured closer in time before the drifts in the detector efficiency, beam current or the detector gains. A Radio Frequency Spin Flipper (RFSF) is used for this fast neutron spin reversal. An RFSF is a resonant based device in which the spin direction of neutron pulses propagating through a set of orthogonal magnetic fields is rotated by 180^0 with respect to B by performing NMR.

The polarized neutrons come out of the ^{3}He polarizer with its spin parallel or anti-parallel to the direction of the 10 G magnetic field. The RFSF was used at 20Hz to flip the spin of the neutrons coming out of the polarizer [65]. The spin sequence used for the experiment is $\uparrow\downarrow\downarrow\uparrow\downarrow\uparrow\uparrow\downarrow$,where $\uparrow$ means neutron pulse spin is not flipped (RFSF off) and $\downarrow$ means pulse spin is flipped (RFSF on). These neutrons then enter

the para-LH_2 target where they were captured by the protons producing gamma.

The RFSF used for the experiment was a 30 cm long solenoid with a diameter of 30 cm enclosed in an aluminium housing. Aluminium was selected for the spin flipper because of its non-magnetic properties. To switch off the RFSF, the current drawn by the coil was switched to a resistor circuit, called the dummy load, for which the impedance was equal to the coil. Because of this, the load on the main power circuit remains constant and therefore, reducing the effect of the SF on-off in all other circuits in the experiment as the RF is always on.

3.7.1 Theory of the Spin Flipper

An RFSF is based on the principles of NMR [3], described in appendix A. The two main types of spin flippers are: adiabatic spin flippers and resonant spin flippers. Spin flippers make use of two types of magnetic field - static magnetic field B_0 perpendicular to the direction of beam propagation and a perpendicular RF magnetic field. In an adiabatic spin flipper, the static magnetic field changes the magnitude along the length of the beam and the RF field magnitude varies with a maximum in the middle. In resonant spin flippers, the static field is constant and the RF frequency is chosen to match the Larmor precession frequency in some region of space. The field gradient in adiabatic spin flipper will effect the magnetic field outside the spin flipper and therefore the path of the neutrons. This will cause spin correlated spatial shift in the neutron distribution inside the liquid hydrogen target leading to false asymmetry in the detectors as the solid angle seen by the detectors will change. As the NPDGamma experiment aimed to measure the asymmetry to very high accuracy resonant spin flipper was chosen for the experiment.

Before entering the RFSF, the polarized neutrons precess in the static magnetic field of 10G. After entering the spin flipper where both static and time dependent

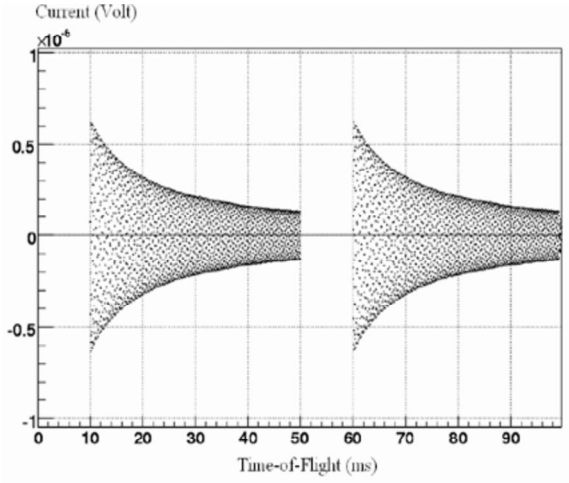

Figure 3.14: Amplitude of the B field applied to the solenoid. The dependence of the B field on time of flight can be seen in this figure. Each neutron pulse is 50 ms long but we were recording data for only 40 ms.

fields are present the neutrons precess with the angular frequency $\omega_1 = \frac{\mu_n B_1}{\hbar}$ about the effective magnetic field, $B_{eff} = (B_0 - \frac{\omega}{\mu_n}\hbar)\hat{y} + B_1\hat{z}$, where μ_n is the magnetic moment of the neutron. To perform a spin flip of π radians on the neutrons passing through the spin flipper, the neutrons will have to stay inside the flipper for a time $t = \frac{L}{v} = \frac{k\pi\hbar}{\mu_n B_1}$ where k=1,3,5,...and L is the length of the spin flipper. The velocity of the neutrons is given by $v = d/t_{tof}$ where d is the distance of the flipper from the moderator and t_{tof} is the time of flight. Therefore, to achieve high spin-flip efficiency for each neutron velocity, the RF field amplitude should be

$$B_1(t_{tof}) = \frac{n\pi\hbar}{\mu_n}\frac{d}{L}\frac{1}{t_{tof}}, \tag{3.19}$$

which implies that the field B_1 has to be varied during each neutron pulse as $\frac{1}{t_{tof}}$. Figure 3.14 shows dependence of B_1 on time of flight t_{tof}.

3.8 The Liquid Hydrogen Target

NPDGamma experiment used a liquid hydrogen target as the proton target for neutron capture. 16 liters of liquid hydrogen was stored in a 30 cm long and 30

cm diameter target vessel made of aluminium. The target was designed to capture about 60% of the incident neutrons. Dimensions of the target were decided using a Monte Carlo calculation taking into account the double differential scattering cross sections for the scattering of cold neutrons in liquid para-hydrogen target [17].

The target vessel was surrounded by a vacuum chamber. Both target vessel and vacuum chamber were made up of Al. Because of its non-magnetic properties polarized neutrons were efficiently transported into the target without depolarizing the neutrons. Upstream and downstream windows of the vacuum chamber and the target vessel were very thin for the maximum transmission of neutrons. The upstream window of the target vessel was ≈3.2 mm and ≈6 mm respectively. The downstream window of the vessel was ≈3.8 mm thick [37].

The detector array of the NPDGamma experiment had 48 detectors, four rings with 12 CsI(Tl) detectors in each ring around the cylindrical 16 L hydrogen target [38]. Alignment of the detectors in one ring is shown in figure 3.15. Current mode gamma detectors were used for the experiment. Detection was performed by converting the scintillation light from the CsI detectors to current signals using vacuum photo diodes (VPD). This photocurrent was converted to voltage and amplified by low-noise solid-state electronics.

The signal at each of the detectors is a function of neutron polarization P_n, spin flip efficiency ϵ, geometry factor $g_d(\theta,\phi)$, neutron depolarization S, capture locus $h(z,E_n)$ and number of neutrons in the beam times gain factor $V_d = \kappa_d N_{\uparrow,\downarrow}$ and gamma energy deposition $f_d(\vec{x},\theta,\phi)$. In terms of all these parameters, a detector signal is given by [37]

$$Y_d = \frac{V_d}{4\pi}[1 + A_\gamma P_n(E_n)\epsilon(E_n)S(E_n)g_d(\theta,\phi)]h(z,E_n)f_d(\vec{x},\theta,\phi). \tag{3.20}$$

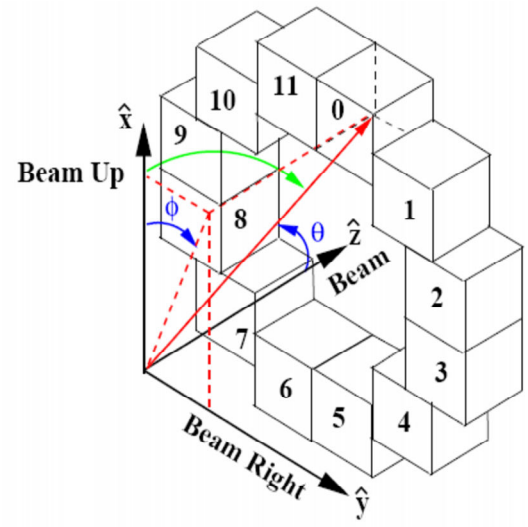

Figure 3.15: The figure shows one of the four rings in the detector assembly. There are 12 CsI detectors in each ring with four rings in total. For a given γ-ray source point and direction (red), the cosine of the angle γ-ray makes with the x-axis is given by the standard spherical coordinate direction cosine (green)

Using these signals from detector pairs the asymmetry is given by,

$$A_{raq,p}(t_i) = \frac{Y_{A_p,\uparrow}(t_i) - Y_{B_p,\uparrow}(t_i) - Y_{A_p,\downarrow}(t_i) + Y_{B_p,\downarrow}(t_i)}{Y_{A_p,\uparrow}(t_i) + Y_{B_p,\uparrow}(t_i) + Y_{A_p,\downarrow}(t_i) + Y_{B_p,\downarrow}(t_i)}. \tag{3.21}$$

Thus asymmetry was calculated using signals from different detector pairs for all the 4 rings of detectors.

3.8.1 Neutron Scattering by Ortho and Para Hydrogen

For an asymmetry experiment which aims to measure the asymmetry to 10^{-8} level, it is important to preserve the neutron polarization in the LH_2 target. At room temperature 75% of the hydrogen is in the ortho-H_2 state and 25% is in the para-H_2 state. The capture of cold neutrons has a smaller cross section than the scattering cross section for both ortho-H_2 and para-H_2 leading to scattering of polarized neutrons, at least once before being captured. Interaction of neutrons with ortho-H_2 lead to coherent or incoherent scattering. For ortho-H_2 the incoherent scattering cross section is larger than the coherent scattering which can cause depolarization

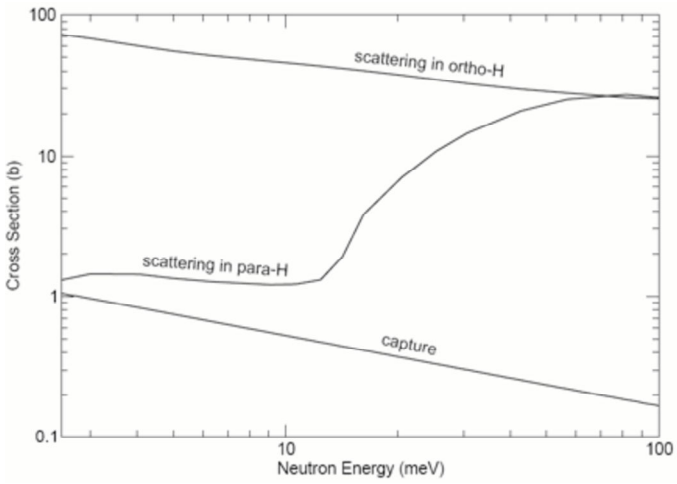

Figure 3.16: Plot showing the capture and scattering cross section of ortho and para hydrogen. Scattering cross section is higher for ortho-hydrogen than the cross section for para-hydrogen for cold neutrons [17].

of neutrons. For ortho-H_2, $\sigma_{coh} = 0.439 \pm 0.003$ b and $\sigma_{incoh} = 20.052 \pm 0.014$ b for neutrons at $v = 2200m/s$ [53]. But, in the ground state of the hydrogen molecule, para-H_2 capture and coherent scattering are the only allowed processes in the interaction of cold neutrons. Therefore, to preserve the neutron polarization inside the target it is required to keep the concentration of ortho-H_2 in the target as low as possible. Figure 3.16 shows the scattering and capture cross section for hydrogen [51].

To avoid neutron spin depolarization inside the target due to incoherent scattering it is required to convert ortho-H_2 to para-H_2. The energy difference between the ground state (para-H_2) and the excited state (ortho H_2) is 14.3 meV [13]. To convert the ortho-H_2 to para-H_2, the hydrogen and the heat radiation shield (located around the vessel) were cooled using two cryogenic refrigerators. In this cooling process, hydrogen which is mostly in the ortho-H_2 state at room temperature gets converted to para-H_2 state. The conversion from ortho to para hydrogen depends on the natural ortho-to-para conversion rate, $K_n = 12.7 \times 10^{-3} h^{-1}$[73]. If f_i is the initial fraction

of ortho-H_2 in the target, f_o is the fraction of ortho-H_2 at any time t and f_e is the equilibrium fraction, then the time constant for the conversion of ortho-H_2 to para-H_2 is given by [45]

$$t = \frac{1 - f_e}{K_n f_e} ln \left[\frac{f_i(f_o - f_e)}{f_o(f_i - f_e)} \right]. \tag{3.22}$$

For liquid hydrogen at 17K, if at the beginning we have $f_i = 0.75$ and we want to reach $f_o = 0.0004$ with the natural conversion rate, the time constant for this conversion is ≈ 30 years. Therefore, we need to catalyze the process so as to reach the required concentration in a shorter time period.

The conversion process is catalyzed by the interaction of hydrogen with paramagnetic surfaces introducing inhomogeneous magnetic field that flips the spin of the atoms adsorbed on the surface of the paramagnetic material and therefore catalyzing the conversion. The NPDGamma experiment used two FeO_2 ortho-to-para converters for the conversion to reduce the time to reach the equilibrium. With the use of these converters the conversion time constant was reduced to 2-4 days. The location of these two converters in the target is shown in fig.3.17. For the NPDGamma experiment we were able to attain the equilibrium fractions of 99.98% and 99.99% for the August-September and November-December runs respectively[13]. Figure 3.17 shows the location of the ortho-to-para converters in the hydrogen target.

3.9 Polarization Calculations and Results

Neutrons were polarized in the experiment using a ^{3}He polarizer. The neutron beam polarization was analyzed using the data from monitors M1 and M2. Neutrons coming from the source have a Boltzmann distribution as seen in M1 signal (figure 3.18). The signal obtained at the first monitor (M1) depends on the neutron flux and therefore was used for the normalization of the signals recorded at other monitors (M2

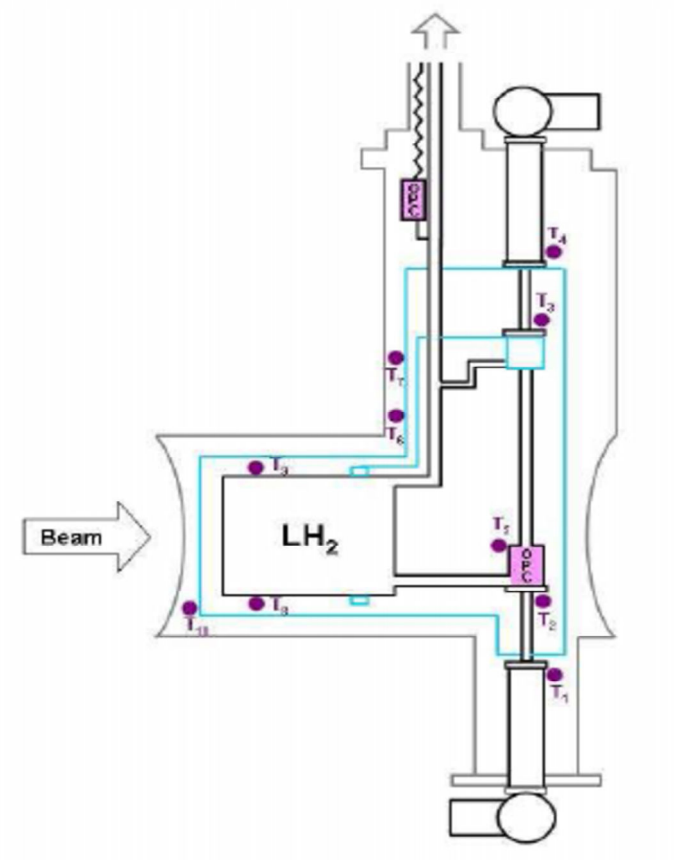

Figure 3.17: A schematic diagram showing the locations of the ortho to para converters (OPC) in the LH_2 target. The upper OPC is located in the filling line and was operated at about 30K. The second OPC is located in the recirculation loop, where the final conversion occurs.

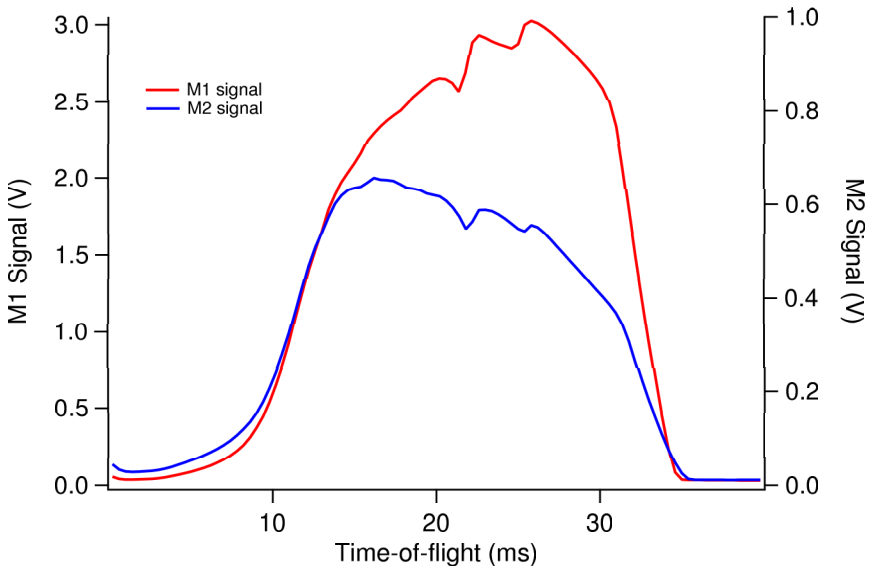

Figure 3.18: Raw time-of-flight spectrum for M1 and M2. The dips near 22 ms and 26 ms are due to the Bragg edges from aluminium windows.

and M3). The normalization was done to take care of the fluctuations in neutron flux due to change in proton current, moderator temperature fluctuation etc. This section discusses the analysis done for the measurement of ^{3}He and neutron polarization.

3.9.1 Interpolation

Positions of M1 and M2 are different in the experiment, one before the polarizer and one after the polarizer (figure 3.1). Therefore, the time required by the neutrons to reach different monitors is different and a given time of flight corresponds to a different wavelength/velocity at different monitors. Therefore, we interpolate the data from one monitor with respect to the other monitor to obtain the data at the same wavelength. Data from M2 was linearly interpolated to the data obtained at M1.

Time of flight was converted to wavelength for both M1 and M2 using the de Broglie wavelength equation, and then M2 was interpolated to the wavelength at M1

$$\lambda = \frac{h}{mv} = \frac{ht}{md}, \tag{3.23}$$

where h is the Planck's constant, m is the mass of the neutron, v is the velocity of the neutron, t is the time of flight and d is the distance of each monitor from the source. The interpolation was done using

$$M2_i^{int} = \frac{M2[i+1] - M2[i]}{\lambda_2[i+1] - \lambda_2[i]}(\lambda_1[i] - \lambda_2[i]) + M2[i], \tag{3.24}$$

where λ_1 and λ_2 are the wavelengths at monitor 1 and 2, respectively, given by,

$$\lambda_1 = \frac{h}{mL_1}t_1, \lambda_2 = \frac{h}{mL_2}t_2 \tag{3.25}$$

and L_1 and L_2 are the distances of M1 and M2 from the moderator. The analysis was done with M1=21.123 m.

3.9.2 Pedestal Correction

Figure 3.18 shows typical raw time-of-flight data, averaged over 10,000 pulses, for M1 and M2 with the ^{3}He spin filter in place. Electronic offsets, beam-off background, including that due to long-lived activation are periodically monitored with beam-off runs, measured for 40ms data acquisition window triggered by the proton pulse. These beam-off runs were called the pedestal runs and were used to do the background subtraction from the raw data. Figure 3.19 shows several beam-off runs for the two monitors, M1 and M2. It can be seen from these plots that the pedestals are typically less than 1% of the beam-on signal. The pedestal is also not constant over the 40 ms acquisition window with fluctuations on the order of 10^{-3} V and some small oscillations. The data for each beam-on run for the M1 and M2 were separately corrected by assuming a constant offset,M_{offset}, determined from two beam-off runs one before and one after the beam-on run. For example, M1 signal was corrected using

$$M1_{corrected} = M1_{raw} - M1_{offset}. \tag{3.26}$$

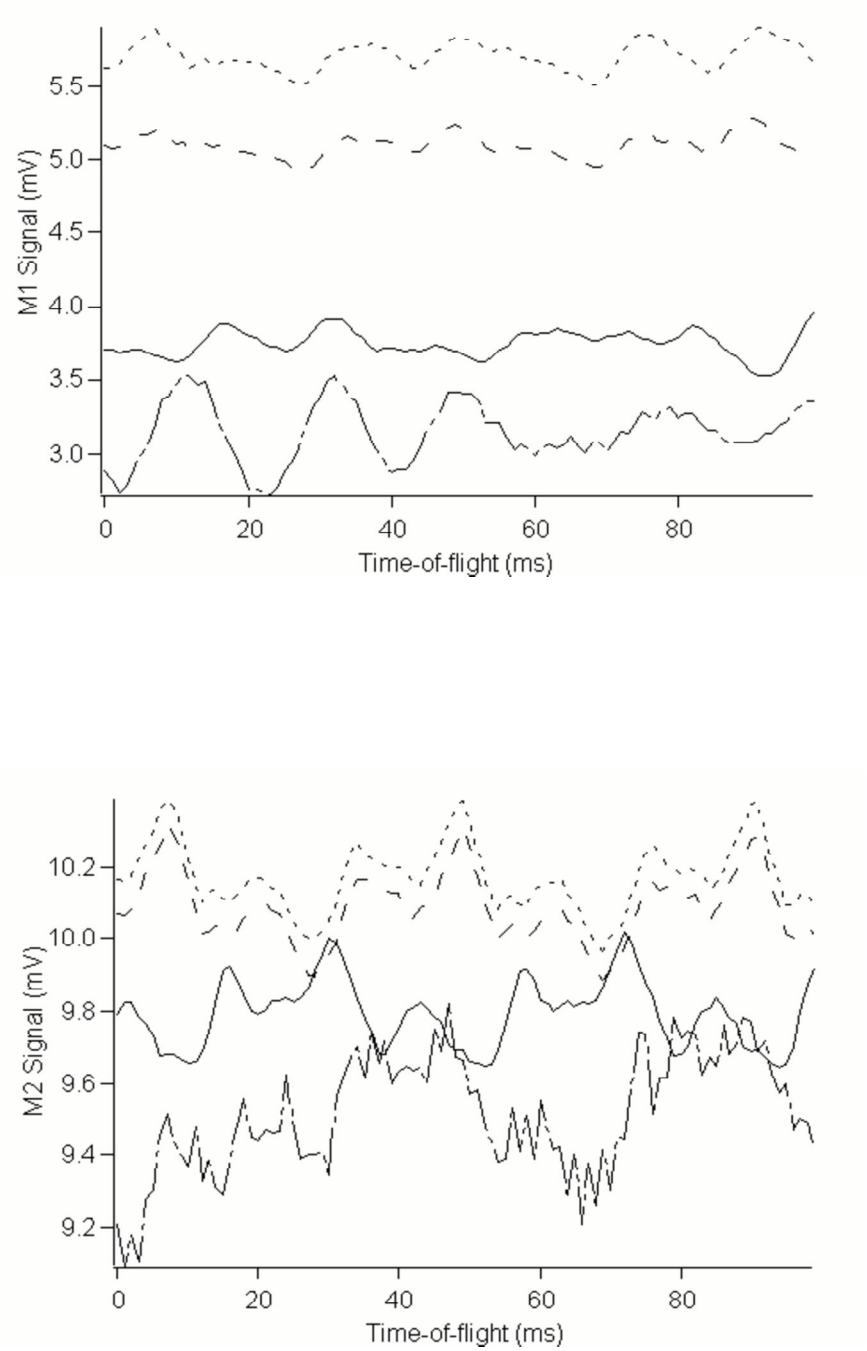

Figure 3.19: Beam-off (pedestal) data for M1 and M2. Each trace is the average of 1000 pulses. The four pedestals are taken at different times. Although the pedestal signal is small corrections are made to the analysis by subtracting the pedestals.

Time of flight dependent background also include beam related neutrons and short lived activities. Neutrons incident on the monitors during the 40 ms window are predominantly the moderated neutrons from the proton pulse but may also include "wrap around" slow neutrons from earlier pulses (see figure 3.3). These neutrons may also include beta-delayed neutrons from fission products in the tungsten target and also scattered neutrons. The activation also produces gamma-rays and will be incident on M1 and M2 with different intensities, but will taken care of in the ratio M2/M1 if the gamma background remains constant.

3.9.3 Cell Thickness Determination

First task in the determination of ^{3}He or neutron polarization is to determine the thickness, nl, of the polarizer cell. Thickness is defined as the number of ^{3}He atoms per unit length. For thickness determination, runs with four different configurations were taken: 1.With unpolarized ^{3}He polarizer between M1 and M2, 2.With the oven intact with the Silicon wafers but the polarizer cell removed from the oven, 3. A piece of GE180 glass between the monitors and 4.Pedestal runs, with the neutron beam off.

The neutron transmission through the oven with unpolarized polarizer cell, T_{UP} is

$$T_{UP} = [T_{gl}(\lambda)]^{d/5} T_{Si} T_{He}, \tag{3.27}$$

and the transmission through empty oven i.e. silicon wafers only, T_{oven} is

$$T_{oven} = T_{Si}, \tag{3.28}$$

where T_{gl} is the transmission through the GE180 glass (figure 3.8), T_{Si} is the neutron transmission through the silicon wafers on the oven and T_{He} is the transmission

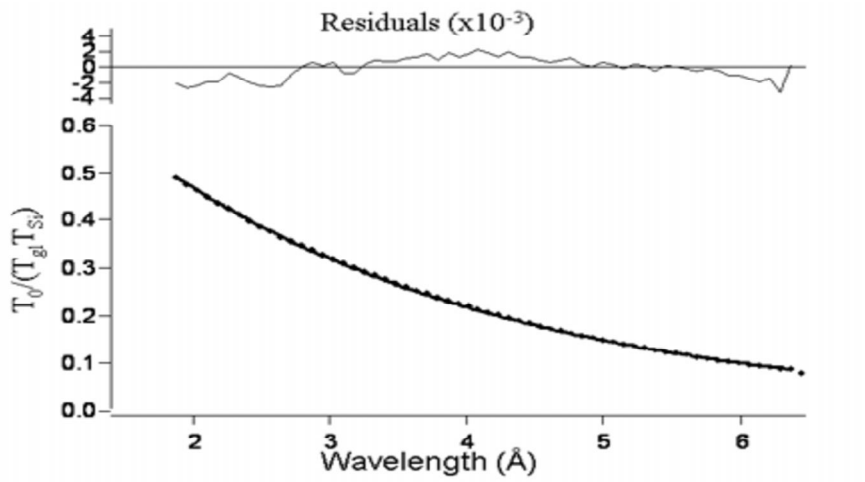

Figure 3.20: Transmission through unpolarized polarizer cell. Cell thickness was calculated from this plot by doing an exponential fit.

through the ^{3}He inside the cell. Therefore, dividing equation 3.27 by equation 3.28,

$$\begin{aligned} T_{He} &= \frac{T_{UP}}{T_{oven}} = [T_{gl}(\lambda)]^{d/5} exp(-nl\frac{\sigma_0}{\lambda_0}\lambda) \\ &= Aexp(-\alpha\lambda). \end{aligned} \tag{3.29}$$

Here d is the thickness of the glass on the cell walls, front and back combined. Value of d was determined by the best fit of the data in figure 3.20. Transmission through an empty oven is shown in figure 3.9. Thus, if we take the transmission ratios of the transmission through the unpolarized cell and empty oven, thickness of the polarizer cell can be determined. The T's are $\frac{M2}{M1}$ ratios and are extracted from background corrected M1 and M2 data.

If we plot the quantity defined in equation 3.29 vs wavelength and do an exponential fit, the "average thickness" of the cell can be determined from the fit parameters as shown in figure 3.20. The average thickness for a cell is the thickness integrated over the entire cell volume considering all possible neutron trajectories inside the cell. One important thing about the cell thickness is that it varies with the size of the neutron beam used to do the measurements. The thickness variation as a function

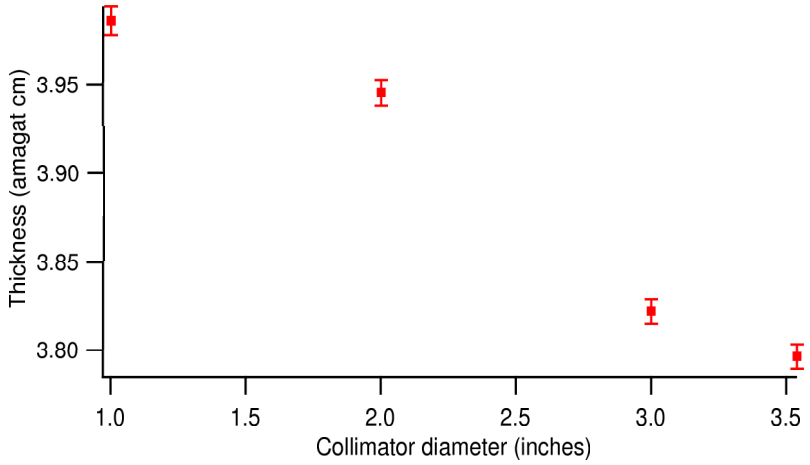

Figure 3.21: Cell thickness as a function of neutron beam size or collimator size.

of collimator size is shown in figure 3.21. The polarizer cells have a curved surfaced making it thicker at the center than the edges. Because of this neutrons are attenuated more at the center than the edges. Also, when the beam size is big there is more divergence in the neutron beam and therefore less attenuation. Because of the excess attenuation at the center than the edges, cells are thicker when the collimation is small. Because of the thickness dependence on the size of the neutron beam, it is important to use the correct thickness value based on the beam size to determine neutron polarization precisely.

3.9.4 ^{3}He and Neutron Polarization

Once the thickness of the cell is known ^{3}He and neutron polarization can be measured using the transmission ratios through polarized and unpolarized cell. We did the analysis for the data taken in February 2006, during the commissioning of the NPDGamma experiment. The cell used in the commissioning run was "Boo Boo". From equations 3.14 and 3.15 it is seen that the ratio of the polarized transmission to the unpolarized transmission through a ^{3}He cell obeys the $\cosh(\frac{nl\sigma_0}{\lambda_0}(\lambda_1 - \lambda_{off}))$ relation (figure 3.22) and the neutron transmission obeys $\tanh(\frac{nl\sigma_0}{\lambda_0}(\lambda_1 - \lambda_{off}))$ (figure

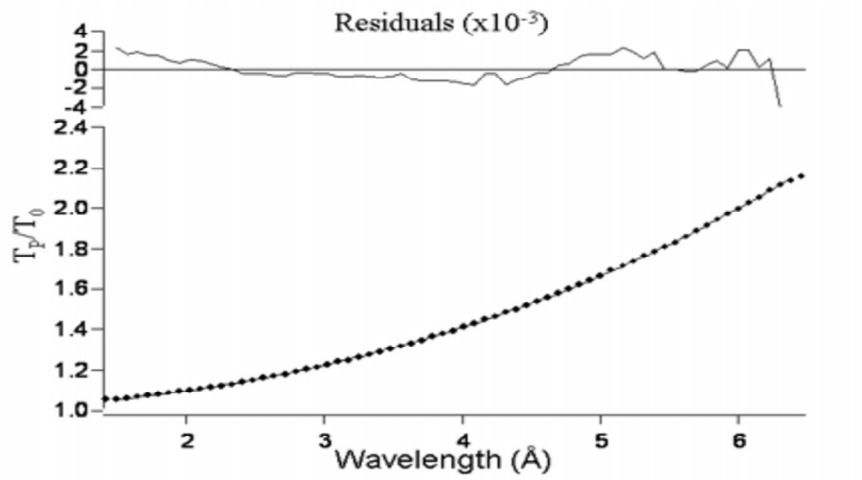

Figure 3.22: Transmission through a polarized cell. ^{3}He polarization was determined from this graph using the value of cell thickness obtained from figure 3.20.

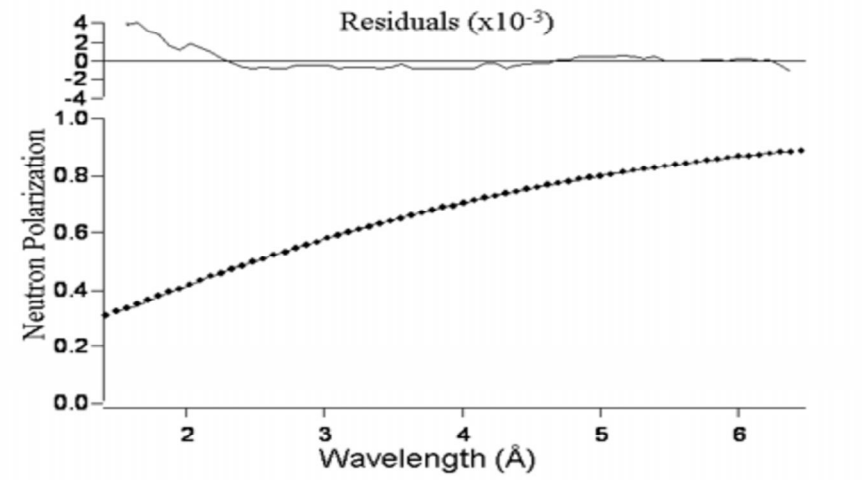

Figure 3.23: Neutron polarization versus wavelength

3.23), respectively. Therefore, the quantity $\frac{T_P}{T_0}$ as a function of wavelength (at M1), can be fitted to the following functional forms:

$$\frac{T_P}{T_0} = \cosh(\beta(\lambda_1 - \lambda_{off}) \tag{3.30}$$

and

$$P_n(\lambda) = \sqrt{1 - (\frac{T_0}{T_P})^2} = \tanh(\gamma(\lambda_1 - \lambda_{off})). \tag{3.31}$$

T_P is the transmission through a polarized ^{3}He cell, $P_n(\lambda)$ is the polarization of the neurons emerging from the polarized ^{3}He and λ_{off} accounts for an offset in the

timing (wavelength) with respect to the proton pulse signal. The free parameters in equations 3.29, 3.30 and 3.31 are A, d, α and β, where α, β and γ are given by,

$$\alpha = \frac{nl\sigma_0}{\lambda_0}, \tag{3.32}$$

$$\beta = \alpha P_{He}, \tag{3.33}$$

and

$$\gamma = \alpha P_{He}, \tag{3.34}$$

where P_{He} is the ^{3}He polarization in the neutron spin filter. Figures 3.20, 3.22 and 3.23 show that the data fit well with the analysis. Residuals are shown in the figures. The residual indicates wavelength dependent systematics of a few tenths of 1% which is much greater than the statistical error. With this analysis the cell thickness, nl was calculated to be 4.71 ± 0.02 amagat cm and ^{3}He polarization, $P_{He} = 0.578 \pm 0.012$. The uncertainty in the polarization values are discussed in next section.

3.9.5 Backgrounds

There are several sources of wavelength dependent backgrounds in both M1 and M2. In addition to the wrap around neutrons, short lived activation and scattered neutrons also have a significant contribution. The sizes of these effects were not directly measured, but a significant effort was made to understand the effects. This will be discussed chapter V. The main sources of uncertainty in the polarization analysis are: wavelength calibration, thickness determination, wrap around neutrons, time dependent backgrounds etc. We therefore need to take care of these factors in the analysis.

While doing the analysis for the NPDGamma experiment, we did some simulations to understand the background effects. We did two kind of simulations: 1. Simulation of the M2 signal based on a model of the spin filter and windows with added

backgrounds and 2. Simulated corrections to M1 and M2 with a generic background linear in time of flight.

The simulated M2 signal, $M2'(\lambda_1)$, was generated using monitor 2 signal, $M1(\lambda_1)$, taking into account the transmission through the polarized cell. $M2'(\lambda_1)$ was calculated using

$$M2'(\lambda_1) = \alpha T_{emp}(\lambda_1) M_1(\lambda_1) \exp\left(-\frac{\sigma_0 t_3 \lambda}{\lambda_0}\right) \cosh\left(\frac{\sigma_0 t_3 P_{He} \lambda}{\lambda_0}\right), +(A\lambda + B) \quad (3.35)$$

where α is the wavelength dependent attenuation, A and B are coefficients that represent a linear wavelength dependent background difference for M1 and M2 and $t_3 = nl$ is the thickness of the cell. This model approximates any of the backgrounds mentioned before (scattered neutrons, "wrap-around" neutrons, activation effects etc.). The simulated data are then analyzed in the same way as explained before. Results for $A = 0.002V/\mathring{A}$ and B=-0.01 V are shown in figure 3.24. For the simulated data with 3-5% background added to M1 or M2, the change in residuals of the fit to neutron polarization at 5 $\mathring{A}$ is $\approx 0.1\%$ and the change in ^{3}He polarization is 1%. This provides a reasonable estimate of the uncertainty on the ^{3}He polarization for these low-background data. It also emphasizes the importance of understanding the backgrounds better for attaining precision neutron polarimetry.

Another source of uncertainty in the polarization determination is the curved surface of the polarizer cells. Due to the nature of the blown glass, it is difficult to make the surface of the polarizer cells perfectly flat or parallel leading to non-uniform cell thickness. With non-uniform ^{3}He thickness the neutron polarization also becomes non-uniform over the beam size leading to systematic effects.

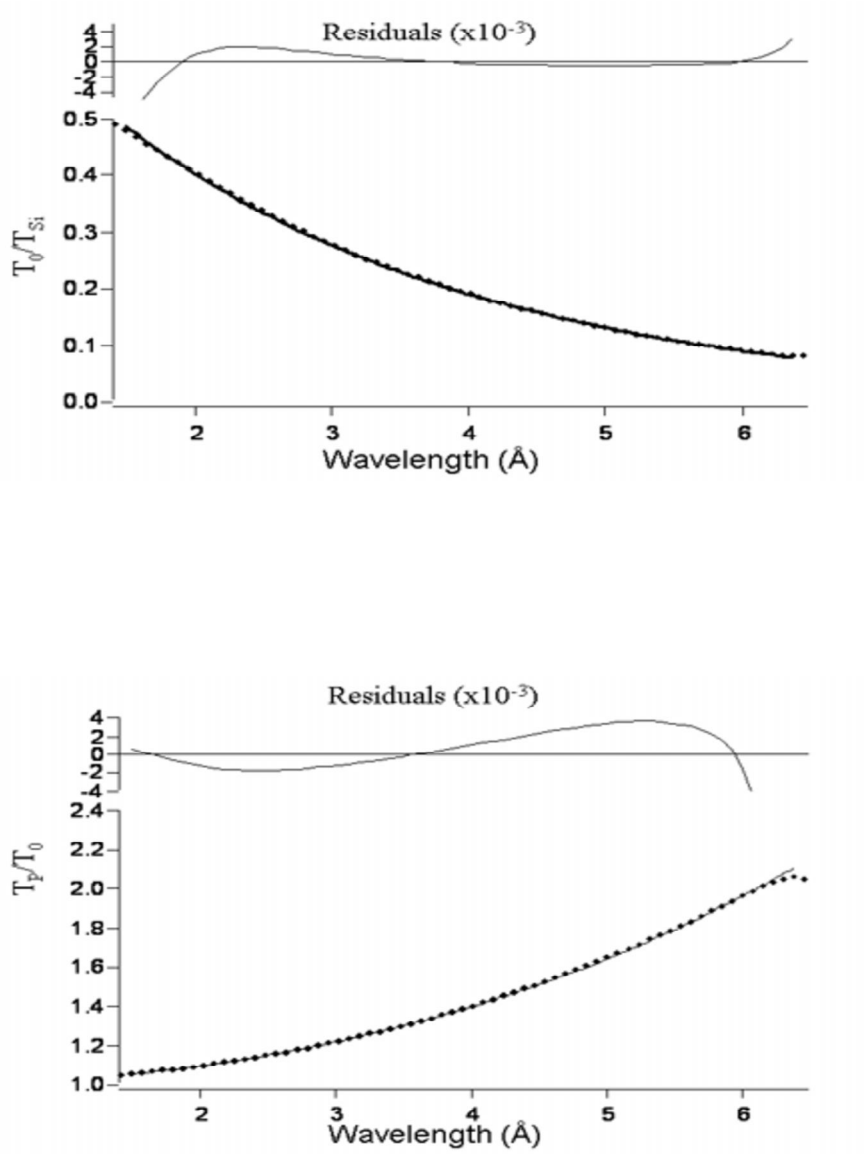

Figure 3.24: Results for simulated data with background added to the signal from M1. M2 was simulated using M1 signal for both polarized and unpolarized transmissions.

3.10 Neutron Polarization in the NPDGamma Experiment

The NPDGamma experiment was done in two phases: commissioning period and the production period. The analysis shown above is with the data which were taken during the commissioning period when there was no H_2 target and therefore low background conditions. The results discussed below are from the second phase of the NPDGamma experiment when the 16 L hydrogen target was in the beamline.

The hydrogen target data were taken in two stages - August-September 2006 and November-December 2006. For the August-September run, a cell named "Pebbles" was used and for the November-December run "Dino" was used. ^{3}He polarization was calculated using the same method described in the previous section. ^{3}He polarization for Pebbles and Dino are shown in figures 3.25 and 3.26.

Figure 3.25 shows the ^{3}He polarization for "Pebbles" for August and September 2006. From this figure it is seen that there is a sudden change in ^{3}He polarization on 1^{st} September 2006. The analysis was done as before with an offset in the wavelength i.e. λ_{off} is a free parameter in $\cosh(\alpha(\lambda-\lambda_{off}))$. But if we make $\lambda_{off} = 0$, the sudden change in polarization disappears. It was important to understand the polarization behavior for these runs as incorrect values of polarization would lead to incorrect value of asymmetry in the n-p capture.

In an effort to understand this jump in the polarization, we addressed two issues: 1. Background effects because of the 16L hydrogen target, a H_2 target can cause scattering because of the presence of some amount of ortho hydrogen in it and 2. Change in neutron time-of-flight spectrum around September 01 2006.

The main factor responsible for the change in ^{3}He polarization was thought to be the background due to the neutron back-scattering from the hydrogen target.

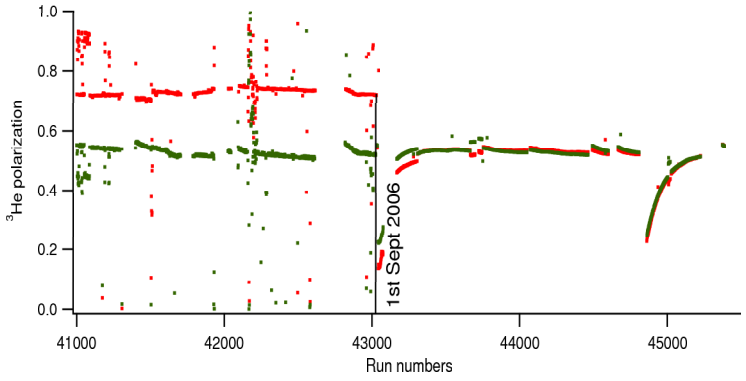

Figure 3.25: ^{3}He polarization for "Pebbles" for all the runs taken during Aug-Sep 2006 calculated using two different fitting equations. The red dots are with $\cosh(\alpha(\lambda - \lambda_{off}))$ and green dots are with $\cosh(\alpha\lambda)$. A sudden change in polarization was seen on 1^{st} September in the red dots.

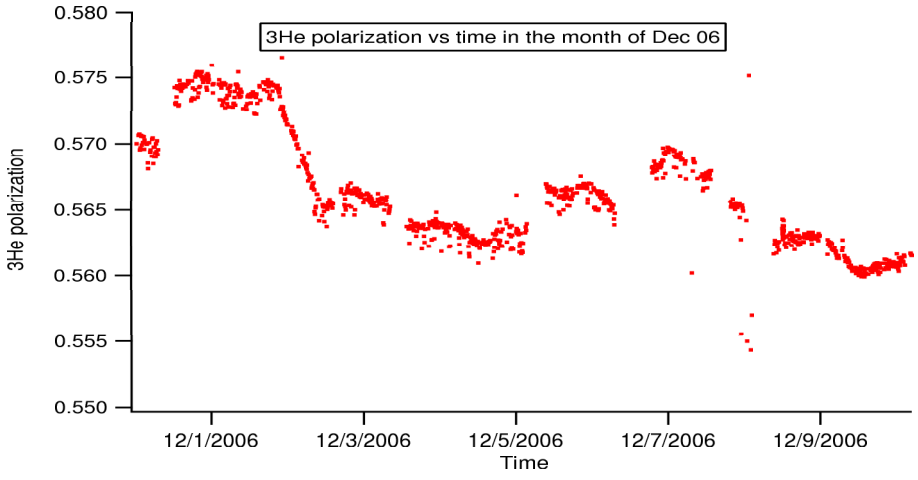

Figure 3.26: ^{3}He polarization for "Dino" for all the runs taken during Nov-Dec 2006.

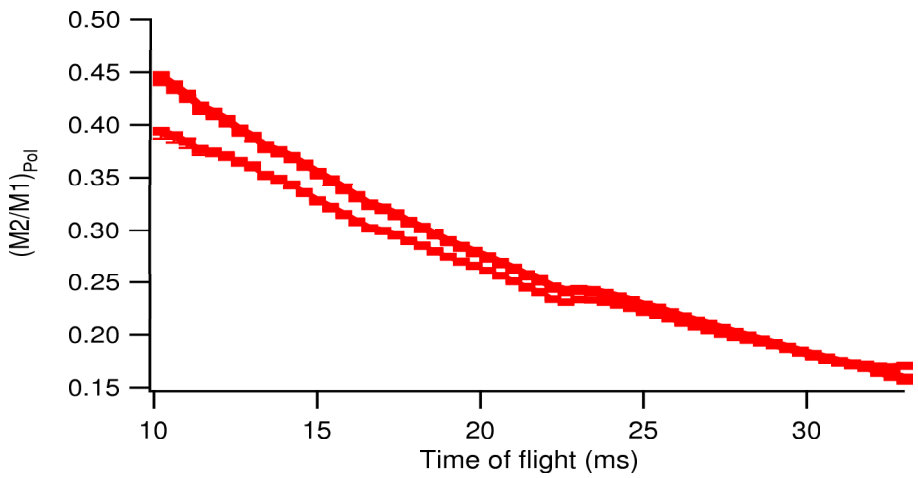

Figure 3.27: M2/M1 ratio for some runs before and after 1^{st} September. The ratios were different before and after this day.

Fig.3.28 shows λ_{off}, obtained when $\cosh(\alpha(\lambda - \lambda_{off}))$ was used to fit the transmission ratios for a polarized cell for the August-September runs plotted versus run numbers. If λ_{off} is a measure of backgrounds in the monitor ratios we should have seen a gradual decrease in its value but this plot also shows a jump in λ_{off} around the same time. The background due to the hydrogen target was a significant contributor to the backgrounds in the analysis. But, this possibility was ruled out for the sudden change in polarization because if the back-scattering was responsible for the high values of λ_{off} one would expect it to decrease gradually with time rather than a sudden jump, as back-scattering would decrease with increasing para-H_2:ortho-H_2 ratio. This possibility of back-scattering with ortho-H_2 was therefore ruled out.

We therefore decided to look at the monitor spectrum before and after 1^{st} September 2006 to see if there was any change in neutron time-of-flight spectrum around that time. Figure 3.27 shows the $\frac{M2}{M1}$ ratio for some runs before and after 1^{st} September 2006. From this figure, it is seen that the ratios are different before and after 1^{st} September indicating something changed in the M1 spectrum around that time. With this problem, it was decided to eliminate the λ_{off} from the fit equations 3.30

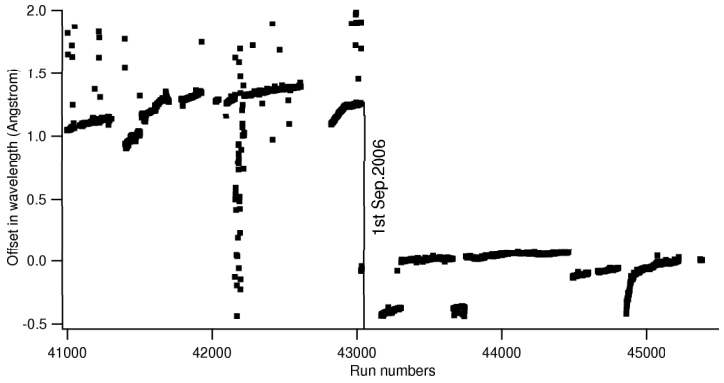

Figure 3.28: A plot showing λ_{off} obtained when T_P/T_0 was fitted to $\cosh(\alpha(\lambda - \lambda_{off}))$ to obtain ^{3}He polarization. The λ_{off} values are not affected by scattering from the LH_2 target during the ortho-H_2 to para-H_2 coversion.

and 3.31 and continue the analysis with,

$$\frac{T_P}{T_0} = \cosh(\beta\lambda_1) \tag{3.36}$$

and

$$P_n(\lambda) = \sqrt{1 - (\frac{T_0}{T_P})^2} = \tanh(\gamma\lambda_1), \tag{3.37}$$

as without λ_{off} in the equations we were getting reasonable values of ^{3}He polarization as seen from figures 3.25 and 3.26.

Because of the unclear background issues it was difficult to assign values for ^{3}He polarization and neutron polarization for every run with known uncertainty. Therefore, it was decided to make histogram for the ^{3}He polarization values and take the mean and the second moment as the ^{3}He polarization and uncertainty respectively. This method of obtaining the ^{3}He polarization by mean and error bars by taking the second moment worked for the NPDGamma experiment because the NPDGamma aimed to measure the f_π^1 coupling constant to 10% of the DDH value and this method introduced an error of less than 3% in the ^{3}He polarization.

^{3}He polarization histogram for "Pebbles" and "Dino" are shown in figures 3.29 and 3.30. With this method, the ^{3}He polarization values for "Pebbles" was 0.524

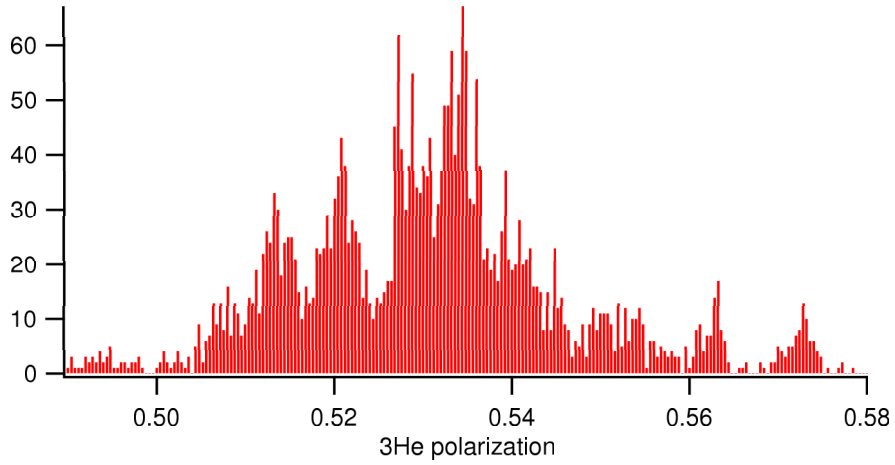

Figure 3.29: ^{3}He polarization histogram for "Pebbles"

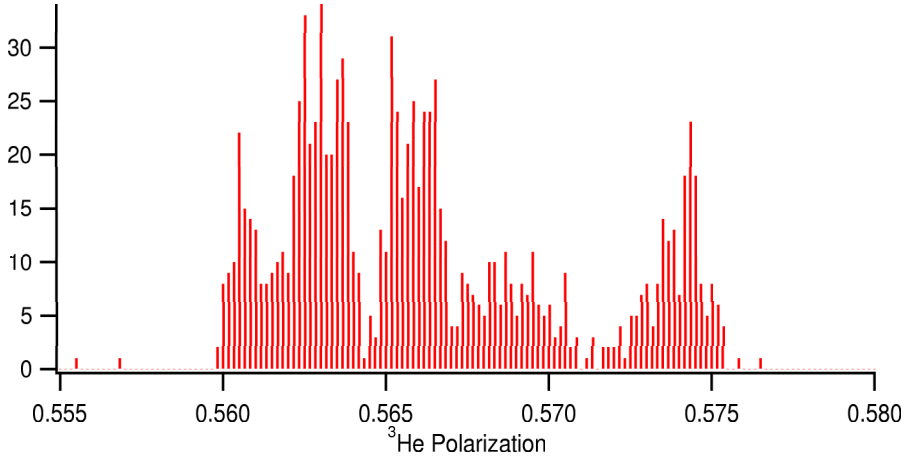

Figure 3.30: ^{3}He polarization histogram for "Dino"

$\pm$ 0.021 and "Dino" was 0.572 $\pm$ 0.012. Once ^{3}He polarization is known neutron polarization P_n can be calculated using equation 3.37 and the polarization values can be used in equation 3.20 to calculate the asymmetry value given all other parameters in the equation are known. The errors on the polarization values are higher than the values we measured for the runs taken during the commissioning period. The higher error bars on these values have been attributed to the background effects due to the hydrogen target.

3.11 Conclusions

All the components of the NPDGamma experiment were described in detail in this chapter. ^{3}He polarizer cells were used to polarize neutrons. The theory and functioning of the polarizer cell were provided in the first part of the chapter. Polarization analysis method was discussed using the runs taken during the commissioning period of NPDGamma experiment in February 2006. The data shows that given low background conditions it is possible to measure ^{3}He polarization to $\pm 1\%$. If the backgrounds are understood properly it is even possible to go below 1%.

Measurement of neutron polarization is important as it is a required parameter in the asymmetry determination as shown in equation 3.20. The NPDGamma experiment aimed to measure the value of pion-nucleon coupling constant f_π^1 to 10% of the DDH proposed value by measuring the directional asymmetry in the gamma emitted in n-p capture with respect to the neutron spin. For a 10% measurement of f_π^1 it is required to measure neutron polarization up to an accuracy of $\approx$5%. The above analysis shows that we have measured the ^{3}He polarization values to $\pm 3\%$. But, we are still limited by the unknown backgrounds in the analysis.

After solving the problem of the sudden change in ^{3}He polarization, the asymmetry analysis moved forward. The spin flip efficiency was reported to be $(0.98\pm0.8)\%$, ortho-H_2 to para-H_2 ratio in both the phases of the NPDGamma experiment was reported to be $(99.98\pm0.02)\%$ and the spin flip scattering was calculated to be 2%. With all these values current asymmetry value from the analysis is $A_\gamma = (-1.1 \pm 2.1) \times 10^{-7}$. The analysis is still under progress. NPDGamma experiment finished the experiment at LANSCE in fall 2006 and has been moved to SNS.

Also, there are some notable features in figure 3.25 and figure 3.26. The steady

state ^{3}He polarization appears to be slowly but steadily decreasing throughout the run. There are several possible sources of this decrease in maximum attainable ^{3}He polarization: cell degradation, changing magnetic field environment, laser drift and magnetic alignment changes. This degradation in ^{3}He polarization in the presence of neutron beam became a major concern and experiments were performed to understand this decay behavior. The degradation of ^{3}He polarization and the effort for its understanding is discussed in the next chapter.

CHAPTER IV

Depolarization in ^{3}He Spin Filters

4.1 Introduction

In chapter III we saw depolarization in ^{3}He polarization in spin filter cells when exposed to the neutron beam. This depolarization was observed for the first time in the cell named "Boo Boo". "Boo Boo" was used in the commissioning run of the NPDGamma experiment. The depolarization effect was observed again a different cell "Pebbles" used during the production run of the experiment, confirming that neutron beam is responsible for the depolarization in the ^{3}He polarizers. Two types of depolarization were seen when the spin filter cells were exposed to the neutron beam for a long time: short term depolarization and long term depolarization. This depolarization behavior limited the maximum attainable polarization in these polarizer cells.

We considered several possible sources of this decrease in maximum attainable polarization: cell degradation, drifts in magnetic field environment, laser drift and optical alignment changes. Cell degradation could affect the ^{3}He polarization relaxation time, the density and/or polarization of the rubidium at a given temperature, and the coupling or transmission of laser light into the cell. The ^{3}He relaxation depends on the ^{3}He density, the cell walls, contaminants, magnetic field gradients,

Rb density and temperature. At the end of the run ^{3}He relaxation time was measured using NMR and found to be ≈100 hrs which was consistent with the previous measurements.

In the experiments with ^{3}He spin filters performed before the NPDGamma experiment ^{3}He polarization was stable provided the laser properties and cell temperature were stable but there was no prior experience then with GE-180 cells pumped at high-temperatures for 1.5 years. This was the first time a polarizer cell was exposed to the neutron beam for such a long time. To understand this depolarization in the ^{3}He cells we performed an experiment at the Los Alamos Neutron Science Center in Summer 2007 followed by another experiment at Institut Laue-Langevin at Grenoble, France. The details of the experiments, idea behind the experiment and our approach towards the better understanding of this depolarization effect in the ^{3}He polarizer cells are discussed in this chapter.

4.2 Polarization Decay in the ^{3}He Cells and Implications

During the course of the NPDGamma experiment two types of relaxations were observed: (1) Long term relaxation (figure 4.1) and (2) Short term relaxation (figure 4.2). In the long term relaxation, polarization decreases continuously with time when the cell is exposed to the neutron beam and this decay is not recoverable. Short term relaxation is an effect which is observed in shorter time scale, ^{3}He polarization decays when the cell is exposed to the neutron beam and with the beam off, polarization recovers, at least partially. These two types of relaxation are seen in figure 4.1 and 4.2, respectively.

Figure 4.1 shows the ^{3}He polarization for September 2006 for the polarizer cell ("Pebbles") used in the NPDGamma experiment. "Pebbles" was exposed to the

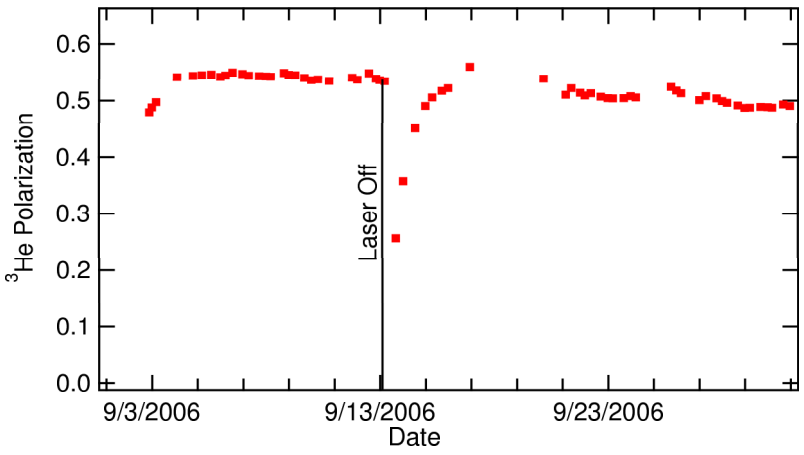

Figure 4.1: ^{3}He polarization vs time for "Pebbles" used at LANSCE in September 2006. It shows the long term behavior of the polarizer, the polarization was slowly decreasing with time.

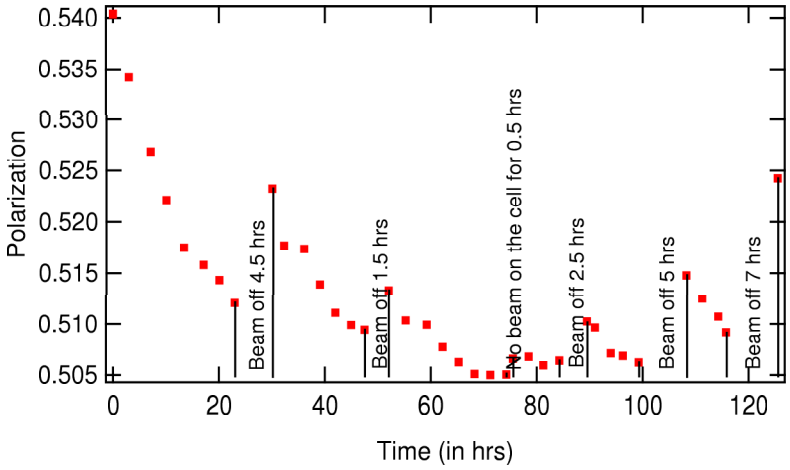

Figure 4.2: Effect of neutron beam on ^{3}He polarization in shorter time scales. The rate of decay is (1/12 h), which was consistent with 1' of the cell.

neutron beam for more than two months. ^{3}He polarization values were calculated using the neutron transmission ratio method explained in chapter III. Though the ^{3}He polarization appears relatively constant over the long term there is a slow downward drift. Beginning in September 2007 the equilibrium ^{3}He polarization was 56.8%, which over a period of a month decreased to 50.6%. The long term depolarization in the ^{3}He polarizer cells can be seen in figure 4.1.

The long time constant decay of the polarization appears to be due to the milky white coating that builds up on the cell walls with time and therefore, reduces the transmission of laser light into the cell. The build up is probably due to the formation of Rb compounds on the inner walls of the cell possibly due to reaction with hydrogen (^{1}H and ^{3}H) produced by neutron absorption on ^{3}He. For the LANSCE experiment about 10^{15} hydrogen atoms are produced per month, and several micrograms of RbH would be produced. A similar effect was observed for a pure Rb cell at 170 ^{0}C placed in the full flux PF1B beam at ILL for one hour, however a potassium-rubidium hybrid cell was exposed to the neutron beam for over 10 hours at the normal operating temperature of 210^{0}C, but no visible coating was produced. One hour exposure at PF1B is equivalent to about 2 days exposure at LANSCE FP12 [67].

Figure 4.2 shows the ^{3}He polarization for the same cell ("Pebbles") on shorter time scales, for ≈130 hrs. When the neutron beam is on, the ^{3}He polarization decays, and with the neutron beam off, the polarization recovers. The amount of recovery depends on the time for which the neutron beam is off as seen from the plot. The polarization recovery was greater when the beam was off for 4.5 hrs than when the beam was off for 1.5 hrs.

^{3}He polarization is governed by an exponential time dependence with rate con-

stant, $\Gamma = (1 + X_{cell})\gamma_{SE} + \Gamma_R$ and the equilibrium polarization given by

$$P_3^{eq} = P_{Rb}\frac{\gamma_{SE}}{\Gamma} \tag{4.1}$$

where $\gamma_{SE} =< \sigma_{SE} v > [Rb]$ is the velocity averaged spin-exchange constant which is typically $\frac{1}{10}h^{-1} - \frac{1}{15}h^{-1}$ (Figure 4.3). Γ_R is the intrinsic ^{3}He relaxation rate which is a sum of all the relaxation rates responsible for depolarizing ^{3}He in the cells: cell wall interactions, impurities, ^{3}He dipole-dipole relaxation and magnetic field gradients. The rate Γ_R is generally 10-50 times smaller than γ_{SE}, thus $\Gamma \approx (1 + X_{cell})\gamma_{SE}$. P_{Rb} is the volume averaged rubidium electron polarization and X_{cell} accounts for an observed reduction in ^{3}He polarization that varies from cell-to-cell [11].

Figure 4.2 shows that the neutron beam causes the ^{3}He polarization to go below the equilibrium value, P_{eq} at a rate of approximately (1/12 h), which is consistent with Γ. It was not possible to measure the ^{3}He polarization with neutron beam off as P_{He} values are calculated using the neutron transmission ratio method. However, the increase of ^{3}He polarization is consistent with a similar rate constant as Γ. From this figure Γ=(1/13.5) h^{-1}. Figure 4.3 shows that the building up of ^{3}He polarization in "Pebbles" has a similar time constant. Since Γ does not change appreciably, the most likely cause is the drop of rubidium polarization, P_{Rb}. This led us to the study of the effect of neutron beam on Rb polarization.

The short term decay in the polarizer cells was also confirmed with NMR data. After observing the effect of neutrons on the cell "Pebbles", we started taking NMR data for the second cell "Dino", used in the second phase of the NPDGamma run. Figure 4.4 shows the comparison of the NMR values for ^{3}He polarization simultaneously with the measurement of ^{3}He polarization using the neutron transmission method discussed in chapter III. The left axis of the plot shows the amplitude of the NMR signal and the right axis is the ^{3}He polarization. It is seen from this plot that

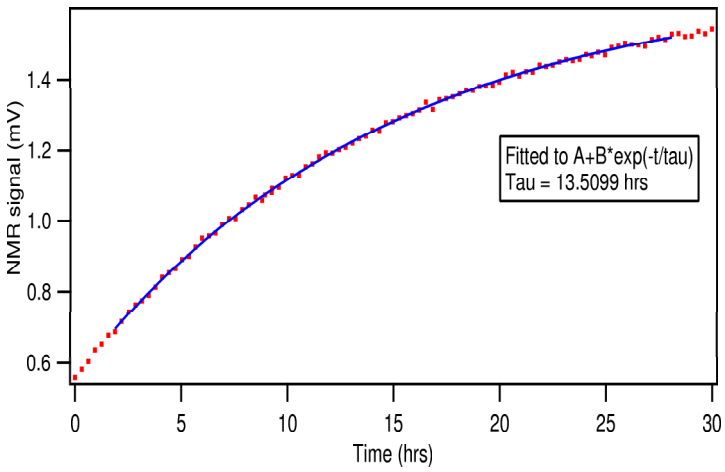

Figure 4.3: Plot showing the pumping up of ^{3}He polarization in Pebbles. The rate constant for the pump up was 1/(13.5 hrs).

NMR is following ^{3}He polarization confirming that the short term decay in polarization was real. Both, NMR and transmission method showed a drop of approximately $\approx$2.4%.

Ionization effects on rubidium optical pumping were observed for the first time in work with 180 particle-nA beam of 18 MeV alpha-particles [27]. It was seen there that the depolarization rate depends on the total pressure of the target, the presence of the N_2 impurities and on the magnetic field. But, for use in neutron beams this effect was considered to be negligible as the ionization energy loss is 100 to 10,000 times less. We therefore decided to measure the effects of the neutron beam on the alkali-metal polarization in high-flux neutron beams.

4.3 Scaling of the Depolarization with Neutron Flux

Neutron sources also produce gammas along with neutrons. After seeing ^{3}He depolarization in polarizer cells when exposed to neutron beam, the major concern was to know if the depolarization was caused by neutrons or by gammas. If the depolarization was due to neutrons and proportional to the neutron flux then the

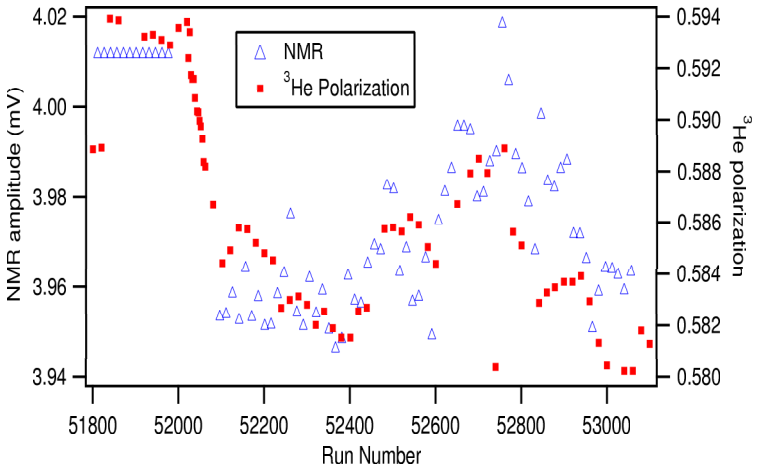

Figure 4.4: ^{3}He polarization and NMR data. Left axis is the NMR data for the cells and right axis is the ^{3}He polarization measured using transmission ratio method. From both the measurements polarization drop was ≈2.4%.

effect would be worse at the SNS where the neutron flux will be higher. But if the effect is due to the gammas the cells will not see any depolarization at SNS as the flight path at SNS is curved and the gammas will not reach the experiment. Therefore it became important to understand the effect of neutron flux, theoretically and experimentally. This section shows the depolarization estimation for the SNS beamline, where the SNS neutron flux is scaled to LANSCE neutron flux.

The ^{3}He polarization is given by [11]

$$P_{He} = P_{Rb}\frac{k_{SE}[Rb]}{k_{SE}[Rb](1+X)+\Gamma_r}; \tag{4.2}$$

where P_{Rb} is the volume averaged Rb polarization. For Pebbles, $\gamma_{SE} = k_{SE}[Rb] = (1/12)h^{-1}$ and $\Gamma = (1/240)h^{-1}$ and therefore the maximum achievable polarization for Pebbles is 95.2%, which is considered to be the X factor limited polarization if rubidium polarization is 100%. X factor limited polarization is defined such that $1/(1+X)$ limits the maximum attainable polarization when Rb is 100% polarized. For the runs shown in figure 4.1 the maximum polarization that we achieved for "Pebbles" was approximately 54.0% which decayed to approximately 50.6% when

the beam was on for 13 hours (figures 4.1 and 4.2).

As we believed that it was the Rb polarization which was affected because of the neutron flux, we started with the effect of neutron beam on Rb polarization and therefore on ^{3}He polarization. The rubidium polarization in a polarizer cell in the absence of neutron beam is given by [11],

$$P_{Rb} = \frac{\gamma_{opt}}{\gamma_{opt} + \Gamma_{SD}} \tag{4.3}$$

where γ_{opt} is the photon scattering rate per alkali-metal atom for an unpolarized vapor, Γ_{SD} is the alkali-metal polarization relaxation rate. But in the presence of beam ^{3}He polarization starts to decrease with a time constant of approximately (1/13) hrs. We can therefore add a term, Γ_{beam}, to the denominator of equation 4.3. Γ_{beam} is responsible for the relaxation of the alkali-metal polarization in the presence of neutron beam. Thus, P_{Rb} is given by,

$$P_{Rb} = \frac{1}{1 + \frac{\Gamma_{SD}}{\gamma_{opt}} + \frac{\Gamma_{beam}}{\gamma_{opt}}} \tag{4.4}$$

where $\frac{\Gamma_{SD}}{\gamma_{opt}}$ is the ratio between the alkali-metal polarization relaxation rate to the photon scattering rate per alkali-metal atom for an unpolarized vapor and $\frac{\Gamma_{beam}}{\gamma_{opt}}$ is the ratio between the alkali-metal polarization relaxation rate to the photon scattering rate per alkali-metal atom for an unpolarized vapor in the presence of neutron beam. For LANSCE conditions when the Rb polarization dropped to 50.6%, equation 4.4 in terms of the value of $\frac{\Gamma_{SD}}{\gamma_{opt}}$ and $\frac{\Gamma_{beam}}{\gamma_{opt}}$ is

$$0.506 = \frac{1}{1 + 0.759 + 0.118}; \tag{4.5}$$

where $\frac{\Gamma_{SD}}{\gamma_{opt}} = 0.118$. With increasing neutron flux if this factor scales up the depolarization in the cells will be more at SNS than LANSCE. Therefore, it became important to understand the effect of neutrons in the ^{3}He polarizer cells.

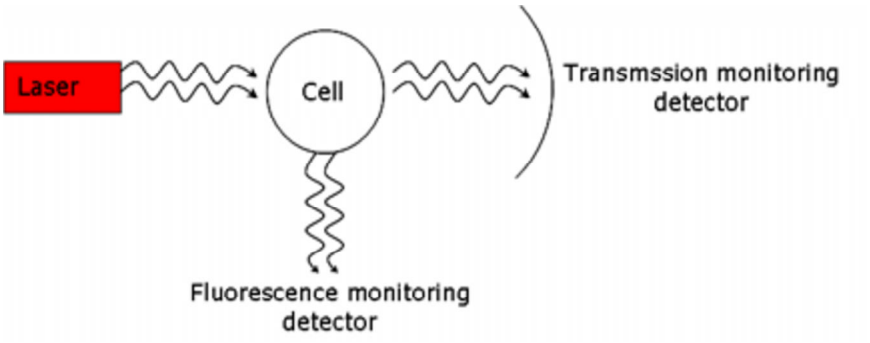

Figure 4.5: Methods to measure Rb polarization: fluorescence monitoring and transmssion monitoring.

4.4 Rb Polarimetry Experiment at LANSCE

Rubidium spin polarization can be monitored using optical methods in which we measure the photon scattering rate which gives information about the degree of spin polarization of the Rb atoms. The measured signal is a combination of two terms: the mean photon scattering rate, R and a second term which is polarization dependent, $-2R < S_z >$. There are two ways to detect this scattering rate: florescence monitoring and transmission monitoring [41]. In florescence monitoring, the amount of florescence scattered light from the optically pumped atoms and in transmission monitoring the attenuation of the pumping light after it has passed through the cell is measured. The two methods are illustrated in figure 4.5. Fluorescence signal is measured in a direction perpendicular to the direction of propagation of the laser light and the transmission signal is measured in the same direction as the direction of propagation of the laser light.

The cells used for the NPDGamma experiments were large and the florescence signal was small due to the size and the presence of the quenching gas, N_2. Nitrogen is present in spin filter cells to eliminate radiation trapping and collisional mixing of the levels. Therefore, it was not practical to do the florescence monitoring on

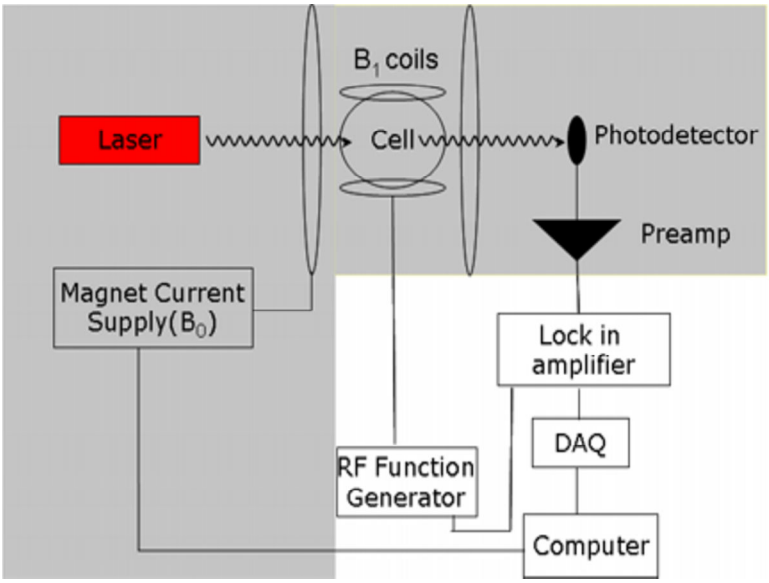

Figure 4.6: A block diagram of the experimental set up used at LANSCE for Rb polarization measurement. Transmitted laser light from the cell during a magnetic field sweep was recorded by a photodetector.

these cells and we decided to do the transmission monitoring to determine the Rb polarization.

4.4.1 Experimental Set Up for the Measurement of Rb Polarization

Figure 4.6 shows the experimental set up for the measurement of Rb polarization in the presence of neutron beam. The experiment was performed at FP12 at the LANSCE in Summer 2007. The cell was placed in an uniform magnetic field, B_0, of about 30 Gauss. One set of coils, which was designed during the NPDGamma experiment, was providing a very homogenous magnetic field of 10 Gauss. Additional 20 Gauss was provided by an extra pair of hand-wound rectangular coils wound around the polarizer oven. A photograph of the pair of hand-wound coils is shown in figure 4.7. The dimensions of the coils were 35.5 cm $\times$ 53.5 cm separated by a distance of 18 cm and each of the coils had 51 turns. A Kepco power supply was used to provide power to the smaller coils to control them externally for the magnetic field sweep. National Instruments Data Acquisition device was used to control the

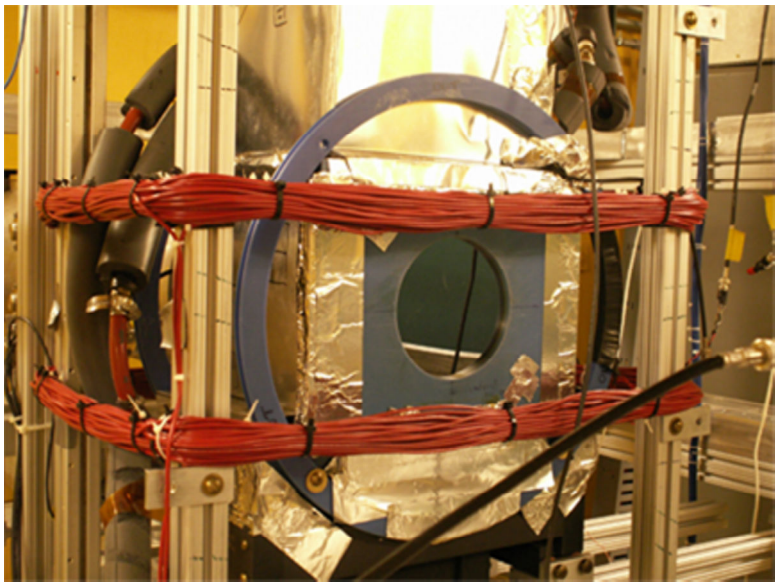

Figure 4.7: The red coils are the hand wound magnetic field coils used to produce 20 Gauss of magnetic field for the Rb polarimetry experiment. Dimensions of the coils were 14 in × 21 in separated by 18 cm and N=51 turns.

magnetic field sweep for the transitions. The RF field, B_1 was provided by a separate set of coils driven by a function generator. The frequency of the amplitude of this signal was also modulated using the function generator. Laser light at 795 nm and 30 Watts was incident on the cell. Laser light transmission through the cell during the sweep was recorded using a photodetector, amplified by a pre-amplifier and then recorded using the DAQ device. The part of the experiment in the shaded region in figure 4.6 was inside the shielded cave and the rest of the experiment was outside the cave.

4.4.2 Theory

Rubidium has two isotopes ^{85}Rb and ^{87}Rb with nuclear spin $I = 5/2$ and $I = 3/2$, respectively. In its natural form, the isotopic fractions of Rb are 72% ^{85}Rb and 28% ^{87}Rb. In the experiment, we measured the signal from ^{85}Rb using Electron Spin Resonance (ESR). ESR signal is obtained due to the coupling of atom's magnetic moment with a magnetic field.

The Hamiltonian for an alkali-metal in a transverse sinusoidal magnetic field of amplitude B_x is [9]

$$H = \sum_m E_m |m><m| + g_s \mu_B S_x B_x \cos(\omega t). \tag{4.6}$$

Using the density of matrix approach the equation of motion for the coherence between states $|m>$ and $|m-1>$, $\rho_{m,m-1}$, is given by

$$i\frac{d\rho_{m,m-1}}{dt} = (E_m - E_{m-1})\rho_{m.m-1} - i\gamma\rho_{m.m-1} + V_{m,m-1}(\rho_m - \rho_{m-1}) \tag{4.7}$$

where ρ_m and ρ_{m-1} are the probabilities to be in state $|m>$ and $|m-1>$ with energy E_m and E_{m-1} respectively and γ is the decay rate. Assuming the coherence form to be $\rho_{m,m-1} = \sigma e^{-i\omega t}$ and $V = g_S \mu_B S_x B_x$, equation 4.7 can be solved for σ steady state. In steady state,

$$\sigma = \frac{<m|V|m-1>}{2(\Delta + i\gamma)}(\rho_{m-1} - \rho_m) \tag{4.8}$$

where $\Delta = (\omega - E_m + E_{m-1})$. The behavior of the density of the sublevels $|m>$ and $|m-1>$ are defined by the equations,

$$i\hbar\frac{d\rho_m}{dt} = \frac{<m|V|m-1>\sigma^* - <m-1|V|m>\sigma}{2}, \tag{4.9}$$

$$i\hbar\frac{d\rho_{m-1}}{dt} = \frac{<m-1|V|m>\sigma - <m|V|m-1>\sigma^*}{2}. \tag{4.10}$$

If only one resonance is driven at a time by the RF field, the difference in the population density of the two states $|m>$ and $|m-1>$ is

$$\frac{d(\rho_m - \rho_{m-1})}{dt} = \frac{\gamma}{\Delta^2 + \gamma^2/4}\left(\frac{g_s \mu_B B_x}{2I+1}\right)^2 (F(F+1) - m(m-1))\frac{\rho_{m-1} - \rho_m}{4}. \tag{4.11}$$

Thus, the signal observed for any transition is proportional to $(F(F+1) - m(m-1))(\rho_{m-1} - \rho_m)$. Equation 4.11 gives the area of the peak for one transition. If we

have more than one transition, the ratio of the area under two successive peaks can be written as

$$A = \frac{F(F+1) - m(m-1)}{F(F+1) - (m-1)(m-2)} \frac{\rho_{m-1} - \rho_m}{\rho_{m-2} - \rho_{m-1}}. \tag{4.12}$$

Equation 4.12 can be simplified using the definition of spin temperature. The spin sublevels $|F, m>$ of total spin angular momentum $F = I \pm 1/2$ and azimuthal quantum number m are populated with a probability very close to the spin temperature limit:

$$\rho(F, m) = \frac{e^{\beta m}}{\mathcal{Z}} \tag{4.13}$$

where $\mathcal{Z}$ is called the partition function, $\mathcal{Z} = \sum_{F,m} e^{\beta m}$ [85]. The parameter β is called the spin-temperature and is defined as $\beta = 2 \tanh^{-1} P_{Rb}$. Spin temperature is defined as the temperature at which the observed ratio of parallel to antiparallel spins will be the same ratio as if the gas is in thermal equilibrium. The importance of spin temperature was first discussed by Anderson *et al.* [8]. Using this definition of spin temperature equation 4.12 is

$$A = \frac{F(F+1) - m(m-1)}{F(F+1) - (m-1)(m-2)} e^{\beta}. \tag{4.14}$$

In terms of spin temperature, electron spin polarization is [42]

$$P = 2 < S_z >= \tanh(\beta/2) = \frac{e^{\beta/2} - e^{-\beta/2}}{e^{\beta/2} + e^{-\beta/2}} = \frac{e^{\beta} - 1}{e^{\beta} + 1}. \tag{4.15}$$

Electron spin resonance (ESR) is due to the coupling of the atom's magnetic moment with a magnetic field, intrinsic or applied. It involves the coupling of the energy from the applied field to the atomic spin system with a natural frequency due to the Zeeman splitting. The energy shift, E for a resonance with given F and m at field B_0 is [57],

$$E(F, m) = -\frac{h\delta\nu_{hfs}}{2(2I+1)} - g_I \mu_B B_0 m \pm \frac{h\delta\nu_{hfs}}{2} \sqrt{1 + \frac{4m}{2I+1} x + x^2} \tag{4.16}$$

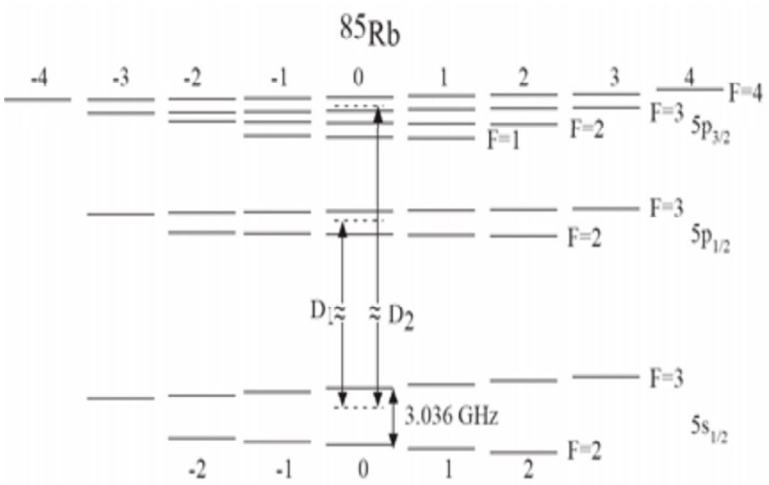

Figure 4.8: Hyperfine splittings of ^{85}Rb

where F is the total spin quantum number, m is the projection of F along the quantization axis and x is,

$$x = \frac{(g_J + g'_I)\mu_B B_0}{h\delta\nu_{hfs}} \tag{4.17}$$

where $h\delta\nu_{hfs} = \Delta E$ is the energy of the hyperfine splitting of the particular alkali-metal isotope and $(g_J + g'_I) \approx g_S$ for ground state alkali-metal atoms ($g_I << g_S$). The magnetic resonance transitions correspond to $\Delta F = 0$ and $\Delta m = \pm 1$. Using equation 4.16, an approximation of the splitting between adjacent transitions can be written as,

$$\nu_{F,m\leftarrow m-1} - \nu_{F,m-1\leftarrow m-2} = \frac{2\mu_0^2}{\delta\nu_{hfs}(2I+1)^2} \tag{4.18}$$

where ν_{hfs} is the hyperfine splitting of the particular alkali-metal isotope. The hyperfine splitting, ν_{hfs}, is 3.036 Hz for ^{85}Rb and 6.835 Hz for ^{87}Rb. Figure 4.8 shows the energy level diagram and the hyperfine splittings for ^{85}Rb. Because of the high value of hyperfine splitting for ^{87}Rb, the ESR lines for this isotope are not resolved. Its easier to resolve the lines for ^{85}Rb and therefore our analysis has been done with data taken with ^{85}Rb.

Figure 4.9 shows the possible ESR spectrum of Rb if all the transitions are properly

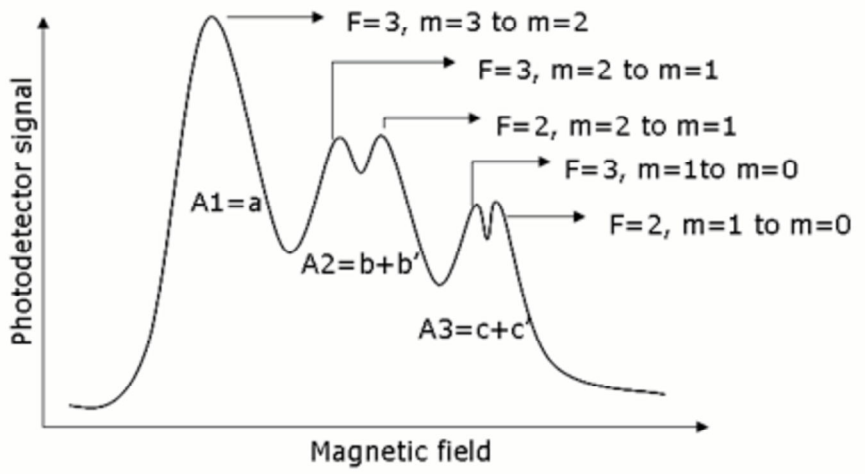

Figure 4.9: A diagram showing the transitions in Rb during a magnetic field sweep. The figure shows resolved and unresolved transitions.

resolved. All the transitions in the diagram are labeled. The area enclosed by the transition $F = 3, m = 3 \rightarrow m = 2$ is given by $A_1 = a$. A_2 is the area enclosed by the two peaks b and b' where b is the transition due to $F = 3, m = 2 \rightarrow m = 1$ and b' is due to the transition $F = 2, m = 2 \rightarrow m = 1$. Similarly, A_3 is the area enclosed by the combined transition of the two peaks c and c' where they are the $m = 1 \rightarrow m = 0$ transitions for both $F = 3$ and $F = 2$. The ratio of the area under two successive peaks is calculated using equation 4.14. The ratio of the area between a and b is calculated to be,

$$\frac{a}{b} = \frac{3}{5}e^{\beta}. \tag{4.19}$$

Similarly, the ratio of the areas for other transitions are

$$\frac{b}{c} = \frac{5}{6}e^{\beta}, \tag{4.20}$$

$$\frac{b'}{c'} = \frac{2}{3}e^{\beta}. \tag{4.21}$$

To calculate the ratios b'/a and c'/c we used the relations for Rb polarization when the peaks are resolved and when they are not resolved. When all the Rb peaks are

resolved i.e. when a and b are properly resolved Rb polarization for ^{85}Rb is given as,

$$P = \frac{5A - 3}{5A + 3} \tag{4.22}$$

where $A = a/b$ and when the peaks are not resolved Rb polarization for ^{85}Rb is given as,

$$P = \frac{7A' - 3}{7A' + 3} \tag{4.23}$$

where $A' = a/(b + b')$. As the polarization remains constant whether the peaks are resolved or not, we equate equations 4.22 and 4.23 and calculate

$$\frac{a}{b'} = \frac{3}{2}e^{\beta}. \tag{4.24}$$

Similarly,

$$\frac{b}{c'} = \frac{5}{3}e^{\beta}. \tag{4.25}$$

We used these ratios in our analysis for obtaining the value of Rb polarization in the cell.

4.5 Analysis and Results

The relationships of the areas of two successive peaks for the Rb absorption spectrum were shown in the previous section. These relationships were used to calculate the rubidium polarization of the data we collected. For our case, the peaks were not resolved properly because of the inhomogeneity of the magnetic field in which the cell was placed and therefore the transitions $m = 2 \rightarrow m = 1$ and $m = 0 \rightarrow m = 0$ for F=2,3 are unresolved.

Figure 4.11 shows the data used to measure the Rb polarization. Here we measured the laser light transmission through the polarizer cell during the magnetic field sweep with varying neutron flux. The blue curve shows the neutron beam off data

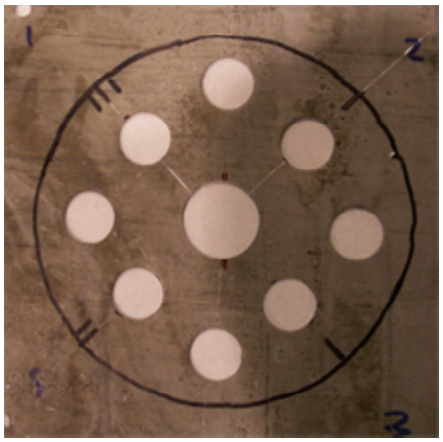

Figure 4.10: "Swiss cheese collimator" used for reducing the neutron flux. With this collimator the neutron flux was reduced to 19% of the maximum.

i.e. no neutrons were incident on the cell. The green curve shows the data taken when the full neutron flux coming from the source was incident on the cell and the red curve is the data for reduced neutron flux. We used Cd collimators upstream of the polarizer to reduce the neutron flux. Cd collimators were used for two reasons: (1) they are good neutron absorbers (2) they do not absorb the gammas from the neutron source and they produce gammas themselves. So, these collimators were helpful in determining whether the decay was caused by the gammas or the neutrons. Figure 4.10 shows the Cd collimator we used. This collimator was passing only 19% of the neutron beam. If the depolarization was caused by the neutrons it was expected that Rb polarization would go down with increasing neutron flux.

We used a Lorentzian function with three peaks to obtain the value of Rb polarization from the data. Using the Lorentzian function, the area under a peak is given by,

$$\begin{aligned} A_P &= \int_{\infty}^{\infty} D \frac{\Gamma/2\pi}{(\omega-\omega_0)^2 + (\frac{\Gamma}{2})^2} \\ &= D\Gamma\pi \end{aligned} \tag{4.26}$$

where Γ is the width of the peak. In our case we had three peaks in the data and

therefore we used a function with three Lorentzian terms. The area of the peaks are different for the three peaks given by A_1, A_2 and A_3 (figure 4.9). We calculated both $A_2 = b + b'$ and $A_3 = c + c'$ in terms of A_1 and an additional parameter $Z = e^{\beta}$. If the area occupied by the first peak is,

$$A_1 = a \tag{4.27}$$

then the ratio of the area occupied by the second unresolved peak which is the combination of b' and b to the first peak is

$$\begin{aligned} \frac{A_2}{A_1} &= \frac{b' + b}{a} \\ &= \frac{7}{3}\frac{1}{Z}. \end{aligned} \tag{4.28}$$

Similarly, the ratio of the area occupied by the third unresolved peak to the first peak is

$$\begin{aligned} \frac{A_3}{A_1} &= \frac{c' + c}{a} \\ &= \frac{3}{Z^2}. \end{aligned} \tag{4.29}$$

Equations 4.27, 4.28 and 4.29 were used to replace the coefficients in the Lorentzian fit equation. The model used for the fitting is

$$F(B_i) = y_0 + \sum_i A_i \frac{(\Gamma/2\pi)^2}{(B_i - B_0)^2 - (\Gamma/2)^2}, \tag{4.30}$$

where y_0 is the offset and A_i is the area of each peak, B_0 is the field at resonance frequency and Γ is the width of the peaks. The fits were done with a single Γ. Thus Z was determined from the fits and Rb polarization was calculated using

$$P_{Rb} = \frac{Z - 1}{Z + 1}. \tag{4.31}$$

Figure 4.11 shows the laser transmission measurement during the magnetic field sweep for different neutron flux incident on the cell. The laser transmission through

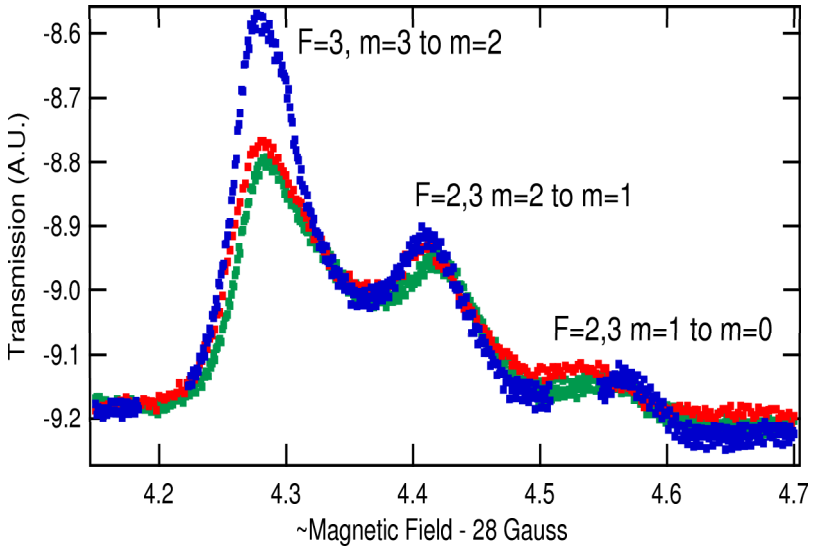

Figure 4.11: ESR spectra of ^{85}Rb for full flux (green), 19% of full flux (red) and no beam (blue) at LANSCE.

the cell was maximum when the beam was off and minimum when neutron flux was the maximum. The values of Rb polarization for varying neutron flux are tabulated in table 4.1.

Neutron Intensity	Rb polarization	Error
0	0.658	0.001
0.19	0.597	0.002
1	0.575	0.001

Table 4.1: Variation of Rb polarization with neutron flux. 0 in the first column beam means no beam on the cell, 0.19 is 19% of the maximum neutron flux is on the cell and 1 is maximum neutron flux on the cell. The third column gives the error on the Rb polarization

4.6 Calibration

If an oscillating field is applied with RF frequency almost equal to the resonance frequency, $\omega_{RF} \approx \omega_0$, there is an effective additional relaxation and Γ changes to,

$$\Gamma = \Gamma_0 + \Gamma_{RF} \tag{4.32}$$

where Γ_0 is the intrinsic combination of wall relaxation and other mechanisms, but does not include the spin exchange, which conserves the Rb polarization. The rate of RF induced transitions, Γ_{RF} depends on the frequency and magnitude of the applied RF field (V_{RF}). The relation between Γ_{RF} and V_{RF}^2 is given by [3],

$$\Gamma_{RF} \propto V_{RF}^2. \tag{4.33}$$

Any change in Γ leads to a change of Rb polarization with exponential time dependence. Therefore, we need to calibrate the polarizer cell to obtain the Rb polarization P_0 in the absence of the RF field i.e. when $V_{RF} = 0$.

In the presence of the RF field, alkali metal polarization can be written as

$$\frac{1}{P_{Rb}} = 1 + \frac{\Gamma_{SD}}{\gamma_{opt}} + \frac{\Gamma_{RF}}{\gamma_{opt}}. \tag{4.34}$$

Therefore, from equations 4.33 and 4.34

$$\frac{1}{P_{Rb}} \propto V_{RF}^2. \tag{4.35}$$

For measurement of P_{Rb} vs V_{RF}^2, the LANSCE set up was used again in Michigan after the run. Again, we used two coils to produce 30 Gauss magnetic field. The rectangular coils shown in figure 4.7 were used to produce approximately 20 Gauss of magnetic field and additional 10 Gauss was provided by a pair of Helmholtz coil. The LANSCE data was taken at $V_{RF} = 4V$ at a cell temperature of 165^0C. Because

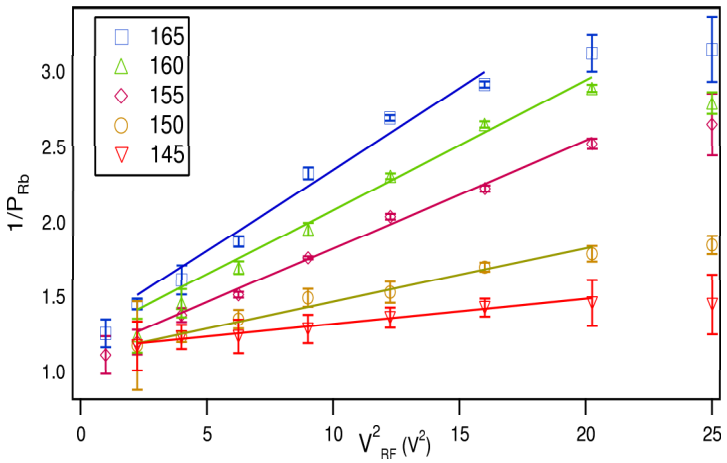

Figure 4.12: $1/\mathrm{P}_{Rb}$ plotted vs V_{RF}^2 at different temperatures. These curves were individually fitted to a line to obtain P_0 at $V_{RF} = 0$. The error bars on the values are obtained from the Lorentzian fits done to the data.

of the inability to reproduce the experimental set up exactly we decided to take the laser light transmission data through the cell as a function of V_{RF} at different temperatures and extrapolate the data to zero for all the temperatures to get P_0' (Polarization at a temperature T when $V_{RF} = 0$). P_0 at $V_{RF} = 0$ was calculated by taking the average of all the P_0''s. The LANSCE data was calibrated using this value of P_0. Figure 4.12 shows the plot for $1/\mathrm{P}_{Rb}$ vs V_{RF}^2 for different temperatures.

4.7 Observations from the ILL Run

The LANSCE run was followed by a different set of runs at ILL. In the ILL runs ESR measurements were performed at 10 Gauss with a hybrid Rb-K cells constructed at NIST. The Zeeman splitting of potassium is much larger than that of Rb and allows each of the ESR resonances of ^{39}K to be fully resolved at 10 Gauss as shown in figure 4.13. The signals from ^{87}Rb and ^{41}K can also be resolved [10]. The rapid spin exchange between the Rb and K allows the ESR of potassium to measure the concentration-averaged electron polarization of all the alkali-metal species [8]. The cell was illuminated with light from two 100 Watt narrowed diode-laser-array-bars

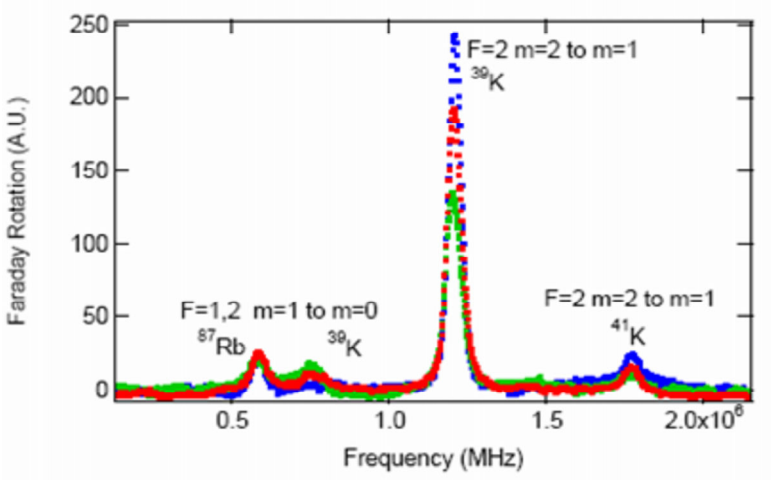

Figure 4.13: ESR spectra of ^{39,41}K and ^{87}Rb ESR for full flux (green) and 8.5% of full flux (red) and 0.9% (blue) at ILL.

[21]. A linearly polarized probe laser tuned near the Rb D2 resonance and directed along the magnetic field was used to measure the Faraday rotation signal, which is proportional to the alkali metal polarization [75]. The RF field was swept over a range of approximately 600 kHz around 7 MHz and the data extrapolated to zero power. For I=3/2, $P_{Rb} = (2R-1)/(2R+1)$, where R is the area under the peak.

Figure 4.14 shows the change $\Delta(1/P_A)$ relative to no beam as a function of neutron capture-flux density ϕ_n for both the LANSCE and ILL data. The ILL experiment used ten-fold-higher power, narrowed lasers, therefore the neutron-beam effects were significantly reduced at a given neutron flux density compared to the LANSCE data. This confirmed that the Rb polarization decays with the neutron flux which explains the depolarization in the ^{3}He cells. It is also confirmed now that the neutrons and not the gammas are responsible for the depolarization. This set of measurements confirmed the decay of the alkali metal polarization when exposed to the neutron beam.

The alkali-metal polarization, which varies with position inside the cell and is

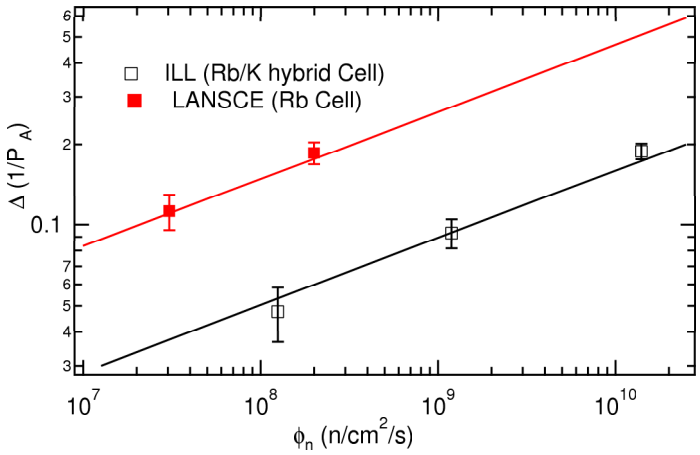

Figure 4.14: Polarization results for both LANSCE (solid squares) and ILL (open squares) plotted as the change in $(1/P_A)$ relative to no beam. The solid lines are proportional to $\phi_n^{1/4}$

written as,

$$\frac{1}{P_A(\vec{r})} = 1 + \frac{\Gamma_{SD}}{\gamma_{opt}(\vec{r})} \tag{4.36}$$

where $\gamma_{opt}(\vec{r})$ is the convolution of the laser spectral profile and the optical absorption cross section at the position $\vec{r}$. The spin destruction rate, Γ_{SD}, is the rate of electron spin-flips per alkali-metal atom. Equation 4.36 shows that the primary effect of the neutron beam must be an increase of Γ_{SD}, therefore electron spin destruction rates were directly measured at ILL using the relaxation in the dark technique [35]. The relaxation in the dark technique makes use of a low power (<0.1 W/cm^2) optical pumping beam to produce a small alkali-metal polarization. The optical pumping light was chopped at 1 Hz, and P_A was measured by Faraday rotation. With the optical pumping beam chopped off, the polarization decays with a time constant that is slower than Γ_{SD}. The slowing factor $S \geq 1$ accounts for the angular momentum stored in the nuclear spins, which couple to the electron spin through the hyperfine interaction [77]. Due to electron spin-exchange, the factor S is an average over isotopes and alkali-metal species in each cell and depends on the alkali-metal polarization. For low polarization, S=10.8 for natural rubidium and S=6 for potas-

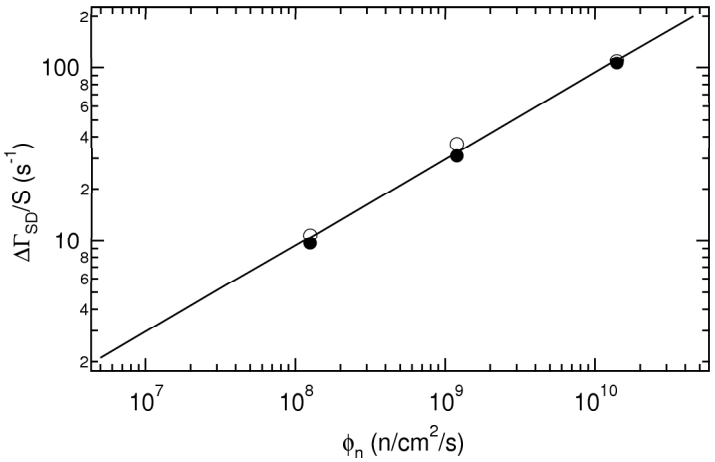

Figure 4.15: ILL results for $\Delta\Gamma_{SD}$ for two cells, a pure Rb (open circles) and a K-Rb hybrid cell (closed circles). The solid line is given by $\phi_n^{1/2}$, provided to guide the eye.

sium. The results for a pure rubidium cell and for the hybrid cell are shown in figure 4.15. The relaxation as a function of the neutron flux showed the form $\Delta\Gamma_A \propto \sqrt{\phi_n}$, which is consistent with relaxation due to a recombination-limited equilibrium ion concentration.

4.7.1 Cause of the Depolarization

The reaction which is happening inside the cell when neutrons are incident on a cell is n+^{3}He$\rightarrow$ p+^{3}H. The reaction also releases 764 keV of energy for every capture. This energy can cause the ionization of the species present inside the cell and can form metastable ^{3}He atoms, molecular ions and radicals of helium and nitrogen. The observed depolarization behavior may be due to one or more of these species. Let the decrease in the relaxation rate be given by $\Delta\Gamma_A = k_e n_e + \sum_j k_j n_j$, where k_j is the relaxation rate constant for the j species, n_e is the density of neutrons produced due to ionization in the cell and n_j is the density of an ion species. The production of the ion species depends on the electron density and therefore, $n_j = f_s n_e$ where f_s is a fraction of the electron density and $f_s = 1$ if there is only one ion species.

The rate equation for the change in the electron density is

$$\frac{dn_e}{dt} = \sum_i \gamma_i \phi_n - n_e \sum_i \alpha_j n_j. \tag{4.37}$$

The first term is the production of electrons due to the ionization caused by the neutrons. The rate of production of electrons due to the ionization of different atoms or molecules is γ_i and ϕ_n is the neutron flux. The second term is responsible for the consumption of the electrons by the different ionized species present inside the cell, α_j is the recombination coefficient for each species. Assuming there is one dominant species present inside the cell equation 4.37 becomes

$$\frac{dn_e}{dt} = \sum_i \gamma_i \phi_n - n_e \alpha_d n_d, \tag{4.38}$$

where n_d is the dominant species and $n_d = f_d n_e$. The steady state solution of the equation is

$$n_e = \sqrt{\frac{\sum_i \gamma_i \phi_n}{\alpha_d f_d}}, \tag{4.39}$$

where α_d and f_d are the recombination coefficient and fraction of the electron density for the dominant species. And as $\Delta\Gamma_A \propto n_e$

$$\Delta\Gamma_A \propto \sqrt{\phi_n}. \tag{4.40}$$

Ddependence of alkali-metal polarization on neutron flux, ϕ_n, was observed from both the LANSCE and ILL data. Electron spin destruction measurements from ILL showed the square root dependence of relaxation on neutron flux. Therefore, it is believed that the decay in the relaxation rate is affected by one dominant species which is produced due to the ionization inside the cell.

4.8 Conclusions

^{3}He polarization measurement in the NPDGamma experiment showed us the depolarization behavior in the spin filter cells exposed to neutron beam. To understand

Figure 4.16: A double cell, "Tweety". In double cells pumping is done at one part and this part is not exposed to neutron beam to avoid the depolarization due to ionization.

the effect of the neutron beam on the polarizer cells we performed an experiment to measure the electron polarization of Rb at LANSCE. This measurement was followed by another experiment at ILL which used hybrid Rb-K cells. In both the runs we observed a decrease in the Rb polarization with increasing neutron flux.

Also, the relaxation rate was measured for the alkali-metal polarization at ILL and this study showed that the electron spin destruction has a square root dependence on the neutron flux. In summary, both the LANSCE and ILL measurements showed that the incident neutron beam increases the alkali metal relaxation rate which decreases the alkali-metal polarization and therefore the ^{3}He polarization decreases. The decrease in Rb polarization explained the ^{3}He depolarization we saw in the polarizer cells during the NPDGamma experiment.

A possible solution to the Rb depolarization is to eliminate the effect of ionization on the Rb optical pumping with the use a double cell [23]. Figure 4.16 shows a photograph of one of the double cells built. A double cell is a target with two chambers. In one of the chamber optical pumping of Rb takes place and the second chamber can be exposed to the neutron beam. Thus, the ionization inside the cells due to exposure of Rb to neutrons can be eliminated. Use of double cells in neutron

experiments could provide a possible solution in future.

These cells can still be used as polarizer with higher laser power. From the ILL data it was concluded that if high intensity narrowed lasers are used the depolarization is less. But for experiments where stable polarization for a longer period is required these cells cannot be used as polarizer. But, they can definitely be used as analyzers in experiments as an analyzer does not require high and stable polarization. ^{3}He spin filter cell was used as an analyzer for the precision polarimetry experiment conducted at LANSCE in Summer 2007. This experiment is discussed in detail in the next chapter.

CHAPTER V

Precision Polarimetry

Since the discovery of the weak interaction, precision measurements in polarized neutron decay have played an important role in the development and understanding of the Standard Model and in probing new physics. Neutron β-decay provides highly sensitive test of the electroweak interaction. Information about the electroweak interactions is contained in the β-decay correlation coefficients. Observables in β-decay are angular correlation between the spins and momenta of the particles involved in β-decay. Within the Standard Model, measurement of these correlation coefficients permits the most precise determination of the relative axial-vector coupling constant λ of the weak coupling constants. Observables in these experiments depend linearly on the product of the neutron polarization and therefore the precision measurement of these coefficients is limited by the precision of the neutron beam polarization measurement. So it becomes important to understand the uncertainties in the neutron polarization. We performed the precision polarimetry experiment with the aim of measuring the neutron polarization to a high precision. Neutron β-decay, its importance and the motivation for the precision polarimetry experiment is discussed in this chapter. The chapter also presents a discussion of the experiment and the analysis carried out for the precision polarimetry.

5.1 Neutron β-Decay

In β-decay, a neutron decays to a proton and an electron along with an antineutrino

$$n \rightarrow p + e \quad + \nu_e,$$

where a down quark converts to an up quark emitting a W^- boson which then decays to an electron and an antineutrino. If J is the vector angular momentum of the neutron and m_e is the mass of the electron, the distribution in electron and neutrino directions and electron energy for an allowed transition from an oriented nucleus is given by[46]

$$\frac{d\Gamma}{dE_e d\Omega_e d\Omega_\nu} \propto G_F^2 |V_{ud}|^2 F(E_e) \left[1 + a\frac{\vec{p}_e.\vec{p}_\nu}{E_e E_\nu} + b\frac{m_e}{E_e} + \frac{\vec{J}}{J}.\left(A\frac{\vec{p}_e}{E_e} + B\frac{\vec{p}_\nu}{E_\nu} + D\frac{\vec{p}_e \times \vec{p}_\nu}{E_e E_\nu} \right) \right] \quad (5.1)$$

Here $\vec{p}_e$ and $\vec{p}_\nu$ are the momenta of the electron and the neutrino, respectively, E_e and E_ν are the energies of the electron and the neutrino, respectively, and G_F is the Fermi coupling constant. V_{ud} is the up and down quark mixing element in the Cabibbo-Kobayashi-Maskawa (CKM) matrix. In equation 5.1, a determines the electron-neutrino correlation, A the beta asymmetry, B the neutrino asymmetry and D is a T-odd term. Within the Standard Model these coefficients are given as

$$\begin{aligned} a &= \frac{1-|\lambda|^2}{1+3|\lambda|^2}, \\ b &= 0, \\ A &= 2\frac{Re(\lambda)-|\lambda|^2}{1+3|\lambda|^2}, \\ B &= 2\frac{Re(\lambda)+|\lambda|^2}{1+3|\lambda|^2}, \\ D &= 2\frac{Im(\lambda)}{1+3|\lambda|^2}, \end{aligned}$$

where λ is the ratio of axial-vector to vector coupling constants, $\lambda = g_A/g_V$. The coefficient b is zero in the Standard Model, but would be non-zero if scalar interactions

exist. The initial and final hadronic state in the β-decay are spin 1/2, thus the allowed decay has both $\Delta J = 0$ and $\Delta J = 1$. $\Delta J = 0$ part is a pure vector and the strength is proportional to,

$$g_V = G_F V_{ud}, \tag{5.2}$$

where G_F is the Fermi coupling constant measured in muon decays, V_{ud} is an element in the CKM matrix. $\Delta J = 1$ part is axial vector and is proportional to g_V,

$$g_A = \lambda g_V. \tag{5.3}$$

The Standard Model predictions have been tested precisely in the weak decays of light quarks. The CKM matrix in the Standard Model relates the quarks in the weak interaction basis (d_W, s_W, b_W) to the quarks in the strong interaction eigenstate basis (d, s, b). This quark mixing matrix is given by,

$$\begin{pmatrix} d_W \\ s_W \\ b_W \end{pmatrix} \begin{pmatrix} V_{ud} & V_{us} & V_{ub} \\ V_{cd} & V_{cs} & V_{cb} \\ V_{td} & V_{ts} & V_{tb} \end{pmatrix} = \begin{pmatrix} d \\ s \\ b \end{pmatrix} \tag{5.4}$$

where V_{ud} is the u and d quark mixing matrix element. The matrix elements of the CKM matrix are determined from the weak decays of the relevant quarks. From equation 5.1, neutron decay rate is proportional to the CKM matrix element squared, $|V_{ud}|^2$. V_{ud} is measured from superallowed nuclear beta decays [43]. The Standard Model gives a constraint on the matrix elements by the unitarity condition. The unitarity condition for the CKM matrix elements is

$$|V_{ud}|^2 + |V_{us}|^2 + |V_{ub}|^2 = 1 - \Delta. \tag{5.5}$$

In the standard model, Δ is zero. But, since 1995 the unitarity test has been found not to hold true for so far unknown reasons, and $\Delta \neq 0$ is suggested [1]. The

contribution of $|V_{ub}|^2$ in equation 5.5 is of $2\times\ 10^{\ -5}$ level and can be ignored [1]. Therefore, the significant contributors to the equation are $|V_{us}|^2$ and $|V_{ud}|^2$. $|V_{us}|$ has been measured from a variety of kaon-decay experiments and it is suggested that the unitarity is solved if the currently accepted value of $|V_{us}|$ is shifted by 2σ [1]. Because of the large magnitude of $|V_{ud}|$, a precise determination of this matrix element therefore becomes important. With more accurate value of V_{ud}, the unitarity problem of the CKM matrix could possibly be resolved.

$|V_{ud}|$ can be derived from neutron β-decay without significant nuclear structure effects. Although there are different ways to determine this factor, e.g. Superallowed Fermi transitions in nuclear β-decay, through $\pi\beta$ decay etc., determining $|V_{ud}|$ using neutron beta decay has an advantage as the determination of $|V_{ud}|$ solely depends on two experimental inputs, the neutron lifetime τ_n and λ calculated from the measurement of angular correlation coefficients in the β-decay. Accurate measurements of the neutron lifetime and the angular coefficients will provide a value for the hadronic vector weak interactions constant. In terms of τ_n and λ, $|V_{ud}|$ is given as

$$|V_{ud}|^2 = \frac{K}{G_F^2\tau_n(1+3\lambda^2)f(1+RC)} = \frac{(4908\pm 1.9)s}{\tau_n(1+3\lambda^2)}, \tag{5.6}$$

where f is the phase space factor and K is a constant and $(1+RC)$ is the electroweak radiative corrections to the neutron decay rate. Thus V_{ud} can be calculated by knowing λ and neutron lifetime τ_n and the CKM unitarity can be tested.

Many experiments have been designed to measure these correlation coefficients in the β-decay. Some of these experiments are abBA, Nab, aCORN, UCNA etc. abBA is an experiment proposed for the SNS FnPB and aims to measure the a, b, B and A in the neutron β-decay. The aCORN experiment plans to measure the angular correlation between the beta electron and antineutrino in the nuclear beta decay, a. Nab is another experiment proposed for the SNS where it plans to measure a and b

in the β-decay. If one wants to measure A and B to a high precision it is important to know the neutron polarization accurately as the observables in these experiments depend on the neutron polarization.

Apart from the coefficients expressed in equation 5.1, there is another parameter which can be measured in the neutron beta decay: the proton asymmetry (C), which is the correlation between the neutron spin and proton momentum in the beta decay. The scientific community has also expressed interest in this parameter and a significant amount of theoretical as well as experimental work has been done for the measurement of this quantity [24, 40, 63]. PERKEO is an experiment which finished data collection for the proton asymmetry and the analysis is in progress [63]. Another experiment which aims to measure the C parameter is the Proton Asymmetry in Neutron Decay Apparatus (PANDA). The importance of the experiment and why it makes the neutron polarization accuracy important is discussed in the next section.

5.2 The PANDA Experiment

Examples of angular correlation coefficients are the electron asymmetry parameter A, the neutrino asymmetry parameter B etc. from where λ can be derived in the Standard Model. They have been measured several times with increasing precision and are still in focus. But, the correlation between the neutron spin and proton momentum in the β-decay has never been measured until 2001. In 2001 the first measurement of the C coefficient was carried out using the PERKEO II electron spectrometer at ILL[63].

The correlation of the recoil proton momentum with the spin of a decaying neutron

in a polarized neutron beta decay can be expressed as

$$\frac{d^3\Gamma}{dE_p d\Omega_P} = G(E_p)[1 + \kappa(E_P, \Omega_P)C]\hat{\sigma}.\hat{p_p}, \tag{5.7}$$

where $\hat{\sigma} = \frac{\vec{J}}{J}$ and C is the coefficient of the parity violating correlation and κ is a kinematic factor. From the Standard Model C can be calculated using the correlation parameters A and B,

$$\begin{aligned} C &= -k(A+B) \\ &= 4k\frac{Re(\lambda)}{1+3|\lambda|^2} \approx 0.866, \end{aligned} \tag{5.8}$$

where k is a kinematical factor which depends on β-energy and proton energy range. Thus C is a new input parameter for the study of neutron decay and "possible" new physics. Precise measurement of C will also lead to a better understanding of the recoil-order terms with the hadronic currents. In the proton asymmetry experiment, the asymmetry can be determined using,

$$A_P = \frac{N_+ - N_-}{N_+ + N} = kCA(1-f)P_n. \tag{5.9}$$

Here N_+ and N_- are respectively, the number of protons emitted with $\hat{\sigma}.\hat{p_p} > 0$ and $\hat{\sigma}.\hat{p_p} < 0$ integrated over all proton energies, P_n is the averaged neutron polarization, A is the analyzing power of the proton detector and f is the fraction of protons due to the background.

Figure 5.1 shows the summary of the status of neutron β-decay. It shows V_{ud} versus λ from different experiments, including PERKEO II, neutron lifetime measurements and Particle Data Group (PDG). Neutron lifetime results from PDG and the most recent precise measurement is shown in the plot. The figure also shows the precision which will be obtained if 0.1% of C measurement is performed successfully.

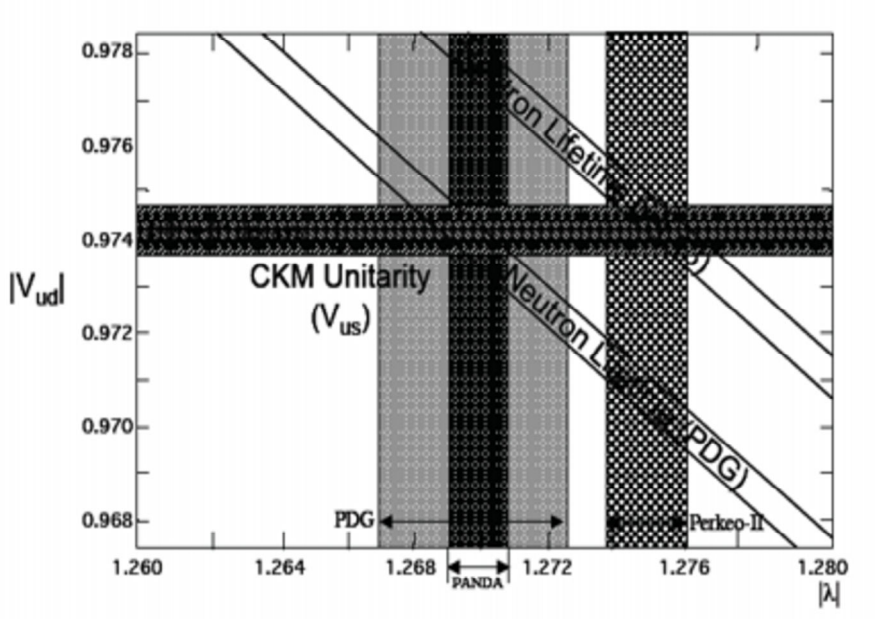

Figure 5.1: Beta decay results and the V_{ud} value obtained from the recent superallowed decays and from $|V_{us}|$+CKM Unitarity. The band labeled PANDA indicates the value of V_{ud} obtained from a 0.1% measurement of the proton asymmetry [24].

λ	-1.2695±0.0029	SM(lowest order)	$\lvert d\lambda/dx\rvert$	$\lvert\frac{\sigma_\lambda}{\lambda}\rvert/\lvert\frac{\sigma_x}{x}\rvert$
a	-0.103±0.004	$\frac{1-\lvert\lambda\rvert^2}{1+3\lvert\lambda\rvert^2}$	3.227	0.2618
A	-0.1173±0.0013	$-2\frac{Re(\lambda)+\lvert\lambda\rvert^2}{1+3\lvert\lambda\rvert^2}$	2.661	0.2459
B	+.983±0.004	$-2\frac{Re(\lambda)-\lvert\lambda\rvert^2}{1+3\lvert\lambda\rvert^2}$	13.66	10.58
C	-0.865±0.013	$4\frac{Re(\lambda)}{1+3\lvert\lambda\rvert^2}$	2.193	1.494
D	-0.0004±0.0006	$\frac{Im(\lambda)}{1+3\lvert\lambda\rvert^2}$		
ϕ	180.06±0.0029			

Table 5.1: Standard Model formulae for neutron beta decay correlation coefficients and accepted λ values [83].

The figure also includes the result from the superallowed $0^+ \rightarrow 0^+$ decays, recent results based on CKM unitarity and $|V_{us}|$ from a variety of kaon decay experiments.

The value of $\lambda = g_A/g_V$ can be calculated using different correlation coefficients of the neutron decay. Table 5.1 shows the currently accepted value of λ and the correlation coefficients. The values of λ from these correlation coefficients and therefore V_{ud} from different experiments with proper corrections becomes a test of the Standard Model as if the value of λ is inconsistent it has to be explained with some new physics. Possibility of a right-handed boson with different couplings and greater mass than the Standard Model W will lead to the modification of β-decay correlation coefficients. These right handed currents will introduce more parameters in the V/A theory and therefore new physics.

The proton asymmetry coefficient, C, is sensitive to the right handed currents. A 0.1% measurement of C would significantly improve the current limits. Table 5.1 shows that λ is less sensitive to C than a or A and at the same time C is almost a magnitude larger than a and A. Therefore, measurement of C is subjected to different and less complicated systematic errors. A 0.1% measurement of C with calculated corrections is therefore feasible and will have a significant impact in the determination of λ and therefore g_A and V_{ud}.

5.3 Importance of Neutron Polarization

The proton asymmetry equation 5.9 shows the dependence of A_P on the neutron polarization and indicates that a 0.1% precise measurement of C requires 0.1% determination of the neutron polarization for both spin states (parallel and anti-parallel to the guide field). It also shows that the significant systematic errors in this measurement arise from neutron polarimetry, backgrounds and detector analyzing

power.

The dependence of the uncertainty of C on the neutron polarization is

$$\sigma_C \propto \frac{\sigma_{P_n}}{P_n^2} \tag{5.10}$$

. Therefore, it becomes important to understand the uncertainties on the neutron polarization to attain our goal of 0.1% measurement of C. Because of the dependence of C on P_n we decided to do the neutron polarization measurement with high precision in the experiment called "The Precision Polarimetry Experiment Using ^{3}He Spin Filters". With ^{3}He spin filters, we can attain high neutron polarization for slow neutrons, low gamma-ray backgrounds and also the extra advantage of using AFP with which we can flip the polarization direction of the neutrons with respect to the magnetic field and thus independently can determine the spin-flipper efficiency.

While performing the NPDGamma experiment we observed that background plays an important role in the determination of neutron polarization. Backgrounds can be due to the wrap around neutrons from the penultimate pulse, scattering from the target, back-scattering from the spin flipper and other equipments in the beamline. These background issues need to be understood properly and proper corrections should be made in order to determine the neutron polarization to a precision of 0.1%. "The Precision Polarimetry Experiment Using ^{3}He Spin Filters" was performed at LANSCE FP12 to understand these issues.

5.4 Precision Polarimetry using ^{3}He Spin Filters

During the NPDGamma experiment, ^{3}He and neutron polarizations were monitored for a long period of time and it was discovered that backgrounds play an important role in limiting the accuracy of the polarization analysis. The oscillations in some of the beam off runs in figure 3.19 are of the order of few $\times 10^{-4}$. For 10,000

pulses and a few percent monitor efficiency , the relative statistical error should also be less than 10^{-4} for a 500 second run. The uncertainties are therefore dominated by systematic effects [26]. A large class of effects are removed in the analysis by taking the transmission ratios however, this assumes the accurate subtraction of the background. But, in addition to the backgrounds there are other sources which may give rise to systematic effects like rate dependence on the monitors and electronics, non linearities etc. In section 3.9.5 we showed that a significant amount of correction was made to the systematics by adding backgrounds to the monitor data. This emphasizes the importance of low and well understood backgrounds for attaining precision neutron polarimetry.

Classical method for the polarization analysis uses a supermirror polarizer as the analyzer [88]. This method uses a polarizer, spin flipper and an analyzer. The limitations of this method are that the spin flipper efficiency and the analyzing power of the analyzer (defined as the polarization which an initially unpolarized beam would have acquired after passing through the analyzer) need to be known for the analysis. One needs to determine the analyzing power of the analyzer which involves the use of three supermirror polarizers and several spin flippers. It is difficult to characterize supermirrors with well defined analyzing power. Also, determining the spin flipper efficiency using a supermirror polarizer is not easy and requires two spin flippers between the beam polarizer and the analyzer.

To overcome the problems of the classical polarization analysis scheme Zimmer proposed a new method of measuring neutron polarization using ^{3}He spin filter as analyzer [88]. ^{3}He analyzers overcame the limitations of the supermirror analyzers. The analyzing power A of a spin filter is

$$A = \tanh(nl\sigma P_{He}), \tag{5.11}$$

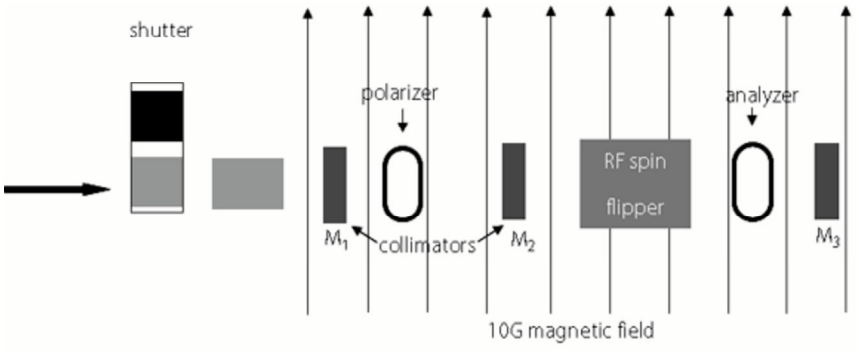

Figure 5.2: Schematics of the experimental set up of the precision polarimetry experiment. The whole experiment was placed in a magnetic field of 10 Gauss. The neutrons pass through different neutron detectors (monitors) placed at different stages of the experiments to measure the transmission of the neutrons.

where σ is the neutron absorption cross section, P_{He} is the ^{3}He polarization, n is the density and l is the thickness of the medium. The quantity $x = nl\sigma P_{He}$ is called the "opacity" of the spin filter. The freedom to choose opacity offers the possibility to reduce the uncertainty in A to the desired level of accuracy by making x large and thus the uncertainty on the value of neutron polarization due to the inaccurate knowledge of the analyzing power is reduced. Another important advantage of ^{3}He spin filter is that they can be polarized either parallel or anti-parallel to the magnetic field. Also, AFP can be performed on the polarizer cells to flip the ^{3}He polarization and the spin flipper efficiency can be determined in a straightforward way (discussed in section 5.8). Neutron polarimetry with ^{3}He spin filters was first demonstrated by Zimmer *et al.* in 1999 [89].

The experimental set up for the precision polarimetry experiment is shown in figure 5.2. Three monitors were used to measure the neutron transmission at different stages of the experiment. The experiment also used a polarizer, a spin flipper and an analyzer. Placing an analyzer after the spin flipper was a significant addition to this experimental set up. The analyzer was used to analyze the polarization of the neutron beam coming out of the spin flipper. Details of the experiment and the analysis are presented in the following sections.

5.5 The Experiment

Precision polarimetry was set up to run in Summer 2007 at the flight path 12 of the Los Alamos Neutron Science Center (LANSCE) and data was collected in July 2007. During the analysis, it was discovered that M2 data was affected by some unexpected oscillations, which affected the quality of the data we collected and hence the precision polarimetry analysis was affected.

The experiment used the basic experimental set up from the NPDGamma experiment with some modifications. The whole experiment was placed inside a 10 Gauss magnetic field, to polarize the neutrons and to transport the neutrons through the experiment downstream of the polarizer. Unpolarized neutrons from the source pass through the polarizer placed after the monitor, M1. The polarizer makes the neutron transversely polarized along the direction of the B field. Neutron transmission through the polarizer was monitored using a second monitor M2. The polarized neutrons then pass through the spin flipper and finally through the analyzer. The transmission through the analyzer was recorded using monitor M3 placed after the analyzer. A picture of the experimental set up is shown in figure 5.3.

A detailed discussion of the experimental set up for the polarizer was provided in chapter III. For this experiment we used the same kind of set up for both polarizer and analyzer except for that both the systems were running on one laser each. The laser light to the polarizer and analyzer was provided using Coherent FAP laser. Each laser was providing about 30 watts of laser power. The system was running at a temperature of $(150 \pm 5)\ ^{0}$C . The details of the ^{3}He spin filter polarization were provided in chapter III. The analyzer was also polarized the same way as the polarizer. "Dino" and "Pebbles" were used as the polarizer and the analyzer, respectively.

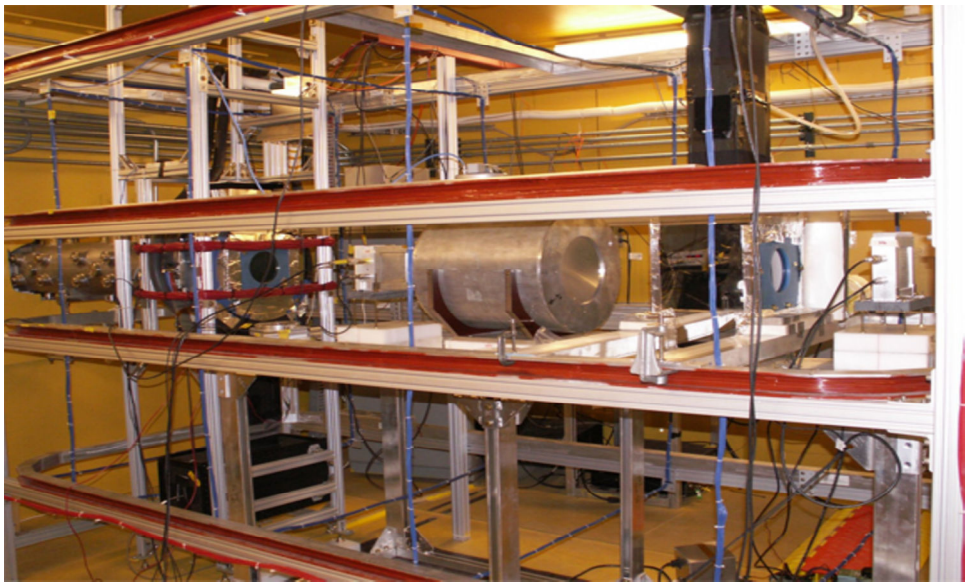

Figure 5.3: Photograph of the experimental set up of precision polarimetry experiment at FP12 at the Los Alamos Neutron Science Center

For the precision polarimetry experiment it was required to define the beam size with proper collimation to reduce the neutron beam divergence. We used a beam of one inch diameter for our studies. The beam was collimated using Cadmium collimators on the monitors. Cd collimators were used for collimation because Cd has a high absorption cross section for neutrons and therefore it absorbs all the unwanted neutrons. There was a 1" collimator after M1 and a second collimator was placed on M2 so that M2 sees the same size beam as the polarizer.

5.6 Neutron Polarization

Experiments have been done in the past by others to measure the neutron polarization precisely [89]. Precision neutron polarimetry was developed with the aim to determine the neutron polarization to 0.1%. The idea of the experiment was to measure the neutron polarization (after the neutrons come out of the ^{3}He polarizer) at two different points: (a) at monitor 2 and (b) after the spin flipper, and to compare these values to see the accuracy.

There are two different ways to determine the neutron polarization using the data recorded by the three monitors. In the first method, we determine the neutron polarization at M2 using the data taken by monitors 1 and 2. In the second method, we determine the neutron polarization after the spin flipper using the data taken by monitors 2 and 3. The two methods are discussed in detail in sections 5.6.1 and 5.6.2 respectively.

To do the polarization measurements we need to determine the thicknesses, $(nl)_x$, of the cells used as the polarizer and the analyzer. These values are obtained using the data taken for the unpolarized ^{3}He cell runs and empty oven runs. Once the thicknesses of the cells are determined, they can be used for the polarization measurement. The thickness measurement for the cells used will be discussed in section 5.9.1.

5.6.1 Neutron Polarization Using M1 and M2

This method uses the same transmission method which was used for the NPDGamma experiment. The data recorded by monitors 1 and 2 were used to determine the neutron polarization at M2, immediately after the polarizer. Unpolarized neutrons from the source after passing through M1 were incident on the ^{3}He polarizer. The neutron transmission of spin up(+) and spin down(-) neutrons through a ^{3}He polarizer is

$$N_{\pm} = \frac{N_0}{2} e^{(-\sigma x_P (1 \mp P_P))}, \tag{5.12}$$

where N_0 is the number of incident neutrons, $x_P = (nl)_P$ is the thickness of the polarizer cell, P_P is the polarization of the ^{3}He polarizer and σ is the absorption cross section which has a wavelength dependence, $\sigma = (\sigma_0/\lambda_0)\lambda$, where σ_0 is the absorption cross section for neutrons at wavelength λ_0. Therefore, when the cell is

unpolarized (P_P=0) the neutron transmission through the polarizer cell, T_0 is,

$$T_0 = \frac{N_+ + N_-}{2} = \frac{N_0}{2} e^{-(\sigma x_P)} \tag{5.13}$$

and the neutron transmission through a polarized cell, T_P, is

$$T_P = \frac{N_+ - N}{2} = \frac{N_0}{2} e^{-(\sigma x_P (1 - P_P))} = T_0 \cosh(\sigma x_P P_P). \tag{5.14}$$

The neutron polarization, P_n, at any wavelength λ is defined as the ratio of the difference in the spin up and down neutrons to the total number of neutrons and is given by,

$$P_n(\lambda) = \frac{N_+(\lambda) - N_-(\lambda)}{N_+(\lambda) + N_-(\lambda)} = \tanh(\sigma x_P P_P) = \sqrt{1 - \frac{1}{\cosh^2(\sigma x_P P_P)}}. \tag{5.15}$$

Because of this known transmission behavior of the neutrons through the polarized and unpolarized ^{3}He cell, we can use the data recorded at M1 and M2 for the polarization analysis of the neutrons coming out of the polarizer. The signal recorded at M1 gives an indirect measure of the neutron flux incident on the experiment. M1 signal is directly proportional to the neutron flux and therefore, used to normalize the signals at M2 and M3. In terms of M1 and M2, the transmission equations are given as

$$T_0 = \left(\frac{M2}{M1}\right)_{UP} = e^{-(\sigma x_P)}, \tag{5.16}$$

$$T_P = \left(\frac{M2}{M1}\right)_{P} = T_0 \cosh(\sigma x_P P_P), \tag{5.17}$$

$$P_n = \sqrt{1 - \left(\frac{T_0}{T_P}\right)^2} = \sqrt{1 - \left(\frac{\left(\frac{M2}{M1}\right)_{UP}}{\left(\frac{M2}{M1}\right)_{P}}\right)^2}. \tag{5.18}$$

Thus, M1 and M2 data can be used to determine the neutron polarization at the second monitor M2.

5.6.2 Neutron Polarization Using M2 and M3

The second method used to determine the neutron polarization is to measure the polarization using the data recorded by M2 and M3. Neutrons coming out of the polarizer were recorded at M2. These neutrons then pass through the spin flipper and the analyzer to reach the third monitor, M3. The signal recorded at M2 and M3 is proportional to the polarization of the polarizer and the analyzer. If the polarization is high the signal will be big and vice versa. Signal recorded at M3 also depends on the spin flipper efficiency. Details of the spin flipper efficiency calculation is discussed in section 5.8. A spin flipper flips the spin of a neutron pulse when the spin flipper is on and when the flipper is off the neutron pulse passes through the flipper unaffected. A detailed discussion of the functioning of the RFSF was presented in Chapter III. We used the same spin flipper from the NPDGamma experiment for this experiment.

An analyzer is another ^{3}He polarizer cell placed after the spin flipper. It is used to analyze the polarization of the neutron beam coming out of the polarizer. The transmission through an analyzer is the same as the transmission through a polarizer. The transmission for spin up and down neutrons through a polarizer which has a polarization P_A and thickness $x_A = (nl)_A$ is

$$T_+^A = e^{(-\sigma x_A(1\mp P_A))}. \tag{5.19}$$

The transmission through the analyzer when the spin flipper is off, just depends on the polarization of the analyzer and is given by

$$\frac{T_{A,P}^{SFOff}}{T_{A,0}} = \cosh(x_A P_A) + \sinh(x_A P_A)\tanh(x_P P_P). \tag{5.20}$$

The transmission through the analyzer when the neutron pulses get flipped by the spin flipper depends on the spin flipper efficiency and the analyzer polarization.

Therefore, it becomes important to determine the spin flipper efficiency accurately. The transmission through the analyzer with spin flipper on is

$$\frac{T_{A,P}^{SFOn}}{T_{A,0}} = \cosh(x_A P_A) + (1-2\epsilon)\sinh(x_A P_A)\tanh(x_P P_P). \tag{5.21}$$

In equations 5.20 and 5.21, $T_{A,0}$ is the transmission through the analyzer when its unpolarized and ϵ is the spin flipper efficiency. A detailed discussion of these derivations is provided in appendix B. To determine the polarization using M2 and M3 data, first we need to determine the polarization of the analyzer which is required to determine the neutron polarization after the spin flipper. Analyzer polarization can be obtained by adding equations 5.20 and 5.21

$$\frac{1}{2\epsilon}\left[(2\epsilon-1)\left(\frac{T_{A,P}^{SFOff}}{T_{A,0}}\right) + \left(\frac{T_{A,P}^{SFOn}}{T_{A,0}}\right)\right] = \cosh(x_A P_A). \tag{5.22}$$

The value of analyzer polarization can be extracted by doing a hyperbolic cos fit to the quantity in equation 5.22. Neutron polarization after the spin flipper, P_n', can be obtained by subtracting equation 5.21 from 5.20,

$$\begin{aligned}\frac{1}{2\epsilon}\left[\left(\frac{T_{APol}^{SFOff}}{T_{A,0}}\right) - \left(\frac{T_{APol}^{SFOn}}{T_{A,O}}\right)\right] &= \sinh(x_A P_A)\tanh(x_P P_P) \\ &= P_n'(\lambda)\sinh(x_A P_A). \end{aligned}\tag{5.23}$$

Using the value of P_A calculated from equation 5.22, neutron polarization as a function of wavelength is written as,

$$P_n'(\lambda) = \frac{1}{2\epsilon T_{A,0}} \frac{T_A^{SFOff} + T_A^{SFOn}}{\sqrt{\cosh^2(x_A P_A) - 1}}. \tag{5.24}$$

Thus neutron polarization for the neutrons coming out of the spin flipper can be calculated using the data collected by the monitors M2 and M3.

5.7 Analyzer

The goal of the precision polarimetry experiment is to analyze the polarized neutron beam coming out of the spin flipper for its polarization. This was achieved using a second ^{3}He polarizer after the spin flipper which we called the analyzer. The position of the analyzer is shown in figure 5.2. Analyzer was used to analyze the neutron polarization in both the states of the neutron spin flipper (on and off) by measuring the transmission of neutrons through it.

The heating system for the analyzer was the same as discussed in section 3.5.2. The analyzer was polarized using 30 watts of laser light from a Coherent FAP laser. The oven had the ability to maintain the cell at (145-155)^{0}C to polarize the Rb inside the cell which in turn polarizes ^{3}He present in the cell. The experimental set up employed a spin flipper between the polarizer and the analyzer. A guide field was applied between the polarizer and the analyzer in order to avoid non-adiabatic transitions of the neutron-spin. The analyzer cell was used for two purposes in the experiment: (a)tuning of the spin flipper for the best value of magnetic field and RF amplitude and (b) analysis of the neutron beam for the polarization.

Analyzers are characterized by the quantity analyzing power given in equation 5.11. The uncertainty in A is

$$\delta A = x\mathrm{sech}x\sqrt{\left(\frac{\delta n}{n}\right)^2 + \left(\frac{\delta l}{l}\right)^2 + \left(\frac{\delta P}{P}\right)^2}. \tag{5.25}$$

Thus the uncertainty in the analyzing power to the desired level of accuracy can be achieved by increasing the opacity, x, of the spin filter and thereby approaching an ideal analyzer [88]. For $x = 3.8$ which implies $nl = 19.09$ amagat cm the analyzing power of the cell is $A \geq 99.9\%$. For the cell we used in our experiment the thickness was measured to be $nl = 3.60 \pm 0.02$ amagat cm and therefore the analyzing power

of the cell was $A \geq 61.5\%$. We were limited by the cells we had available.

5.8 Spin Flipper Efficiency

Precision polarimetry experiment used the same spin flipper that was used in the NPDGamma experiment. The details of this spin flipper were discussed in chapter III. In section 5.6.2, we noticed that the measured neutron polarization depends on the spin flipper efficiency and analyzer polarization. Dependence of neutron polarization on the spin flipper efficiency is given by

$$\sigma_{P_n} \propto P_n \left(\frac{\sigma_\epsilon}{\epsilon}\right). \tag{5.26}$$

Therefore, to do a 0.1% measurement of neutron polarization it becomes important to determine the spin flipper efficiency precisely. The spin flipper and the method used to obtain the spin flipper efficiency is described in this section.

A spin flipper rotates the neutron spin by an angle θ that depends on the neutron velocity or wavelength so that the neutron polarization changes from P_n^+ to P_n^- and are related as $P_n^- = -P_n^+$. A spin flipper can be accurately characterized by averaging $\theta(\lambda)$, $\epsilon =< \cos\theta(\lambda) >$, where ϵ [65] is the spin flip efficiency. The effect of the spin flip efficiency on the polarization in terms of the θ is written as

$$P_n^- = (1 + 2 < \cos(\theta(\lambda)) > P_n^+, \tag{5.27}$$

where P_n^+ is the spin state of the neutrons before the flip and P_n^- is the spin state after the flip. For a perfect spin flipper $< \cos(\theta(\lambda)) >= -1$, i.e. $\theta = \pi$, so that the spin reversal is perfect. But, as we are limited by the experimental conditions there is some deviation from the perfect reversal, so $\theta = \pi - \delta$ so that $P_n^- = (1 - 2 < \cos(\delta(\lambda) >)P_n^+$. Thus for an imperfect spin flipper the efficiency is less than one.

For the experiments which will measure the correlation coefficients precisely, we aim to measure the δ^2 to a precision of 10^{-4} or less. The spin flip efficiency can

be calculated using the crossed polarizer technique. The schematics of the crossed polarized method is shown in figure 5.4. In the crossed polarizer technique, ^{3}He polarization direction in the polarizer is flipped using Adiabatic Fast Passage (AFP). By flipping ^{3}He polarization in the polarizer using the AFP technique a nearly-perfect reversal of neutron beam polarization can be performed. AFP flipped beam can be compared with the spin flipper flipped beam to determine the beam polarization reversal efficiency of the spin flipper.

The crossed polarizer technique needs four sets of measurements: (a) both polarizer and analyzer polarized in same direction and spin flipper off, (T_{SFOff}), (b) polarizer and analyzer polarized in same direction and spin flipper on, (T_{SFOn}), (c) polarizer and analyzer polarized in opposite directions and spin flipper off, (T^{AFP}_{SFOff}) and (d) polarizer and analyzer polarized in opposite directions and spin flipper on, (T^{AFP}_{SFOn}). From figure 5.4 it is seen that the signal at M3 is almost similar for case (a) and (d) and similar for (c) and (d). These four sets of measurements are used to determine the spin flipper efficiency.

Flipping the direction of ^{3}He spins in the polarizer using AFP changes the direction of ^{3}He polarization, and therefore the transmission of neutrons through the polarized cell changes to

$$N^{\pm}_{AFP} = \frac{N_0}{2} T^{\pm}_P = \frac{N_0}{2} e^{-x_P(1\mp P_P)}. \tag{5.28}$$

These neutrons then transmit through the spin flipper and the analyzer. The total transmission of the AFP flipped neutrons recorded by M3 is

$$\begin{aligned} T^{AFP,SFoff}_{A,P} &= \frac{T^{+,AFP}_P T^{+}_A + T^{-,AFP}_P T^{-}_A}{T^{+}_P + T^{-}_P} \\ &= T_{A,0}\cosh(x_A P_A) - \sinh(x_A P_A)\tanh(x_P P_P). \end{aligned} \tag{5.29}$$

Here $T^{AFP,SFoff}_{A,P}$ is the transmission through the polarized analyzer after performing

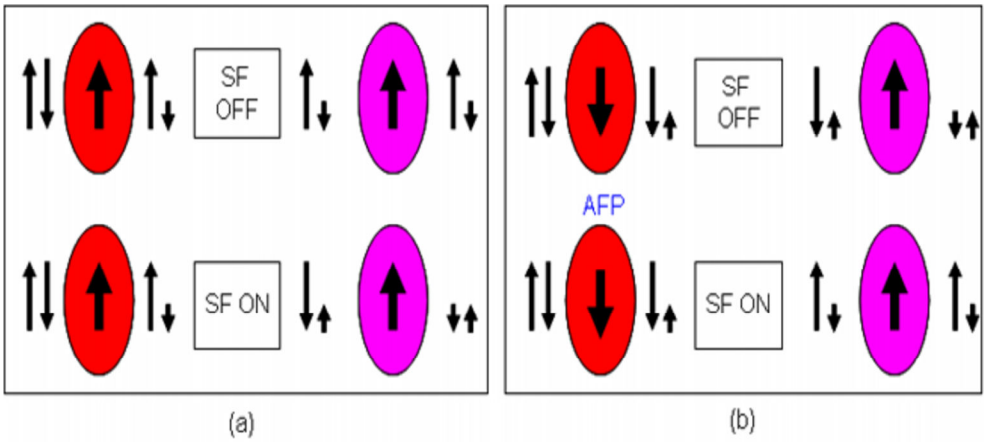

Figure 5.4: Figure showing the crossed polarizer configuration for determining the spin flipper efficiency. Figure (a) depicts the configuration when polarizer and analyzer are polarized in the same direction. Fig (b) is the configuration for polarizer and analyzer polarized in opposite direction. AFP is performed on the polarizer to change the direction of ^{3}He polarization. In both cases, transmission is observed for both spin flipper on and off.

AFP on the polarizer cell and spin flipper off, $T_P^{+,AFP}T_A^+$ is the transmission of the spin up neutrons through the analyzer and $T_P^{-,AFP}T_A^-$ is the transmission of the spin down neutrons through the analyzer. Thus, if we have the data with spin flipper on and off in normal polarization direction and the AFP data for both spin flipper on and off configuration the spin flipper efficiency can be calculated using these transmission signals. There are two ways to determine the spin flipper efficiency. First method is to determine the spin flipper efficiency, ϵ, using the AFP data when the spin flipper is off with the normal polarization data

$$\epsilon = \frac{T_{A,P}^{SFOff} - T_{A,P}^{SFOn}}{T_{A,P}^{SFOff} - T_{A,P}^{AFP,SFOff}}.$$

Second method to determine the spin flipper efficiency of the spin flipper is to use the AFP data with spin flipper on. Neutron transmissions are different with spin flipper on and spin flipper off as can be seen from figure 5.4. When AFP is performed on

the polarizer and the spin flipper is on, the neutron transmission is given by

$$\begin{aligned} T_{A,P}^{SFOn} &= \frac{T_{AFP}^{+,SFOn}T_A^+ + T_{AFP}^{-,SFOn}T_A^-}{T_{AFP}^+ + T_{AFP}^-} \\ &= \frac{(1-\epsilon)T_{AFP}^+ + \epsilon T_{AFP}^-}{T_{AFP}^+ + T_{AFP}^-}T_A^+ + \frac{\epsilon T_{AFP}^+ + (1-\epsilon)T_{AFP}^-}{T_{AFP}^+ + T_{AFP}^-}T_A^- \\ &= T_{A,0}[\cosh(x_A P_A) + (1-2\epsilon)\sinh(x_A P_A)\tanh(x_P P_P)]. \end{aligned} \tag{5.30}$$

Here $T_{A,0}$ is the neutron transmission through unpolarized analyzer, T_A^+ and T_A^- are the transmissions of spin up and down neutrons through polarized analyzer, respectively and T_{AFP}^+ and T_{AFP}^- are the transmissions of spin up and down neutrons through the polarizer after AFP, respectively . Therefore the spin flipper efficiency can be calculated using

$$\frac{T_{SFOff} - T_{SFOn}}{T_{SFOff} - T_{SFOn}^{AFP}} = \frac{\epsilon}{1-2\epsilon}.$$

Solving,

$$\epsilon = \frac{T_{SFOff} - T_{SFOn}}{3T_{SFOff} - 2T_{SFOn} - T_{SFOn}^{AFP}}. \tag{5.31}$$

Thus we have two methods to determine the efficiency of a spin flipper. The efficiency can be calculated using both the methods and can be compared. All the T's in this analysis section are $M3/M2$ i.e. the signal recorded at M3 was normalized using the signal at M2. Once the spin flipper efficiency is calculated, one can calculate the neutron polarization.

Spin flipper efficiency was calculated using both the methods discussed above. Figure 5.5 shows the spin flipper efficiency calculated by averaging the values obtained using the two methods versus wavelength. This figure has few interesting things to be noted. For a perfect spin flipper, $\epsilon = 1$ and for non-perfect spin flippers $\epsilon < 1$. But this plot showed that at certain wavelengths spin flipper efficiency was greater than 1. This was due to the oscillations in M2 and M3 mentioned before.

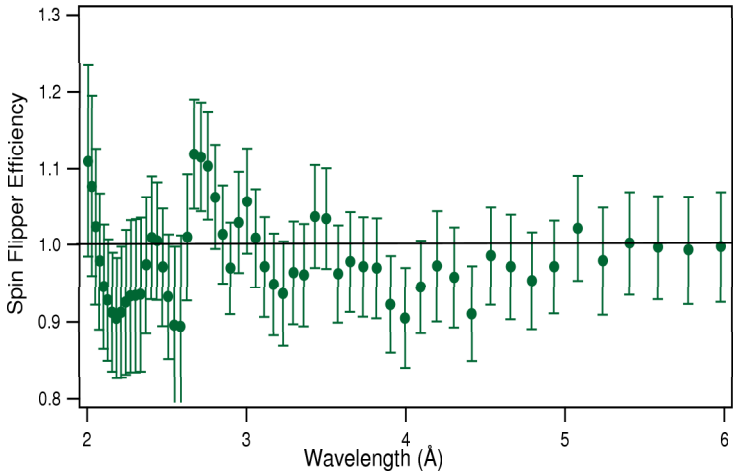

Figure 5.5: Spin flipper efficiency vs wavelength of the spin flipper used for the experiment. The oscillations from M2 and M3 affected the quality of the data which is seen in this plot between 2 $\mathring{A}$ to 3 $\mathring{A}$. In particular, spin flipper efficiency cannot exceed unity.

These oscillations affected the quality of data M2 and M3 recorded and therefore the inappropriate behavior of the spin flipper.

5.9 Analysis and Results

The data for the experiment was collected using an analog to digital converter (ADC). A small fraction of the incident neutron beam was captured by the monitors and a signal was produced. This signal passes through the pre-amplifier to the ADC interfaced with the computer. The schematics of the data acquisition (DAQ) is shown in figure 5.6. The ADC values from the monitors were converted to voltage using

$$V_i = \frac{(ADC)_i - a_i}{b_i}, \tag{5.32}$$

where V_i is the voltage recorded at the ith monitor, $(ADC)_i$ is the value recorded for the i^{th} ADC, a_i is the offset in the ADC's and b_i is the number of ADC counts equivalent to 1 volt. The DAQ was storing 112 samples in every 50 ms with an offset of 3 samples. Figure 5.6 shows the schematics of the data acquisition used for the experiment.

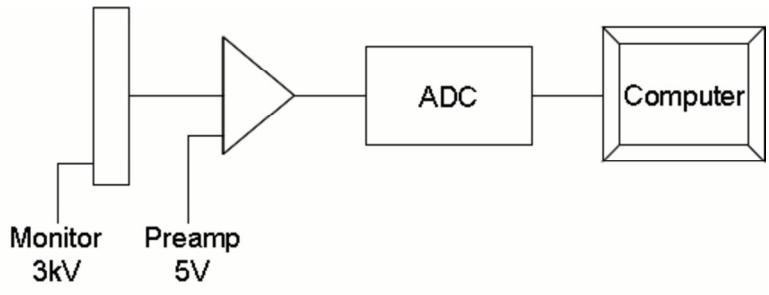

Figure 5.6: Schematics of the data acquisition system used for the experiment. The signal recorded by the monitor was amplified by the pre-amplifier and goes to the ADC which was interfaced with the computer.

5.9.1 Cell Thickness Determination

For neutron polarization analysis the first thing we need to determine are the thicknesses of both the cells. For this we took runs for the unpolarized polarizer, analyzer cell (unpolarized at the same time) and empty oven. The thicknesses were calculated using

$$\frac{T_0}{T_E} = e^{-(nl)_x \frac{\sigma_0}{\lambda_0}\lambda}. \tag{5.33}$$

The analysis method used to determine the thickness values for the cells was discussed in detail in section 3.9. The polarizer thickness was determined using M1 and M2 data were used and for the analyzer M2 and M3 data were used. Figure 5.7 and figure,, 5.8 show the plots for the unpolarized to empty transmission ratios for the polarizer and the analyzer. The thickness values for these two cells were determined using an exponential fit to these plots. For the polarizer the thickness value was (3.84±0.02) amagat cm and the analyzer thickness was (3.60±0.02) amagat cm. Figure 5.9 gives the transmission through the entire experimental set up and therefore measures the thickness of the entire set up, which is almost equal to the sum of thicknesses of the polarizer and the analyzer. This transmission ratio was calculated using M1 and M3 data. The thickness value obtained for the entire set up was (7.5±0.03) amagat cm. The residuals, difference between the experimental value

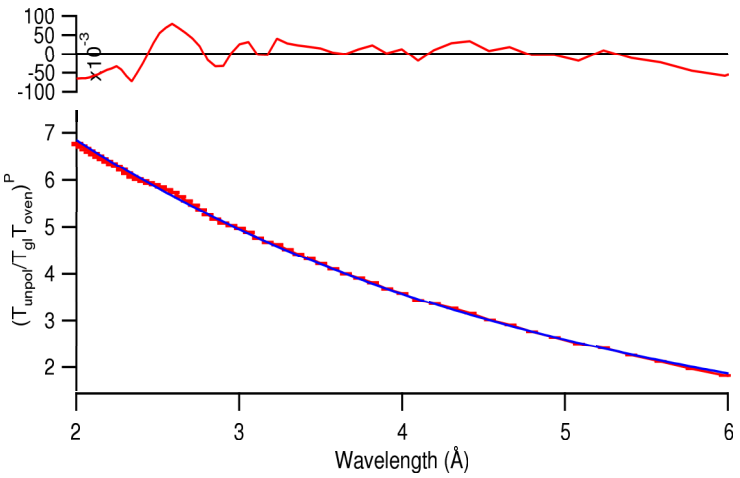

Figure 5.7: Ratio of the neutron transmission through the unpolarized polarizer ("Dino") to the transmission through empty polarizer oven. The red points are the values obtained from the experimental data and the blue line is the fit curve. The residual curve shows the difference between the experimentally observed values and the fit values which is of the order of 1%.

and the fit value, for figures 5.7, 5.8 and 5.9 are of the order of 1%.

5.9.2 Neutron Polarization Analysis

After the thickness and spin flip efficiency measurements the next thing to do is the polarization measurement using the two methods discussed before in sections 5.6.1 and 5.6.2. The polarization analysis using the first method (using the data stored at M1 and M2) is the same as the method we used for the NPDGamma experiment. ^{3}He polarization and neutron polarization values were obtained using equation 5.18 and 5.18, respectively. Figure 5.10 shows the plot for T_P/T_0 using which ^{3}He polarization was calculated for a single run and figure 5.17 shows the plot for neutron polarization P_n for the same run.

To calculate the polarization using M2 and M3, the first challenge was to separate the data with spin flipper on from the spin flipper off data for a single run. Unlike NPDGamma the spin flipper sequence which we used for this experiment was a two pulse sequence given as ↑↓↑↓↑↓↑↓. For this sequence, ↑ means the spin flipper is off

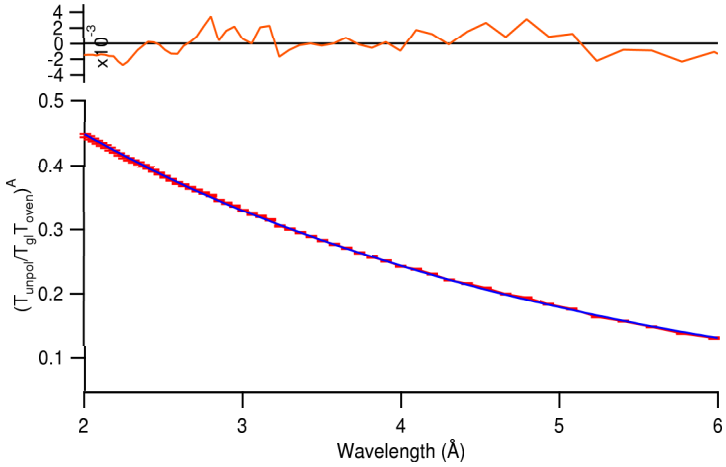

Figure 5.8: Ratio of the neutron transmission through the unpolarized analyzer ("Pebbles") to the transmission through the empty analyzer oven. Residuals are of the order of 1%.

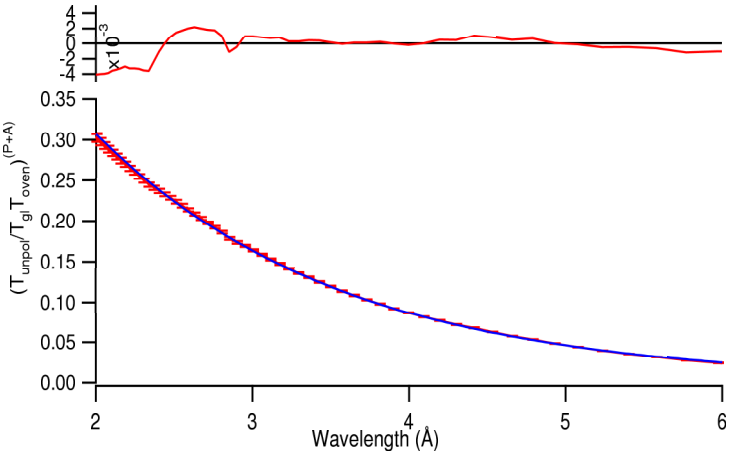

Figure 5.9: Ratio of the combined neutron transmission through unpolarized polarizer and analyzer to the transmission through the empty ovens. This gave the combined thickness value for the polarizer and analyzer.

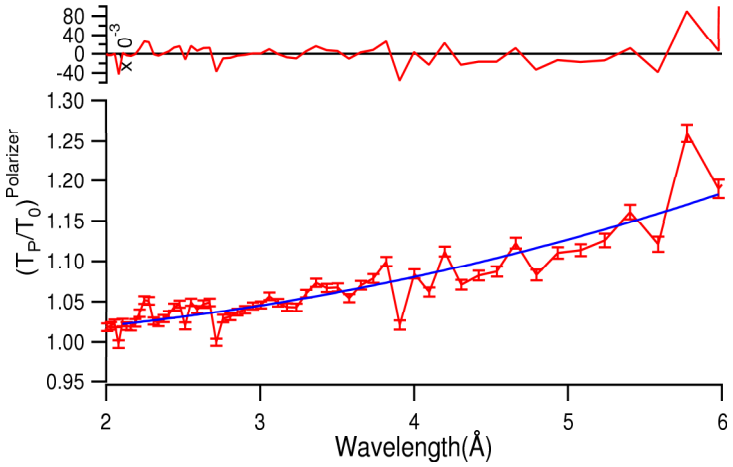

Figure 5.10: Plot shows the ratio of the neutron transmission through the polarized cell to the unpolarized cell versus wavelength (using M1 and M2)

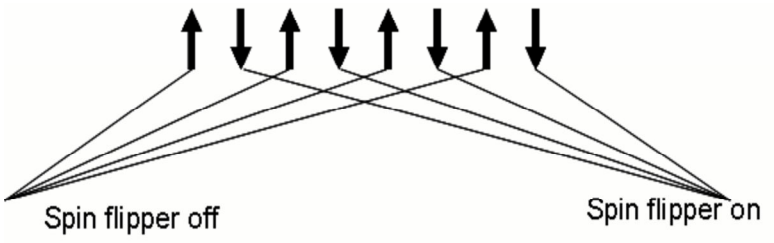

Figure 5.11: The figure shows the two pulse spin sequence for the spin flipper. ↑ means the spin is unflipped and ↓ implies the spin is flipped. For the analysis we separated the transmissions of flipped and unflipped pulses.

and the spin is unflipped and ↓ implies that the spin flipper is on and the spin is flipped for the neutron pulse. For the analysis we needed the transmissions for both spin flipper on and off as seen from equations 5.22, 5.23 and 5.24. These transmissions we had to obtain from the same run by separating the alternate neutron pulses as shown in fig 5.11.

The data separation was done using the fact that if polarizer and analyzer are polarized in the same direction, the bigger signal is for spin flipper off and the smaller signal is for flipper on. But if the two systems are polarized in opposite directions (by performing AFP on one of the systems) bigger signal corresponds to SF on and smaller to SF off. Figure 5.12 shows the variation in the signal size for spin flipper

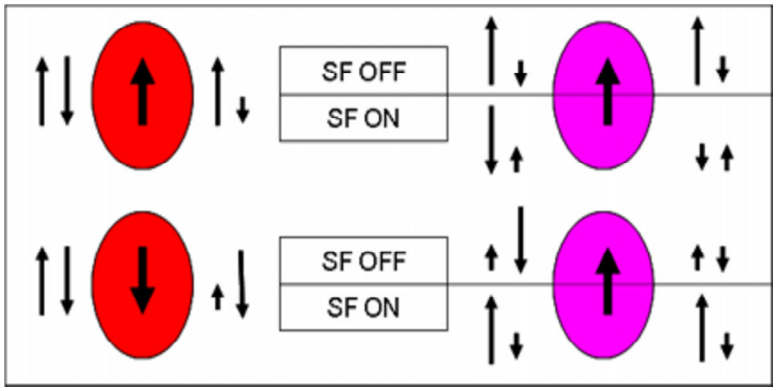

Figure 5.12: Schematics of the method used for separating neutron transmission through the analyzer for spin flipper ON and OFF state. When polarizer and analyzer are polarized in the same direction transmission is bigger for spin flipper on than spin flipper off. And when the polarizer and analyzer are polarized in opposite directions transmission is bigger for spin flipper off than spin flipper on.

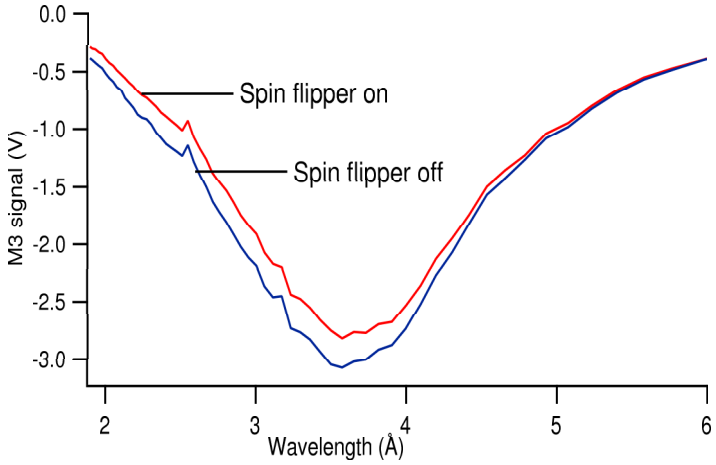

Figure 5.13: Plot shows the transmission through the spin flipper the polarizer and analyzer polarized in the same direction for the ON and OFF states of the spin flipper.

on and off and polarizer and analyzer polarized in the same direction and for spin flipper on and off but polarizer and analyzer polarized in opposite directions. When polarizer and analyzer were polarized in the same direction spin off transmission was bigger than the spin on transmission (figure 5.13) as seen from the data.

After separating the data for T_{SFoff} and T_{SFon}, polarization analysis was performed using equations 5.22 and 5.23. Equation 5.22 was used to determine the value of analyzer polarization, plot is shown in fig 5.14. This value of analyzer po-

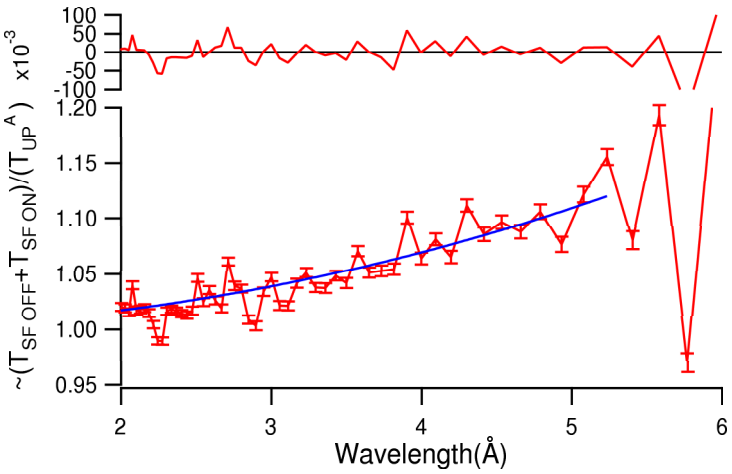

Figure 5.14: Plot shows the quantity $\frac{1}{2\epsilon}\left[(2\epsilon-1)\left(\frac{T_{A,P}^{SFOff}}{T_{A,0}}\right)+\left(\frac{T_{A,P}^{SFOn}}{T_{A,0}}\right)\right]$ versus wavelength and is fitted to $\cosh(x_A P_A)$ to obtain the value of analyzer polarization.

larization combined with equation 5.23 gives the value of ^{3}He polarization in the polarizer. Figure. 5.15 shows the plot for equation 5.23 vs wavelength.

Thus, ^{3}He polarization was calculated for a couple of runs using the two methods described in sections 5.6.1 and 5.6.2. It was observed that for all the runs calculated ^{3}He polarization values using the two methods agree well with each other. Figure 5.16 shows a plot of ^{3}He polarization obtained from the two methods for all the analyzed runs. ^{3}He polarization obtained using the two methods agrees to a percent, but the point to point variation in the data is bigger than a percent due of the presence of the systematics.

It is possible to measure the neutron polarization as a function of wavelength if ^{3}He polarization is known by using $P_n(\lambda) = \tanh(x_P P_P)$. We also compared the values of neutron polarization obtained from the monitors data using the two analysis methods. Figure 5.17 shows the neutron polarization obtained using equation 5.18 and 5.24. From this plot a big disagreement was seen between the neutron polarization values obtained using the two methods. The disagreement in the values

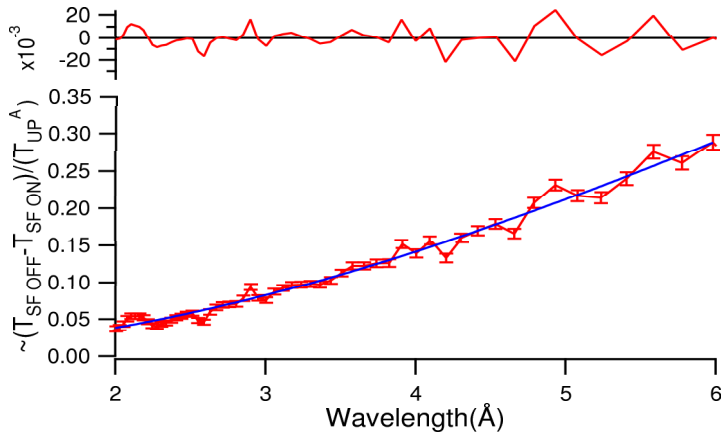

Figure 5.15: The plot shows $\frac{1}{2\epsilon}\left[\left(\frac{T_{APol}^{SFOff}}{T_{Aunpol}}\right)-\left(\frac{T_{APol}^{SFOn}}{T_A^O}\right)\right]$ versus wavelength, fitted to $\sinh(x_A P_A)\tanh(x_P P_P)$ to get the value of ^{3}He polarization using the value of analyzer polarization obtained from figure 5.14

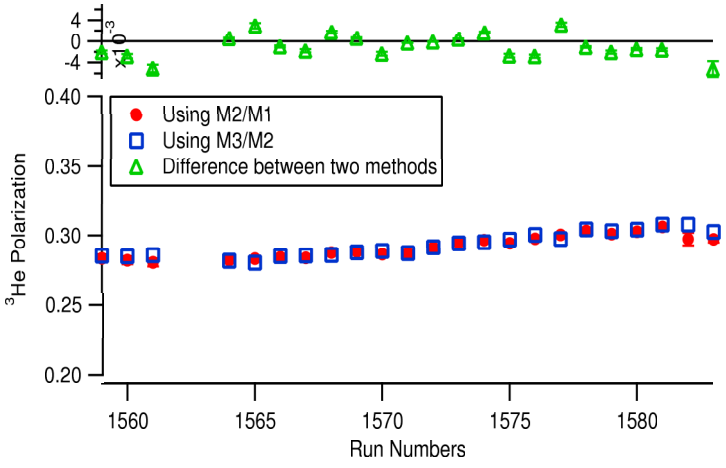

Figure 5.16: Plot showing ^{3}He polarization for a series of runs taken during the Summer 2007 run at LANSCE. Solid circles are from the method using M1 and M2 and squares are from the method using M2 and M3. The triangles at the top show the difference between the two methods.

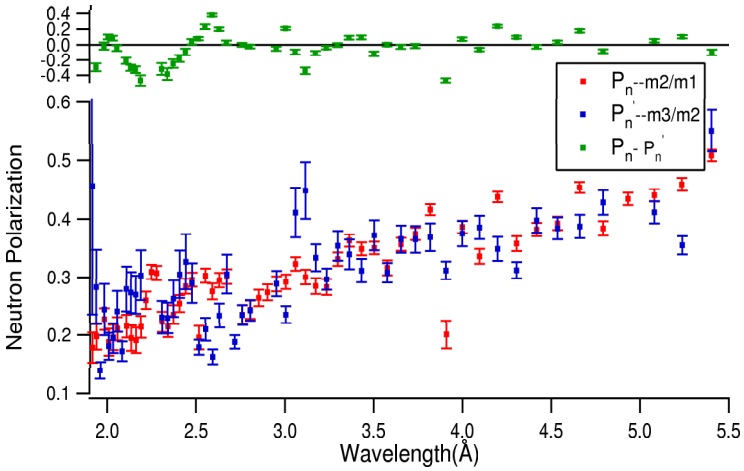

Figure 5.17: Comparison of neutron polarization calculated using the two methods, using M1 and M2 and M2 and M3. The red points show the neutron polarization with M1 and M2. Blue points are the values of neutron polarization with M2 and M3. Green points show the difference of values between the two methods.

obtained from the methods was due to the oscillations in M2 and M3 which affected the quality of the data and therefore affected the analysis. These oscillations are discussed in detail in the next section. The precision polarimetry analysis was thus limited by the data quality. We thus developed an experiment for the precision polarimetry but the verification of the analysis was limited by the quality of the data.

5.9.3 Systematics

It was seen from neutron polarization plot (figure 5.17) and spin flipper efficiency plot (figure 5.5) that there were some systematic effects between 2 $\AA$ to 3 $\AA$. The spin flipper efficiency was greater than 1 in this range, which is unusual as the maximum spin flipper efficiency is 1. Also, between 2 $\AA$ to 3 $\AA$, the neutron polarization deviated a lot from the standard $\tanh(x_P P_P)$ behavior. Figure 5.17 shows that same type of deviation from the standard neutron polarization behavior were observed for the two methods, using M1 and M2 and using M2 and M3. This gave an indication of the possibility that something was wrong with monitor 2 as the only common

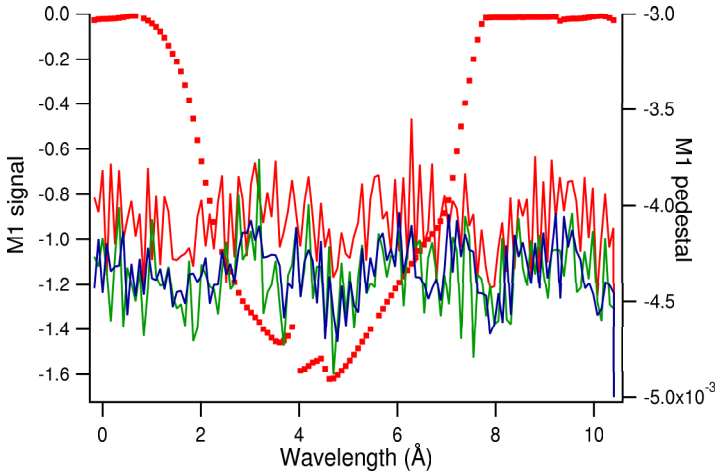

Figure 5.18: Plot showing the comparison of some pedestal runs with the neutron beam on signal at M1. The dotted line shows the neutron beam signal and the solid lines are the pedestal signals. Pedestal signal is about 0.25% of the actual signal

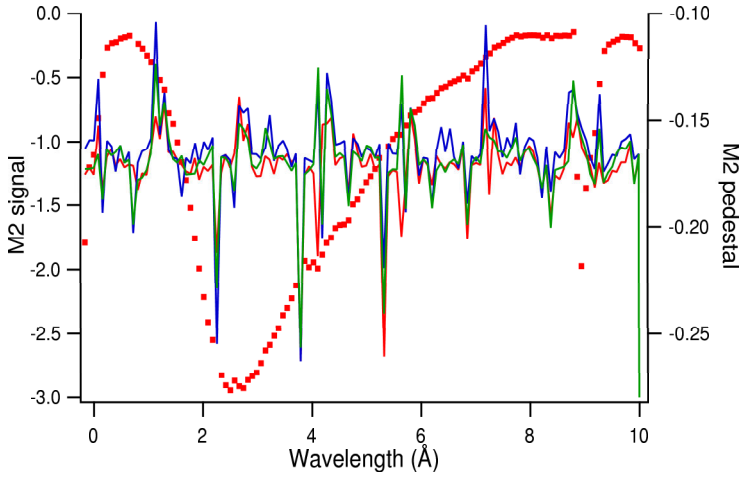

Figure 5.19: Plot showing the comparison of some pedestal runs with the neutron beam on signal at M2. The dotted line shows the neutron beam signal and the solid lines are the pedestal signals. Pedestal signal is about 6% of the actual signal

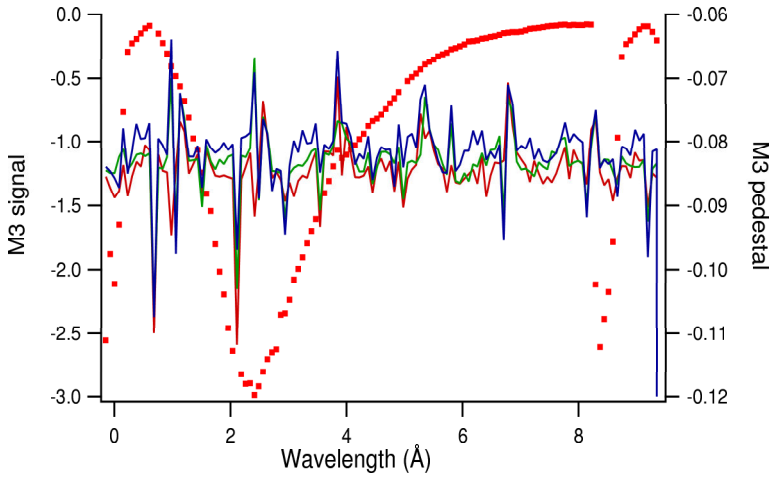

Figure 5.20: Plot showing the comparison of some pedestal runs with the neutron beam on signal at M3. The dotted line shows the neutron beam signal and the solid lines are the pedestal signals. Pedestal signal is about 3% of the actual signal

thing between the two methods was the second monitor. Therefore, we decided to look at the pedestals of all the monitors to compare the behavior of M2 with M1 and M3.

Figure 5.18, 5.19 and 5.20 show the pedestals recorded by the three monitors in comparison with the neutron beam-on signal for the respective monitors. The pedestal level in M1 was 0.25% of the monitor signal, for M3 it was ≈3% but for M2 pedestal signal was ≈6% of the signal which indicates that there was a big source of systematics in the second monitor. From figure 5.19, it was also seen that M2 saw some oscillations at a repetition rate of 120 Hz which is unusual. After investigation it was found that these oscillations were coming from the power source which was connected to the monitors M2 and M3. This affected the quality of the data and therefore analysis was affected. Our data was dominated by the systematics of monitor 2.

5.10 Conclusions

We discussed the importance of the precision neutron polarization measurement in this chapter. There are many experiments which aim at measuring the polarized beta decay correlation coefficients A, B and C. PANDA aims to measure the proton asymmetry C in β-decay to 0.1%. A 0.1% measurement of the proton asymmetry factor, C, is limited by the neutron polarization measurements. Precision polarimetry experiment at LANSCE was designed to measure the neutron polarization precisely keeping in mind the experimental needs of PANDA and abBA.

We performed the "Precision Polarimetry Experiment using ^{3}He Spin Filters" at LANSCE in Summer 2007. Experimental details and the analysis method were presented in this chapter. We successfully demonstrated the working experiment and developed a method to analyze the data. We were able to measure the cell thickness, spin flipper efficiency, ^{3}He polarization and neutron polarization using two different methods.

Although we succeeded in designing and performing the experiment, while analysing we saw the limitations of our data because of the electronic equipments we used in the experiment. Nevertheless, we were able to measure ^{3}He polarization to an accuracy of $\approx$1% which allows us to determine the neutron polarization, but the wavelength dependence of neutron polarization was not directly measured to high precision due to the poor performance of M2.

We also determined the spin flipper efficiency using the data recorded by the monitors and observed that for certain wavelength range the efficiency was going above unity and we were not able to determine the efficiency correctly. Previously, for the same spin flipper efficiency was calculated to be 98.0 $\pm$ 0.8% and had no

dependence on the wavelength [65] but in our analysis we saw a strong dependence on the wavelength which affected the analysis. To eliminate this limitation in the future, in addition to performing AFP on the polarizer, we can also do the AFP on the analyzer. Equation 5.20 gives the ratio of the neutron transmission through a polarized analyzer to the transmission through unpolarized analyzer when the spin flipper is off. Now, if we do the AFP on the analyzer, we can effectively let $P_A \rightarrow -P_A$, and the polarimetry asymmetry can be given as,

$$\left(\frac{T_{A,P}}{T_{A,O}}\right)^{+} + \left(\frac{T_{A,P}}{T_{A,O}}\right)^{-} = 2\cosh(\sigma x_A P_A), \tag{5.34}$$

$$\left(\frac{T_{A,P}}{T_{A,O}}\right)^{+} - \left(\frac{T_{A,P}}{T_{A,O}}\right)^{-} = 2P_n(\lambda)\sinh(\sigma x_A P_A), \tag{5.35}$$

$$\frac{[T_{A,P}/T_{A,O}]^{+} - [T_{A,P}/T_{A,O}]^{-}}{[T_{A,P}/T_{A,O}]^{+} + [T_{A,P}/T_{A,O}]^{-}} = P_n(\lambda)\tanh(\sigma x_A P_A). \tag{5.36}$$

Thus neutron polarization can be calculated using the analyzer without spin flipper and the spin flipper efficiency can be separately determined. Instead of using the second method which we used for our analysis we can use equations 5.34, 5.35, 5.36 to calculate the ^{3}He and neutron polarization using M2 and M3.

CHAPTER VI

Summary

The discussions and results in this dissertation provide insights into three experiments namely, NPDGamma experiment, depolarization in ^{3}He cells and precision polarimetry experiment. We have discussed the motivation behind the NPDGamma experiment and the experimental set up to realize the goal. The discussion includes the depolarization effect which was observed in the ^{3}He cells during the NPDGamma experiment and the experiment performed to understand the depolarization in the cells. Also the need for the determination of accurate neutron polarization and the experiment performed to do the precision polarimetry measurement has been addressed.

Based on the benchmark paper of Desplanques, Donohogue and Holstein (DDH) published in 1980, nucleon-nucleon interaction is described by a strong vertex and a weak vertex [30]. Weak parity violating nucleon nucleon potential is described by the exchange of mesons, namely ρ, π and ω. The meson exchange potential is given by a linear combination of seven meson-nucleon coupling constants. The weak interaction is treated as a perturbation in the Hamiltonian of the system and is responsible for the parity-violating mixing of the states. DDH gave a range of expected values of all the coupling constants for their model in their celebrated paper. Several experiments

have been designed in the last few decades to measure these coupling constants and the NPDGamma experiment is one of them. The NPDGamma experiment measured the directional-asymmetry A_γ in the γ-ray emitted in the n-p capture. With this measurement of A_γ the long range pion-nucleon coupling f_π^1 is calculated using $A_\gamma \approx -0.11 f_\pi^1$. The f_π^1 value calculated from this method is highly significant as recently two different experiments came up with two different values of f_π^1. The value obtained from the NPDGamma experiment will be important as the n-p system is free of any nuclear structural complications.

The NPDGamma experiment was performed at FP12 at the LANSCE spallation source because of the high neutron flux provided by the source. Another advantage from this source was the time of flight spectrum which provided control of systematic effects. Polarized neutrons required for the experiment were produced using ^{3}He neutron spin filter. The cell was maintained within the temperature range 145-155^{0}C and 60 Watts of laser light was provided for the optical pumping of the cell. ^{3}He polarizer was first installed in the FP12 flight path during the commissioning period of the experiment. Some of the data presented in this thesis is from the commissioning period, February 2005. The analysis done with this data showed that we were able to reach a polarization of 57$\pm$1%.

For the NPDGamma production period, 90 Watts of laser light (using three lasers) was provided to the polarizer cells. ^{3}He polarization in the cell and the neutron beam polarization were monitored over time using the data recorded by the monitors used in the experiment. In the production period, we were able to reach a polarization of 0.572 ± 0.021 with "Pebbles" for the first set of runs of the NPDGamma experiment. For the second set of data using "Dino" as the polarizer we reached a polarization of 0.572 ± 0.012. The data collected for the monitors were affected due to the

backgrounds and it was realized that background plays an important role in the polarization analysis.

For the NPDGamma experiment, backgrounds were large due to the possible back-scattering of neutrons from the liquid H_2 target. At room temperature most of the H_2 is in ortho state and has a bigger cross section for neutron scattering. Therefore ortho-hydrogen was converted to para-hydrogen using ortho-to-para converters to reduce neutron scattering inside the target and therefore preventing the neutrons from depolarization before the n-p capture. For our liquid H_2 target we were able to attain 99.98% of para-hydrogen. Presently, the asymmetry value obtained from the NPDGamma analysis is (-1.1$\pm$2.1)$\times$ 10^{-7}. The asymmetry analysis is still under progress. The NPDGamma experiment finished data collection at the Los Alamos Neutron Science Center in Fall 2006 and has been moved to Spallation Neutron Source where it plans to measure the asymmetry A_γ to a level of 10^{-8} with the higher neutron flux.

While monitoring ^{3}He polarization in the NPDGamma experiment we observed ^{3}He depolarization in the cells when exposed to the neutron beam. We observed two kinds of relaxations in the cell: long term relaxation and short term relaxation. Experiments were performed at LANSCE in Summer 2007 to understand this depolarization in which we measured the Rb polarization in a polarizer cell by electron spin resonance technique with varying neutron flux. It was found that Rb polarization decreases with increasing neutron flux. The result was confirmed by another experiment which was performed at Institut Laue-Langevin in Grenoble, France where hybrid alkali metal (Rb-K) cells were used. The spin destruction rate was also measured in the cells with varying neutron flux (ϕ_n). The relaxation rate (Γ_{SD}) as a function of neutron flux showed the form $\Gamma_{SD} \propto \sqrt{\phi_n}$.

We also concluded that the short term depolarization occurs because of the production of electron-ion pairs inside the cells. The processes due to the ionization are created mainly by the capture reaction ^{3}He(n,p)^{3}H which releases 782 keV/capture. This energy is sufficient to cause the ionization of the species inside the cell. It has been established that the spin destruction rate is proportional to the square root of the neutron flux. A possible solution to overcome the short term decay in the polarizer cells will be to use double cells in future experiments.

For the long term depolarization it was concluded that it was due to the formation of a Rb compound inside the cells. The thickness of the white coating deposited on the cell was dependent on the time duration for which it was exposed to the neutrons and the flux incident on it. At higher flux in ILL the cell became white in two hours. One hour exposure at ILL is equivalent to two days exposure at LANSCE beamline [67]. This coating affects the transmission of laser light through the cell and therefore results in a decrease in the polarization. With time the laser light transmission through the cell decreases and therefore we saw the continuous slow decrease of ^{3}He polarization in the cells. It is believed that the coating is of RbH, formed due to the combination of Rb with H produced during the n+^{3}He$\rightarrow$^{1}H + ^{3}H, but it is not confirmed yet. For a complete understanding of the long term depolarization in the cell we will need to confirm the composition of the deposition formed in the cell.

During the NPDGamma experiment we realized that backgrounds play an important role in the polarization measurements and played an important role in limiting us from measuring the neutron polarization accurately. For the NPDGamma experiment we were able to measure the neutron polarization to an accuracy of $\pm$3%. For the NPDGamma experiment accuracy on the polarization value was not a major factor as NPDGamma planned to measure the value of the coupling constant within

10% of the DDH value. But there are experiments with a goal of 0.1% measurement, e.g. PANDA plans to measure the value of proton asymmetry, C, the correlation between the neutron spin and outgoing proton, to a precision of 0.1%. A 0.1% measurement of C means 0.1% measurement of neutron polarization as well. The precision polarimetry experiment was motivated by this requirement and was performed at LANSCE in summer 2007 to see the precision with which we can measure the neutron polarization. The data we recorded for this experiment was affected by some of the unforeseen oscillations in the monitors. With this data we were able to measure the ^{3}He polarization up to 0.4% but the measurement of neutron polarization was inconclusive because of the oscillations in M2 and M3. These oscillations affected all the analysis we did with monitor 2 and monitor 3, including the polarization analysis, spin flipper efficiency analysis.

Nevertheless, we developed a technique for the measurement of neutron polarization using two different approaches. The verfication of the analysis method was limited by the quality of the data, which limited us from reaching the goal. A good way of doing precision polarimetry would be to do AFP on both polarizer and analyzer. Using this the neutron polarization can be calculated using both the methods independent of the spin flipper efficiency.

Polarized neutrons have played an important role in fundamental neutron physics experiments and will continue to do so. They provide opportunities to study the weak interactions in parity violating nucleon-nucleon interactions and in β-decay. Precise measurement of the asymmetries in β-decay requires precise measurement of neutron polarization. It is possible to do precision polarimetry with pulsed neutron beam by taking advantage of the time of flight spectrum and the $1/v$ dependence of the ^{3}He spin filters. ^{3}He polarizers can be used as analyzers for precision polarimetry

experiments. ^{3}He polarizers in its present configuration can also be used as polarizer at times. If the cell were to be exposed to the neutron beam for a longer period of time double cells could be an option. The NPDGamma experiment has been moved to SNS after finishing the first run at LANSCE and is expected to reach improved sensitivity with higher neutron flux.

APPENDICES

APPENDIX A

Adiabatic Fast Passage

A.1 Magnetic Moments in a Magnetic Field

If a magnetic moment $\vec{\mu}$ is placed in an external magnetic field, H, it will experience a torque and the equation of motion is given by

$$\vec{\tau} = \frac{d\vec{J}}{dt} = \vec{\mu} \times \vec{H} \tag{A-1}$$

where $\vec{J}$ is the angular momentum. This can be written as,

$$\vec{\tau} = \frac{d\vec{\mu}}{dt} = \vec{\mu} \times (\gamma \vec{H}) \tag{A-2}$$

as $\vec{\mu} = \gamma \vec{J}$

Assuming the magnetic moment to be in a frame which is rotating with an angular velocity ω, the equation of motion of the magnetic moment, μ, is given by,

$$\frac{\delta\vec{\mu}}{\delta t} + \vec{\omega} \times \vec{\mu} = \vec{\mu} \times (\gamma \vec{H}) \tag{A-3}$$

$$\frac{\delta\vec{\mu}}{\delta t} = \vec{\mu} \times (\gamma \vec{H} + \vec{\omega}) \tag{A-4}$$

If the actual magnetic field $\vec{H}$ in equation A-2 is replaced by an effective magnetic field, $\vec{H_e}$, then the equation of motion of the magnetic moment in the rotating coordinate system is the same as the equation of motion in the laboratory coordinate

system provided,

$$\vec{H}_e = \vec{H} + \frac{\vec{\omega}}{\gamma} \tag{A-5}$$

$\vec{\omega}$ can be chosen such that the effective magnetic field, $\vec{H}_e = 0$ or $\vec{\omega} = -\gamma H_0 \hat{k}$ in a static magnetic field $\vec{H} = H_0 \hat{k}$, and can solve for the motion of $\vec{\mu}$. As $\vec{H}_e = 0$, $\frac{\delta \vec{\mu}}{\delta t} = 0$, and therefore $\vec{\mu}$ remains fixed with respect to the rotating axes. Thus, with respect to the laboratory the spin vector is fixed in a set of axes which rotates with an angular velocity $\vec{\omega} = -\gamma H_0 \hat{k}$. In other words, $\vec{\mu}$ rotates with an angular velocity $\vec{\omega} = -\gamma H_0 \hat{k}$ with respect to the laboratory frame of reference and this frequency is called the Larmor Frequency. For ^{3}He, γ= 3.41 and thus the resonance frequency for ^{3}He spins in a 10 Gauss magnetic field is 34.1 kHz.

A.2 Effect of Alternating Magnetic Field

The equation of motion of a magnetic moment in a magnetic field, $H_0 + H_1(t)$, is given by

$$\frac{d\mu}{dt} = \mu \times \gamma[H_0 + H_1(t)] \tag{A-6}$$

where $H_0 = \hat{k} H_0$ is the static magnetic field in the z direction and $H_1(t) = H_1(\hat{i} \cos \omega_z t + \hat{j} \cos \omega_z t)$ is the alternating magnetic field rotating with a frequency ω_z. In a coordinate system which is rotating about the z-axis at a frequency ω_z, the equation of motion will modify to

$$\frac{\delta \mu}{\delta t} = \mu \times [\hat{k}(\omega_z + \gamma H_0) + \hat{i} \gamma H_1] \tag{A-7}$$

Let $\omega_z = \omega$, then near resonance $\omega = -\gamma H_0$ and the equation

$$\begin{aligned} \frac{\delta \mu}{\delta t} &= \mu \times [\hat{k} \left(H_0 - \frac{\omega}{\gamma} \right) + \hat{i} H_1] \\ &= \mu \times H_{eff} \end{aligned} \tag{A-8}$$

where

$$H_{eff} = \hat{k}\left(H_0 - \frac{\omega}{\gamma}\right) + \hat{i}H_1 \tag{A-9}$$

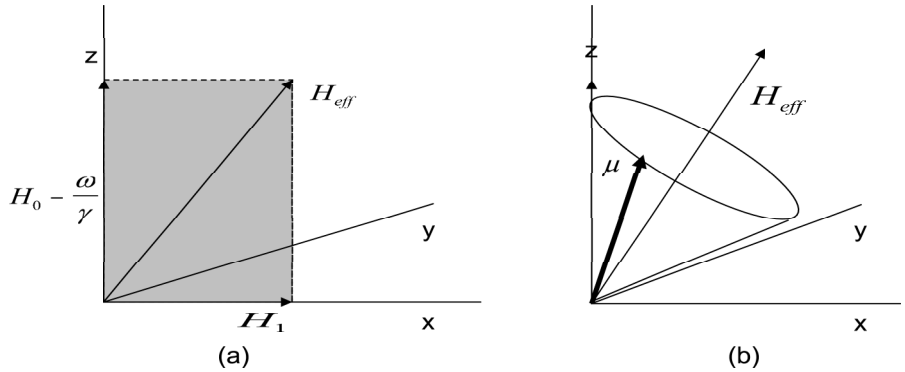

Figure A.1: (a)Effective field (b) Magnetic moment in the rotating coordinate system

Equation A-8 shows that the moment effectively experiences a static magnetic field H_{eff} in the rotating frame. The moment therefore precesses in a fixed angle cone about the direction of effective magnetic field, as shown in figure A.1, at an angular frequency of γH_{eff}. If the resonance condition is met ($\omega = \gamma H_0$) the magnetic moments will precess about the effective field $H_{eff} = \hat{i}H_1$ in the y-z plane. If H_1 is turned on for a short time t_w moment would precess through an angle $\theta = \gamma H_1 t_w$. If t_w is chosen such that $\theta = \pi$ the pulse will invert the magnetic moments and the pulse is called a π-pulse. Similarly pulse is called a 90 degree pulse if a pulse is selected that $\theta = \pi/2$, the magnetic moment is turned from the z direction to y direction [68]. This theory is used to observe the frequency induction decay and adiabatic fast passage in ^{3}He polarizer cells.

A.2.1 Frequency Induction Decay

Frequency induction decay is a commonly used technique for observing resonances. FID is the observable NMR signal by non-equilibrium spin magnetization precessing about the static magnetic field in the z direction. A small tipping angle is provided

to the magnetic moments by applying a resonant radio frequency close to the Larmor frequency of the nuclear spins. This pulse gives a small tip to a small number of ^{3}He atoms in the plane perpendicular to holding magnetic field. The tipped ^{3}He atoms precess around the holding field at the NMR frequency and dephase with a time constant T_2.

The interactions of the spins with their surroundings cause a decay. The duration of the NMR signal is therefore limited by the transverse relaxation time T_2, It depends on the interaction of the gas with the cell walls, field gradients etc.. In liquids, the decay may last for several milliseconds, in solids it is approximately 100 μs. For the NPDGamma experiment the magnetic field was very uniform with a field gradient of 1 mGauss/cm and we observed $T_2 \approx 200ms$ for the cells we used. Block diagram for the FID set up we used is shown in figure A.2. The resulting oscillating magnetization created by the ^{3}He atoms is sensed by a pick-up coil. An FID signal is shown in figure 3.13 in Chapter III .

Transverse magnetization of polarized ^{3}He atoms is given by [3],

$$M = M_z \sin\theta e^{-t/T_2} \tag{A-10}$$

where θ is the tip angle provided by the RF pulse. The precessing magnetic moments will produce a flux through the pick up coil and will induce a voltage. If ϕ is the emf in the coil from the precessing ^{3}He magnetic moments,

$$\phi = M_z nA \sin\theta e^{-t/T_2} \tag{A-11}$$

where A is the area of the pick up coil and n is the number of turns. Therefore, the voltage induced in the pick up coil is given as [25]

$$V_0 = \omega\phi Q \tag{A-12}$$

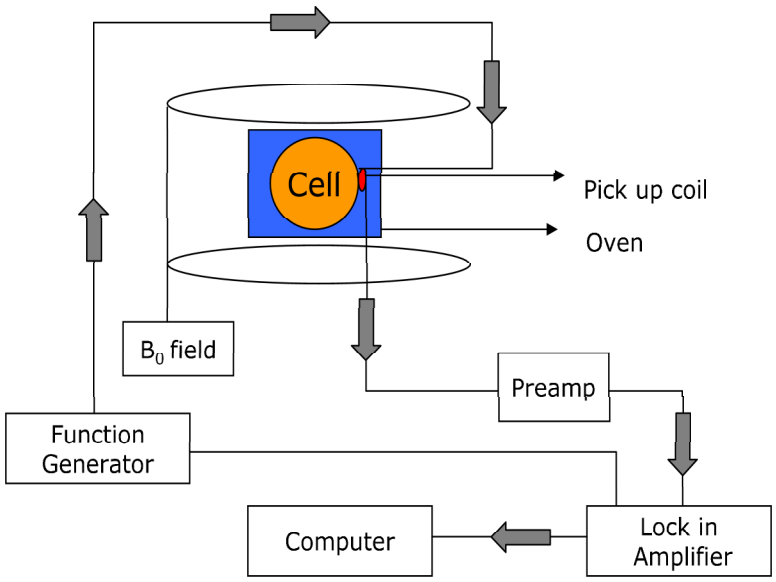

Figure A.2: Experimental set up for Frequency Induction Decay (FID). The tipping angle provided by the RF pulse will produce a flux through the pick up and a voltage will be induced.

Q is the quality factor of a tuned circuit. This voltage signal is observed as the FID signal in experiments. We used FID signal in our experiment to monitor the ^{3}He polarization in the polarizer cells. The signal is proportional to the amount of ^{3}He polarization in the cell.

A.2.2 Adiabatic Fast Passage

AFP is a NMR technique used to rotate the neutron spins from one state to another. There are two ways to do AFP.

- The static field is kept constant and the frequency of the RF signal, ω is passed through the resonance in a time short compared to the relaxation times.
- The RF is kept constant and the static field, H_0 is varied to pass the system through resonance.

As the static field or the frequency of the RF signal is swept from below resonance to above, the nuclear magnetization follows the effective magnetic field in the rotating frame and the spins get inverted i.e. it flips from parallel to opposite H_0. The sweep

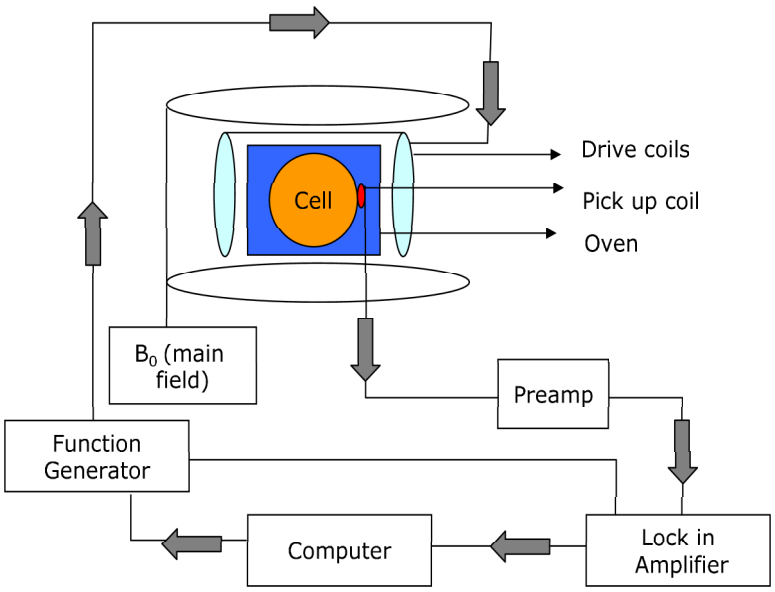

Figure A.3: Experimental set up for Adiabatic Fast Passage. The RF is applied to the drive coil which flips the helium spins.

rate is sufficiently slow to satisfy the adiabatic condition given as,

$$\left|\frac{d\delta}{dt}\right| << |\gamma H_1| \tag{A-13}$$

where

$$\delta = \frac{H_0 - H_\omega}{H_1} \tag{A-14}$$

where $H_\omega = \omega/\gamma$. The condition for adiabatic variation can also be stated as z-field has to pass through an interval comparable to the resonance width H_1 in a time which is long compared to $t_1 = 1/|\gamma H_1|$. The diagram for AFP is shown in figure A.3

We used the first method, changing the frequency of the signal, to do the AFP for flipping the polarization in the polarizer cell during the NPDGamma experiment and the precision polarimetry experiment. Also, the concept of AFP was used in the spin flipper used in these experiments. We also suggest using AFP on the polarizer cell in future.

APPENDIX B

Precision Polarimetry Derivations

When the neutron beam from the source is incident on the polarizer, it has equal number of spin up and down neutrons given by,

$$n_+ = \frac{N_0}{2}, n_+ = \frac{N_0}{2} \tag{B-1}$$

where N_0 is the total number of neutrons incident on the polarizer and n_+ and n_- are the number of neutrons with spin up and spin down, respectively. As we saw in chapter III, when the neutrons pass through a polarizer the transmission of neutrons with spin up and spin down is given by,

$$n_\pm^P = e^{(-\sigma x_P(1\mp P_P))} \tag{B-2}$$

where σ is the absorption cross-section for the neutrons, x_P is the thickness of the polarizer cell and P_P is the ^{3}He polarization in the polarizer cell.

After the polarizer, the polarized neutron beam passes through a spin flipper in the experiment. If the spin flip efficiency of the spin flipper (discussed in Chapter V) is given by ϵ, the neutron transmission through the spin flipper of the two different spin states for the OFF state of the spin flipper is given by,

$$n_\pm^{SFoff} = n_\pm^P \tag{B-3}$$

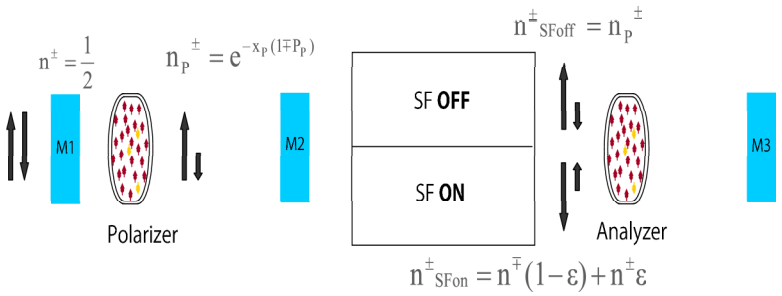

Figure B.1: Neutron transmission through different components of the precision polarimetry set up when the spin flipper is on and off. Using this, the transmission through the analyzer is calculated for both spin on and off state.

i.e. when the spin flipper is OFF the spin flipper the neutron transmission is not affected by the presence of spin flipper. And for the ON state of the spin flipper the neutron transmission is given by,

$$n_{\pm}^{SFon} = (1-\epsilon)n_{\pm}^{P} + \epsilon n_{\mp}^{P} \tag{B-4}$$

This transmission for the spin flipper ON state can be explained in the following way. If we are looking at the neutrons with spin up transmission, when the spin flipper is ON all the neutrons with spin down will change to spin up i.e. $n^P \rightarrow n_+^P$ depending on the spin flipper efficiency and some of the neutrons will not get flipped because of the imperfect spin flipper. For a spin flipper with spin flip efficiency, $\epsilon \approx 1$, the number of spin up neutrons after the spin flipper is $n_+^{SFon} = (1-\epsilon)n_+^P + \epsilon n_-^P$ where the first term is the number of spin up neutrons that remain unflipped and the second term is the number of neutrons flipped by the spin flipper.

Similar to a polarizer, neutron transmission through an analyzer which has a polarization P_A and thickness x_A is given by,

$$n_{\pm}^{A} = n_{\pm}^{SF} e^{(-\sigma x_A(1\mp P_A))} \tag{B-5}$$

where $n_{\pm}^{SF}$ is the transmission for any state of the spin flipper, x_A is the thickness of the analyzer and P_A is the polarization of the analyzer.

For the analysis, we need the transmission through the analyzer for both spin flipper on and off state. The transmission through the analyzer when the spin flipper is off depends on the polarization of the polarizer and the analyzer and is given by,

$$\begin{aligned} T_{A,P}^{SFOff} &= \frac{n_P^+ n_A^+ + n_P n_A}{n_P^+ + n_P^-} \\ &= e^{-\sigma x_A} \frac{\cosh(x_P P_P + x_A P_A)}{\cosh(x_P P_P}) \\ &= T_{A,0}[\cosh(x_A P_A) + \sinh(x_A P_A) \tanh(x_P P_P)] \end{aligned} \tag{B-6}$$

Therefore,

$$\frac{T_{A,P}^{SFOff}}{T_{A,0}} = \cosh(x_A P_A) + \sinh(x_A P_A) \tanh(x_P P_P) \tag{B-7}$$

where $T_{A,P}^{SFOff}$ is the transmission through polarized analyzer when the spin flipper is off and $T_{A,0} = e^{-\sigma x_A}$ is the transmission through the unpolarized analyzer.

We also need to look at the neutron transmission through the analyzer when the spin flipper is on. The transmission through the analyzer when the spin flipper is on depends on the polarization of the polarizer and the analyzer and also on the spin flipper efficiency. The transmission is given by,

$$\begin{aligned} T_{A,P}^{SFOn} &= \frac{n_{SFOn}^+ n_A^+ + n_{SFOn}^- n_A^-}{n_P^+ + n_P^-} \\ &= \frac{(1-\epsilon) n_P^+ + \epsilon n_P^-}{n_P^+ + n_P^-} n_A^+ + \frac{\epsilon n_P^+ + (1-\epsilon) n_P^-}{n_P^+ + n_P^-} n_A^- \\ &= T_{A,0}[\cosh(x_A P_A) + (1-2\epsilon) \sinh(x_A P_A) \tanh(x_P P_P)] \end{aligned} \tag{B-8}$$

Therefore, the ratio of the transmission through polarized analyzer with spin flipper on to the transmission through unpolarized analyzer is

$$\frac{T_{A,P}^{SFOn}}{T_{A,0}} = \cosh(x_A P_A) + (1-2\epsilon) \sinh(x_A P_A) \tanh(x_P P_P) \tag{B-9}$$

where $T_{A,P}^{SFOn}$ is the transmission through polarized analyzer when the spin flipper is on. All the T's in this section are the ratio of M3 to M2.

After determining the transmission through the analyzer for both spin flipper on and off states we determine the analyzer polarization. Adding equations B-7 and B-9 we can determine the analyzer polarization from,

$$\frac{1}{2\epsilon}\left[(2\epsilon-1)\left(\frac{T_{A,P}^{SFOff}}{T_{A,0}}\right)+\left(\frac{T_{A,P}^{SFOn}}{T_{A,0}}\right)\right]=\cosh(x_A P_A) \tag{B-10}$$

And the ^{3}He can be determined by subtracting B-9 by B-7 and using the value of analyzer polarization obtained from equation B-10

$$\frac{1}{2\epsilon}\left[\left(\frac{T_{APol}^{SFOff}}{T_{Aunpol}}\right)-\left(\frac{T_{APol}^{SFOn}}{T_A^O}\right)\right]=\sinh(x_A P_A)\tanh(x_P P_P) \tag{B-11}$$

As we know the neutron polarization at M2 is given by $P_n(\lambda)=\tanh(x_P P_P)$, the neutron polarization at M2 in terms of analyzer polarization and spin flipper efficiency can be written as,

$$P_n(\lambda)=\frac{1}{2\epsilon T_A^0}\frac{T_A^{SFOff}+T_A^{SFOn}}{\sqrt{\cosh^2(x_A P_A)-1}} \tag{B-12}$$

Thus, we developed a method to determine the neutron polarization using two different methods. We successfully analyzed the neutron beam polarization using ^{3}He analyzer.

BIBLIOGRAPHY

BIBLIOGRAPHY

[1] Hartmut Abele. The neutron. its properties and basic interactions. *Progress in Particle and Nuclear Physics*, 60:1–81, 2008.

[2] Y.G. Abov *et.al.* On the existence of an internucleon potential not conserving spacial parity. *Physics Letters*, 12:1:25–26, 1964.

[3] A. Abragam. *Principles of Nuclear Magnetism*. Oxford university Press, 1982.

[4] E.G. Adelberger and W.C. Haxton. Parity violation in the nucleon-nucleon interaction. *Annual Review of Nuclear and Particle Science*, 35:501–558, 1985.

[5] E. G. Adelberger *et al.* Beta decays of ^{18}Ne and ^{19}Ne and their relation to parity mixing in ^{18}F and ^{19}F. *Physical Review C*, 27(6):2833–2856, 1983.

[6] G. Ahrens *et al.* Search for parity violation in the 1081 kev gamma transition of ^{18}F. *Physical Review A*, 390:486, 1982.

[7] J. Als-Nielsen and O. Dietrich. Slow neutron cross sections for ^{3}He, B and Au. *Physical Review*, 133:B925–B929, 1964.

[8] L.W. Anderson and *et al.* Hyperfine structure of hydrogen, deuterium and tritium. *Physical Review*, 120:1279–1289, 1960.

[9] E.D. Babcock. *Spin Exchange Optical Pumping with Alkali-Metal Vapors*. PhD thesis, University of Wisconsin-Madison, 2005.

[10] E. Babcock *et al.* Hybrid spin-exchange optical pumping of ^{3}He. *Physical Review Letters*, 91:1230033, 2003.

[11] E. Babcock *et.al.* Limits to the polarization for spin-exchange optical pumping of ^{3}He. *Physical Review Letters*, 96:0830031–4, 2006.

[12] C. A. Barnes *et al.* Search for neutral-weak-current effects in the nucleus ^{18}F. *Physical Review Letters*, 40:840–843, 1978.

[13] L. Barron-Palos. Determination of the ortho-para fraction in the npdgamma LH_2 target. *Technical Note, NPDGamma collaboration*, 2007.

[14] Bass and C.D. *et al.* Measurement of the parity-violating neutron spin roation in ^{4}He. *Journal of Research of the National Institute of Standards and Technology*, 110:205–208, 2005.

[15] A.R. Berdoz *et al.* Parity violation in proton-proton scattering at 221 mev. *Physical Review Letters*, 87:272301, 2001.

[16] M. A. Bouchiat *et al.* Nuclear polarization in ^{3}He gas induced by optical pumping and dipolar exchange. *Physical Review Letters*, 5(8):373–375, 1960.

[17] J.D. Bowman *et.al.* Measurement of the parity-violating gamma asymmetry A_γ in the capture of polarized cold neutrons by para-hydrogen, $n + p \rightarrow d + \gamma$. *A report submiited to the U.S. Department of Energy in 1998*, 1998.

[18] M.A. Box *et al.* Parity mixing in nuclei as a test of theories of the weak interaction. *Journal of Physics G*, 1:493, 1975.

[19] J. Byrne. *Neutrons, Nuclei and Matter.* Institue of Physics Publishing, 1993.

[20] J.F. Cavaignac *et al.* Search for parity violation in neutron-proton capture. *Physics Letters*, 67B:2:148–150, 1977.

[21] B. Chann *et al.* Production of highly polarized ^{3}He using spectrally narrowed diode laser array bars. *Journal of Applied Physics*, 94:6908–6914, 2003.

[22] T.E. Chupp and K.P. Coulter. Polarization of ^{21}Ne by spin exchange with optically pumped Rb vapor. *Physical Review Letters*, 55:1074, 1985.

[23] T.E. Chupp *et al.* Tests of high density polarized ^{3}He target for electron scattering. *Physical Review C*, 45:915–932, 1992.

[24] T.E. Chupp *et al.* Panda precision measurement of the proton asymmetry in neutron decay. *Letter of Intent*, 2007.

[25] T.E Chupp *et.al.* Polarized, high density, gaseous ^{3}He targets. *Physics Review C*, 36(6):2244–2251, 1987.

[26] T.E Chupp *et.al.* A large area polarized ^{3}He neutron spin filter. *Nuclear Methods and Instruments in Physics research A*, 574:500–509, 2007.

[27] K.P. Coulter *et al.* Measurement of ^{3}He depolarization rates during bombardment with a ^{4}He beam. *Nuclear Instruments and Methods in Physics Research A*, 276:29–34, 1989.

[28] K.P. Coulter *et al.* Neutron polarization with a polarized ^{3}He spin filter. *Nuclear Instruments and Methods in Physics Research A*, 288:1463–466, 1990.

[29] M. Dabaghyan. Determination of the length of fp12 using the bragg edge transmission method. *Technical Note, NPDGamma collaboration*, 2006.

[30] B Desplanques, J.F. Donohogue, and B.R. Holstein. Unified treatment of the parity violating nuclear force. *Annals of Physics*, 124:449–495, 1980.

[31] A. Dianoux and G. Lander, editors. *Neutron Data Booklet.* Institut Laue-Langevin, Grenoble, 2002.

[32] K. Elsener *et al.* Investigation of parity violation in ^{19}F. *Physics Letters*, 117B:167, 1982.

[33] E. Fermi. *Z. Phys.* 88:161, 1934.

[34] V.V. Flambaum and D.W. Murray. Anapole moment and nucleon weak interactions. *Physical Review C*, 56:1641–1644, 1997.

[35] W. Franzen. Spin relaxation of optically aligned rubidium vapor. *Physics Review*, 115:850–856, 1959.

[36] M. Gell-Mann. Test of the nature of the vector interaction in β decay. *Physical Review*, 111(1):362–365, 1958.

[37] M.T. Gericke. *The NPDGamma Experiment: The Weak Interaction Between Nucleons and Parity Violation in Cold Neutron Capture.* PhD thesis, Indiana University, 2004.

[38] M.T. Gericke *et al.* A current mode detector array for γ-ray asymmetry measurements. *Nuclear Instruments and Methods in Physics Research A*, 540:328–347, 2005.

[39] R.C. Gillis. *^{3}He ionization chambers as neutron beam monitors for the NPDGamma experiment.* M.Sc. Thesis, University of Manitoba, 2006.

[40] V. Gudkov. Asymmetry of recoil proton in nuclear β-decay. *Physical Review C*, 77:045502, 2008.

[41] W. Happer and W.A. Van Wijngaarden. An optical pumping primer. *Hyperfine Interactions*, 38:435–470, 1987.

[42] William Happer. Optical pumping. *Reviews of Modern Physics*, 44:169–250, 1972.

[43] J.C. Hardy and I.S. Towner. Superallowed $0^+ \rightarrow 0^+$ nuclear beta decays: A critical survey with tests of the conserved vector current hypothesis and the standard model. *Physical Review C*, 71:055501, 2005.

[44] B.R. Holstein. Nuclear parity-violation parameter in $h_\rho^{\prime(1)}$. *Physical Review D*, 23:1618–1622, 1981.

[45] E.B. Iverson and J.M. Carpenter. *Kinetics of Irradiated Liquid Hydrogen.* ICANS-XVI, Dusseldorf-Nuess, Germany, 2003.

[46] J.D Jackson *et.al.* Possible tests of time reversal invariance in beta decay. *Physics Review*, 106(3):517–521, 1957.

[47] K. S. Krane *et al.* Observation of 1.5% parity-nonconserving γ-ray asymmetry. *Physical Review Letters*, 26(25):1579–1581, 1971.

[48] M. Kreuz *et al.* The crossed geometry of two super mirror polarisers-a new method for neutron beam polarisation and polarisation analysis. *Nuclear Instruments and Methods in Physics Research A*, 547:583–591, 2005.

[49] T.D. Lee and C.N. Yang. Questions of parity conservation in weak interactions. *Physical Review*, 104-1:254–258, 1956.

[50] R. Machleidt *et al.* The Bonn meson-exchange model for the nucleon-nucleon interaction. *Physics Reports*, 149,1:1–89, 1987.

[51] MCNP. *A General Monte Carlo N-Particle Transport Code.* http://laws.lanl.gov/x5/MCNP/index.html.

[52] E. Merzbacher. *Quantum Mechanics.* John Wiley&Sons Inc., 1999.

[53] S.F. Mughabghab *et al.*, editor. *Neutron Cross Section Series.* Academic Press, 1981.

[54] N. R. Newbury *et al.* Gaseous $^3-^3$He magnetic dipolar spin relaxation. *Phys. Rev. A*, 48(6):4411–4420, 1993.

[55] L. Passell and R. I. Schermer. Measurement of the spin dependence of the ^{3}He(n, p)T reaction and of the nuclear susceptibility of adsorbed ^{3}He. *Physical Review*, 150:146–151, 1966.

[56] A.K. Petoukhov *et al.* Recent advances in polarised ^{3}He spin filters at the ILL. *Physica B: Condensed Matter*, 385-386:1146–1148, 2006.

[57] N.F. Ramsey. *Nuclear Moments.* Wiley&Sons Inc., 1953.

[58] M.J. Ramsey-Musolf and S.A. Page. Hadronic parity-violation: A new view through the looking glass. *Annual Review of Nuclear and Particle Science*, 56:1–52, 2006.

[59] D. R. Rich *et al.* Spin exchange optical pumping at pressures near 1 bar for neutron spin filters. *Applied Physics Letters*, 80:2210, 1993.

[60] D.R. Rich *et al.* A measurement of the absolute neutron beam polarization produced by an optically pumped ^{3}He neutron spin filter. *Nuclear Instruments and Methods in Physics Research A*, 481:431–453, 2002.

[61] L.D. Schearer and G.K. Walters. Nuclear spin-lattice relaxation in the presence of magnetic-field gradients. *Physical Review*, 139:A1398, 1993.

[62] R. Schiavilla *et al.* Parity-violating interaction effects in the np system. *Physical Review C*, 70:044007, 2004.

[63] M. Schumann *et.al.* Measurement of the proton asymmetry in neutron beta decay. *Physical Review Letters*, 100(151801), 2008.

[64] P.-N. Seo *et al.* A measurement of the flight path 12 cold H_2 moderator brightness at lansce. *Nuclear Instruments and Methods in Physics Research Section A*, 517:285–294, 2004.

[65] P.-N. Seo *et al.* High-efficiency resonant rf spin rotator with broad phase space acceptance for pulsed polarized cold neutron beams. *arXiv:0710.2871v1*, 2007.

[66] A. Serebrov *et al.* Measurement of the neutron lifetime using a gravitational trap and a low-temperature fomblin coating. *Physics Letters B*, 605:72–78, 2005.

[67] M. Sharma *et al.* Neutron beam effects on spin-exchange-polarized ^{3}He. *Physical Review Letters*, submitted, 2008.

[68] C.P. Slichter. *Principles of Magnetic Resonance*. Springer, 1989.

[69] E.C.G. Sudarshan and R. Marshak. Chirality invariance and the universal fermi interaction. *Physical Review*, 109:1860, 1958.

[70] M. Taketani *et al.* On the method of the theory of nuclear forces. *Progress of Theoretical Physics*, 4(4):581–586, 1951.

[71] N. Tanner. Parity in nuclear reactions. *Physical Review*, 107:501–558, 1957.

[72] W.T.H. van Oers. Symmetries and symmtery breaking. *Physical Review D*, 684:266–276, 2001.

[73] B.I. Verkin *et al.* *Handbook of Properties of Condensed Phases of Hydrogen and Oxygen*. Hemisphere Publishing Corporation, 1990.

[74] P.A. Vetter *et.al.* Precise test of electroweak theory from a new measurement of parity non-conservation in atomic thallium. *Physical Review Letters*, 74:14:2658–2661, 1995.

[75] E. Vliegen *et al.* Faraday rotation density measurements of optically thick alkali metal vapors. *Nuclear Instruments and Methods in Physics Research Section A*, 460:444–450, 2003.

[76] M. Wagshul and T.E. Chupp. Optical pumping of high-density rb with a broadband dye laser and GaAlAs diode laser arrays: Application to ^{3}He polarization. *Physics Review A*, 40:4447, 1989.

[77] M. Wagshul and T.E. Chupp. Laser optical pumping of high-density Rb in polarized ^{3}He targets. *Physics Review A*, 49:3854–3869, 1994.

[78] G. K. Walters *et al.* Nuclear polarization of ^{3}He gas by metastability exchange with optically pumped metastable ^{3}He atoms. *Physical Review Letters*, 8:439–442, 1962.

[79] W.S. Wilburn and J.D. Bowman. Consistency of parity violating pion-nucleon couplings extracted from measurements ^{18}F and ^{133}Cs. *Physical Review C*, 57:3425–3429, 1998.

[80] R. Wilson *et al.* *The Investigation of Fundamental Interactions with Cold Neutrons.* NBS, 1986.

[81] C.S. Wood *et.al.* Measurement of parity nonconservation and an anapole moment in cesium. *Science*, 275:1759–1763, 1997.

[82] C.S. Wu *et al.* Experimental test of parity conservation in beta decay. *Physical Review*, 105:1413–1415, 1957.

[83] Yao and W.M. *et al.* Review of particle physics. *Journal of Physics G*, 33:1, 2006.

[84] B.G. Yerozolimsky. Problems of precise neutron beam polarization measurements. *Nuclear Instruments and Method in Physics Research A*, 420:232–242, 1999.

[85] A.R. Young and *et al.* Three-dimesional imaging of spin polarization of alkali-metal vapor in potical pumping cells. *Applied Physics Letter*, 70-23:3081–3083, 1997.

[86] la.B. Zel'Dovich. Electromagnetic interaction with parity violation. *Soviet Physics JETP*, 6:1184–1186, 1958.

[87] J. N. Zerger *et al.* Polarization of ^{129}Xe with high power external-cavity laser diode arrays. *Applied Physics Letters*, 76:1798, 1993.

[88] O. Zimmer. A method for precise neutron beam polarisation analysis using an opaque spin filter. *Physics Letters B*, 461(307-314), 1999.

[89] O. Zimmer *et al.* High precision neutron polarisation analysis using opaque spin filters. *Physics Letters B*, 455(62-68), 1999.